POLITECNICO DI MILANO

School of Industrial and Information Engineering

Department of Chemistry, Materials and Chemical Engineering

“Giulio Natta”

Master of Science in Chemical Engineering

CFD simulation of aeration and mixing processes in a full-scale oxidation ditch

Academic Supervisor:
Prof. Alberto CUOCI

Company Supervisor:
Dr. Thomas HOEHNE

Candidate:
Tural MAMEDOV
Student I.D. 873912

Academic Year 2018-2019

To my mother and father

Abstract

In Wastewater Treatment Plants (WWTP), effluent quality is mainly dependent on aeration and mixing performances in the oxidation ditch process. Typically, the design of oxidation ditches is based on the heuristic methods in which a detailed analysis of the fluid flow field is not possible. Computational Fluid Dynamics (CFD) is a widely used design tool for analyzing, modelling and simulating fluid flow patterns in wastewater treatment processes over the last two decades. The aim of this study is to accomplish a hydrodynamic analysis of aeration and mixing processes in a full-scale oxidation ditch by using CFD. Multiphase flow model was built in a three-dimensional computational geometry by using the commercial software ANSYS CFX. Unstructured mesh elements were generated due to the complexity of computational geometry. The Euler-Euler approach has been chosen for multiphase modelling, and the continuous phase was set for water, whereas air was modelled as the dispersed phase. The SST turbulence model was specified which predicts turbulence eddies in free stream and wall-bounded region with high accuracy. The momentum source term approach and transient rotor-stator approach were applied for modelling of submersible agitators in the oxidation basin. Hydrodynamic analysis has been successfully performed for four different scenarios. Despite the computational limitations, the results of transient rotor-stator approach are more accurate in comparison with the momentum source term one. Moreover, the results show that the model of submerged agitators is able to generate the required thrust to obtain adequate bulk flow throughout the oxidation ditch. Minimum horizontal flow velocity was also achieved to get high mixing performance. The effect of normal forces on the blades was investigated by the positioning of agitators based on the manufacturer's best practice guidelines. Higher thrust fluctuations were obtained when the distance between the agitators and the first row of diffuser grids is short. Also, the contribution of the air injection to the mixing process has been studied. The result indicates that it is not possible to obtain the required mixing quality without agitators due to the air-induced recirculation zones. Despite the high computational resources needed for a full-scale study of the oxidation ditch process, the objectives of this work were achieved with doing considerable simplifications in computational geometry.

Keywords: Oxidation ditch; Wastewater Treatment; Biological Treatment; CFD; Multiphase Flow; Aeration; Fine Bubble Diffusers

Acknowledgements

First and foremost, I would like to express my sincere gratitude to my supervisor Dr. Thomas Hoehne for his support, patience, and guidance throughout this work at Helmholtz-Zentrum Dresden-Rossendorf (HZDR) in Germany. To be part of the HZDR family was a unique experience in my academic career and my sincere thanks go to my supervisor for giving me this opportunity. My sincere thanks also go to Prof. Alberto Cuoci who supported and guided me as a supervisor from Politecnico di Milano.

A special thanks to my family and my grandparents for their love and full support through all my life. Mainly, my mum and dad, I would not be where I am today without you. I also thank my girlfriend for giving me confidence throughout my studies abroad.

Finally, I wish to express my appreciation to all my teachers, mentors, friends and those who contributed to my success.

Table of Content

List of Figures

List of Tables

Nomenclature

Abbreviations

2D	Two Dimensional
3D	Three Dimensional
BNR	Biological Nutrient Removal
BOD	Biochemical Oxygen Demand
CFD	Computational Fluid Dynamics
CPU	Central Processing Unit
CSTR	Continuous Stirred Tank Reactor
DNS	Direct Numerical Simulation
EAAS	Extended Aeration Activated Sludge
GGI	General Grid Interface
HPOAC	High Purity Oxygen Activated Sludge
LES	Large Eddy Simulation
MLSS	Mixed Liquor Suspended Solid
OD	Oxidation Ditch
OTE	Oxygen Transfer Efficiency
PFR	Plug Flow Reactor
RAS	Return Activated Sludge
RMS	Root Mean Square
RSM	Reynolds Stress Model
SAE	Standard Aeration Efficiency
SBR	Sequencing Batch Reactor
SOTE	Standard Oxygen Transfer Efficiency
SOTR	Standard Oxygen Transfer Rate
SRT	Solid Retention Time
SST	Shear Stress Transport
UNESCO	United Nations Educational, Scientific and Cultural Organization
VOF	Volume of Fluid
WAS	Waste Activated Sludge
WWTP	Wastewater Treatment Plant

Symbols

A_d	Particle cross-section
A_{lg}	Interfacial area density
B_j	Body force in j direction
$C_{1\varepsilon}$	Coefficient of Low-Reynolds-number turbulence model
$C_{2\varepsilon}$	Coefficient of Low-Reynolds-number turbulence model
C_D	Drag coefficient
C_{VM}	Virtual mass force coefficient
C_V	Turbulent viscosity coefficient
$C_{\varepsilon 1}$	Closure coefficient of standard $k-\varepsilon$ model
$C_{\varepsilon 2}$	Closure coefficient of standard $k-\varepsilon$ model
D_g	Mean diameter of gas phase
D_p	Diameter of a particle
e	Thermodynamic internal energy
Eo	Eotvos number
F_k	Interaction force
f_1	Damping function of Low-Reynolds-number turbulence model
f_1	Damping function of Low-Reynolds-number turbulence model
f_μ	Damping function of Low-Reynolds-number turbulence model
g	Gravitational acceleration
g_i	Gravitational vector in direction i
k	Turbulent kinetic energy
l	Turbulent length scale
l_*	Wall length scale
$\dot{m}_{kl}$	Mass transport from phase k to phase l
n	Number of particles
P	Pressure
q_i	Heat flux in direction i
Re_d	Reynolds number of dispersed phase
S	Source term
t	time
u_i	Fluid velocity in direction i
$\langle u_i \rangle$	Averaging component of fluid velocity in direction i
u_i'	Fluctuating component of fluid velocity in direction i
u_*	Wall friction velocity
u^+	Dimensionless velocity
$u_{i,dr}$	Drift velocity in direction i
V_d	Volume of particle
y^+	Dimensionless length
α_f	Volume fraction of continuous phase

α_d	Volume fraction of dispersed phase
ρ	Density of fluid
φ	Flow variable
ω	Specific dissipation rate
ε	Turbulent energy dissipation rate
τ_{ij}	Stress tensor
μ	Dynamic viscosity
σ_κ	Prandtl Schmidt number
κ	Karman constant
Γ	Diffusion coefficient
ρ_m	Mixture density
μ_m	Mixture dynamic viscosity

Chapter 1

Introduction

1.1 Wastewater Generation and Treatment

Water quality is continually deteriorating due to the various human and natural activities in the world. It is a fact that contaminated water sources pose a significant threat to the environment and human health, where wastewater treatment is a reliable method to eliminate toxic and dangerous substances from its ingredients and recover freshwater to nature. The extent of water quality degradation usually depends on fields of usage, thereby wastewater composition can vary, and successful treatment steps are the key factors to avoid threats of these pollutants completely. Wastewater is mainly composed of nutrients, toxic chemicals, heavy metals, biodegradable organics, inorganic substances, pathogens and non-pathogenic microorganisms, etc. and when discharged without treatment processes, they have a bad impact on the aquatic ecosystem as well.

Meanwhile, these pollutants, especially pathogens, are the principal causes of wastewater-related diseases such as diarrhea, cholera, typhoid or skin infections in the human body. The statistics regarding wastewater-related diseases show that annual death from diarrhea and cholera is around 780,000 because of inadequate water and sanitation. Recent worldwide investigations on the water quality show that over 80% of wastewater discharges to the environment without being treated (UNESCO, 2019).

Globally, water consumption has been gradually increasing by approximately 1% per year since the 1980s, and this trend will continue rising at a similar rate until 2050. Nowadays, water consumption is mainly related to three primary sectors which are agricultural, municipal, and industrial sectors. The statistics show that these three major water use sectors are the primary wastewater generators as well. Main constituents of wastewater may vary due to its numerous generation sources, and potential hazards to the ecosystem depend on them (UNESCO, 2019).

Wastewater treatment ensures that the resultant effluent after the treatment process possesses such a quality that comply with environmental regulations requirements

and allowed to discharge back to the environment without causing any pollution. Conventional wastewater treatment involves three principal successive stages so-called primary, secondary and tertiary treatments and each of these stages deal with different contaminants. The resultant effluent becomes cleaner as wastewater passes through these steps. These stages cover physical, biological and chemical processes to remove suspended solids, toxics, organic and inorganic substances from wastewater. During the primary treatment process, solid matters in wastewater are mechanically removed by special equipment. Heavier solid matters settle to the bottom of separation tank, while light solid wastes are floating at the tank surface. The efficiency of this process related to the retention time of feedstock in the wastewater tank, and it removes only a small amount of coarse solid wastes which might inhibit the regular operation of secondary treatment process units. Then the effluents are pumped to the tank of secondary treatment process which is also known as the activated sludge process. The principal aim of this process is to get rid of the organic content of wastewater. The seed sludge addition and air supply to the system lead to the growth of bacteria and microorganisms. These small organisms consume the natural ingredients of wastewater and settle down at the bottom of the tank as large particles. The next step involves more deep treatment operations to remove all residual impurities from the effluent of activated sludge processes. The resultant effluent quality of tertiary treatment is similar to that of drinking water.

In addition to these core processes, there are other auxiliary steps such as odor control, screening of large objects, disinfection, etc. for increasing efficiency of treatment. Many contaminants cause a terrible smell, and they are treated by the addition of chemicals at the beginning of the wastewater treatment process. Also, not all the impurities treated during main treatment processes, and there are still pathogen contents that must be disinfected with chlorine-based chemicals. Disinfection process makes the feedstock cleaner to protect human and animal health. All the procedures play a crucial role to remove pollutants from wastewater, and they take place in a wastewater treatment plant (WWTP).

1.2 Motivation for Study

The secondary treatment or more precisely biological treatment process is the main and integral part of WWTP in order to get rid of biodegradable organic wastes and suspended solids. This treatment method commonly uses an aerobic activated sludge

process to remove pollutants. Oxidation ditch is the modified activated sludge process with the advantage of minimizing mixing limitations in comparison with large bioreactors applications. In addition to this, the amount of energy consumed to satisfy the oxygen demand of large bioreactors is not sufficient to keep the solid-liquid mixture as suspension (Grady, et al., 1999). Oxidation ditches are closed-loop bioreactors and oblong shape geometry is widely used in the industry. Aeration plays a vital role in an oxidation ditch process, and the fundamental objectives are both to transfer oxygen and to provide velocity to the media.

Up to this point, many valuable works and analyses have been done to improve the performance of the wastewater treatment plants. In terms of energy consumption in a biological treatment process, aeration can account for up to 70% of overall energy expenditure. From this point of view, optimizing aeration process is one of the focal points to minimize operating costs and to provide a highly efficient treatment in such installations (Fayolle, et al., 2007). Oxidation ditch plants with fine bubble aeration are commonly installed in the world, and the main variables for a bubble are its rising velocity, bubble size, rate of oxygen transfer, and coalescing with other bubbles during the process.

Furthermore, fully submerged agitators with a horizontal rotation axis are used in order to sustain the mixing process with the typical flow velocity. The hydrodynamics of such a system generally created by agitators as well as by the drag of the liquid with the gas phase. To predict the hydraulic behavior and flow patterns of multiphase flow inside the process tank are complicated and time-consuming issues via experimental studies.

Computational Fluid Dynamics (CFD) is commonly used for the solution of complex fluid flow problems in wastewater treatment in the last two decades. CFD enables to model the wastewater treatment systems and predicts its hydraulic behavior to a certain extent. Moreover, CFD analyses and modellings allow to better understand the optimal design for new facilities with high precision technique.

In this study, CFD-aided modelling aims to identify the effect of operating parameters such as air flowrate, submerged impeller thrust, water depth, etc. on both aeration and mixing processes in the oxidation ditch, and to obtain optimal operating conditions for the existing tank model.

In literature, although the single-phase CFD modelling of full-scale oxidation ditch is a comprehensive approach because of less computational time, this study will focus on the multiphase modelling by using the advantages of CFD.

1.3 Scope of Thesis

The objective of this thesis is to utilize CFD modelling to describe mixing and aeration processes in a full-scale oxidation ditch, and hence

- predict fluid pattern and assess mixing performance throughout the tank
- investigate the relation between generated thrust by submerged agitators and aeration flow for efficient oxygen transfer and avoiding sedimentation
- achieve effective bulk flow
- optimize operating conditions to maintain energy-efficient process

Apart from the goals mentioned above, understanding the effects of diffuser grid arrangement on the hydraulic behavior in the tank is another point of interest for this study.

Despite the rapid development of computer technology, modelling of complex multiphase flow in full-scale biological treatment tanks requires extremely high computational power (Karpinska & John, 2015). These existing challenges make considerable simplifications necessary for geometries and operating parameters such as impeller modelling and using a single bubble mean diameter, respectively.

As a result, the geometry of the aeration grid is modelled as a plane surface or rectangular block at the bottom of the tank for the sake of simplicity. On the other hand, there is wall friction, obstacle and bend loss, and diffuser grid's geometrical shape which are hydraulic resistances in such a tank. Also, recirculation patterns might be formed in the aeration zone by high air flowrate that will be a barrier to the bulk flow. In order to avoid this, a higher hydraulic thrust input will be required and experimental study of such a system with trial and error is a quite challenging and complicated issue in terms of economy and time. CFD tools have been already approved as a robust designing and modelling tool by the research community in the wastewater treatment sector. As a result, CFD modelling of multiphase flow will be applied to achieve targets of this study.

1.4 Thesis Outline

In this section, the structure of this thesis is indicated with a brief description of the topics that are relevant to the chapters.

Chapter 2 introduces the principles of the biological wastewater treatment process and its various types which are common in the industry. A detailed explanation of the activated sludge processes has been given which included its main parts, biochemical reaction mechanisms and the variations of the process. Moreover, the oxidation ditch process described in this chapter as well.

Chapter 3 contains the theory of CFD modelling and shows a brief description of CFD application in wastewater treatment plants. Also, the reliability and validity of CFD technique in wastewater treatment sectors were given.

Chapter 4 is about the development of CFD model for this study. The description of the computational geometry and mesh generation techniques was shown in the beginning. They were followed by the simulation setup and solution methodology, respectively.

Chapter 5 shows the result of CFD simulation which includes four different scenarios. In addition to this, the mesh independence study results were given for the validation of CFD model.

Chapter 6 describes the conclusion of this project and gives recommendations for future studies.

Chapter 2

Biological Wastewater Treatment

2.1 Principles of biological wastewater treatment

The water pollutants are categorized as soluble and insoluble organic or inorganic substances. The insoluble constituents are easily removed by the physical operation of sedimentation in preliminary and primary treatment steps. The residual effluents that are mainly composed of soluble constituents need further treatment which occurs in the biological treatment section. Biological wastewater treatment is a process that occurs by biological mechanisms as the name suggests. The principle behind biological wastewater treatment is to convert harmful organic and inorganic matters into an innocuous form with biochemical operations and separate them from water by further processes.

The end products of biochemical operations are microbial biomass or sludges, carbon dioxide, nitrogen, and other wastes. There are various biochemical operations used in industry, and they are classified from three different points of view (Grady, et al., 1999):

1) the biochemical transformation
2) the biochemical environment
3) the bioreactor configuration

The purpose of classification is to define the most appropriate operation for a specific requirement.

The biochemical transformation describes methodologies to deal with different types of contaminants such as soluble organic matter, insoluble organic matter, and soluble inorganic matter. The removal of soluble organic matter is the principal target of biochemical operations, and they are food sources for microorganisms. As a result, carbon dioxide and biomass formed, and gases sent to the atmosphere while solid particulates removed by settling. The stabilization of insoluble organic matter is another critical requirement for the treatment process. The sedimentation does not entirely avoid insoluble organic matters, and they are present as colloidal in the influent of the biological treatment process. During soluble organic matter removal, some of the colloids are entrapped with the biomass and become stable waste by

losing its biological activity. However, taking advantage of soluble organic matter removal is not effectively eliminate insoluble ones. Therefore, operations designed for the removal of insoluble organics are necessary.

On the other hand, the solubility of inorganic pollutants is the cause of eutrophication effects, and a particular approach must be applied to get rid of them. Nitrogen and phosphorus are the prime inorganic pollutants that give rise to eutrophication problem. Conversion of these soluble inorganics to the unharmful end products is another biochemical transformation method applied in biological wastewater treatment. Nitrogen and Phosphorus are present in domestic wastewater as the form of various chemical compounds. The specific bacteria are used for each of the chemicals to transform them into nontoxic products.

The biochemical environment is the key factor that has a massive impact on the effluent quality due to the growth of microorganisms with different metabolic pathways (Grady, et al., 1999). These metabolic pathways are based on three-terminal electron acceptors that characterize the biochemical environment. They are oxygen, organic compounds, and inorganic compounds. The environment in the presence of dissolved oxygen is defined as aerobic one, and the microorganism growth rate is quite high in this process. In contradiction to the process that occurs in an aerobic environment, there is another one that happens in the absence of oxygen. It is known as the anaerobic treatment process where organic compounds or carbon dioxide are primary terminal electron acceptors. If the electron acceptor is nitrite or nitrate without the presence of oxygen, the biochemical operation occurs in the anoxic environment. The latter situation is more efficient than anaerobic one for a living organism growth rate, but the aerobic environment is the most favorable.

There are several types of wastewater treatment bioreactors in use and categorized as suspended and attached growth bioreactors. These two major categories depend on the microorganism grow manner in wastewater. The name of each category indicates the nature of operations in reactors where microorganisms grow in suspension for suspended growth bioreactor, while they create a biofilm on solid supports for attached growth ones. The suspended growth bioreactors require well-mixing quality to keep the concentration of all constituents uniform throughout the operation. Hence, continuous stirred tank reactors (CSTR), batch reactors, plug-flow reactors (PFR) are suitable bioreactors for that purpose. Also, packed tower, rotating disc, and fluidized bed bioreactors are recognized as attached growth bioreactors.

2.2 Industrial processes

There are plenty of biochemical processes in industry and each method has different operating conditions due to the wastewater contaminants. The reactor configuration, operating environment, and characteristic of pollutants define the types of industrial processes. The most common operation is called activated sludge process which is subdivided into many processes. However, all activated sludge processes are widely used in the industry, and the primary target of them is the removal of soluble organic substances. Activated sludge process takes place in an aerobic bioreactor where microorganisms grow in suspension and detach as biomass. Initially, batch operations were used, and formed sludges were removed by settling after air injection. Then, continuous operations have been used with long aeration chamber because it treats a high amount of wastewater in comparison with batch operations. This is known as the conventional activated sludge process. Nowadays, both reactors are in use with various modifications.

The system is so-called biological nutrient removal (BNR) removes soluble inorganics and is a complex system. Aerobic, anaerobic, and anoxic environment are chosen depending on inorganics characteristics. For example, sequencing batch reactors remove phosphorus and nitrogen by imposing anaerobic and anoxic conditions. In order to extract insoluble organic matter, aerobic digestion is suitable with suspended growth reactors, especially CSTR. This process is famous for its long retention time that maintains the oxidation of organic matters to carbon dioxide. On the other hand, there is an anaerobic digestion that uses anaerobic cultures for stabilization purposes of insoluble organic contents.

The process separates the soluble organic matters in an anaerobic environment is called anaerobic contact. Also, as in the activated sludge process, both insoluble and soluble organic substances are treated in this operation. Two groups of microorganisms are used, and the first group converts organic matters into acetic acid, hydrogen and carbon dioxide. Then, these products are transformed into methane gas using the second group. In comparison with the activated sludge process, the advantages of anaerobic contact are methane generation, less energy consumption, and less solid wastes. The drawback is the residual pollutants that cannot be treated without oxygen supply. Up to now, suspended growth bioreactors are feasible for all these processes.

Furthermore, there are many kinds of processes that operate with the attached growth bioreactors. The operation in use with a fluidized bed bioreactor can employ any of three environments in order to remove the soluble organic matters and nitrogen-based substances. Fluidized bed bioreactors are commonly chosen for industrial wastewater treatment. Another operation is rotating biological contactor for transforming inorganic and organic matters. It is a more energy-efficient process since half-submerged rotating-disc configuration support oxygen transfer, and biofilm attached to the discs. In addition to these, packed bed bioreactors, aerobic filter and tricking filter operations exist in the industry, and selection of them depends on the scale of operation and diversity of pollutants. For this study, activated sludge, which is a reliable and efficient process, is the area of interest.

2.2.1 Activated Sludge Processes

The activated sludge processes are commonly used biological wastewater treatment process which developed in England during the early 1900s (Grady, et al., 1999). The operation takes place in an aerobic environment with the application of suspended growth bioreactors. Removal of the soluble organic contents is the primary target of the activated sludge process besides nitrification and stabilization of insoluble organics. The core principle of all activated sludge processes is to use living organisms that consume carbon-based wastes and form settleable harmless particles through air supply. It is one of the most popular biological treatment process alternatives due to its high-quality effluent and relatively economic advantages. The unit operations must be carefully controlled to complete the process and reach the desired effluent quality. The activated sludge process is capable of treating larger volumes of wastewater which makes its application widespread in the world.

Although numerous activated sludge process variations exist in the industry, a typical activated sludge process can be divided into five main parts.

1. Aeration tank
2. Aeration source
3. Clarifier
4. Recycle
5. Waste disposal

An aeration tank is a bioreactor where the transformation of water pollutants into the harmless particulates occurs. The aeration tank is an open tank with a single or multiple tank configuration composed of mixing and air injection equipment. As the microorganisms are suspended in an aeration basin, the contents of the tank are referred to as mixed liquor suspended solids (MLSS). The typical depth range of the aeration basins is between 3 – 7.5 m (Grady, et al., 1999). However, based on the mixing and oxygen transfer performance in specific processes, these values can be adjustable. Steel and concrete are used in the construction of the aeration tanks. Configuration of bioreactors may vary due to the special cases of treatment processes. Furthermore, the shape of bioreactors is designed in such a manner that it keeps MLSS in suspension.

Aeration source provides a system with oxygen and support mixing process. Air is injected into the bioreactor with diffused air configuration, floating, or fixed mechanical surface aerators. By the use of diffused air configuration from the bottom of a tank, both fine and coarse bubble injections are possible. Some bioreactors use only a single aerator to maintain suspension. In large bioreactors, aeration is inadequate to suspend solid particles in the tank medium. Therefore, auxiliary mixers are used to obtain high mixing performance and desired operating conditions.

The formed solid wastes or heavier biomass are separated from treated water in a tank that is referred to as a clarifier. Biomass settles to the bottom of the secondary clarifier as activated sludge and effluent water sent for further processing in the water treatment plant. The most common configuration for the secondary clarifier is circular, but the rectangular shape is also used. The effect of tank configuration on the treatment performance is not so crucial as bioreactor configuration (Grady, et al., 1999). However, the proper sizing of a clarifier vessel is of prime importance. The clarification and thickening are two functions of the secondary clarifier. The former deals with the removing of biomass, while the latter concentrates the heavier biomass which returns to the bioreactor. Concentrated sludge with hungry microorganisms sent to the bioreactor to begin the same process all over again. These concentrated solids are commonly called return activated sludge (RAS). It is a source of microorganisms, and the concentration of hungry microorganisms in the bioreactor can be controlled by RAS flowrate. The food content of incoming wastewater is always changeable, and RAS flowrate control allows to ensure the required food/microorganisms ratio. Another important factor regarding the RAS is the amount of time that the sludge remains in the secondary clarifier.

The excessive retention time leads to deterioration of living microorganisms due to the lack of oxygen in the tank. Accordingly, the RAS might lose its functionality in bioreactors.

The excess solids in the secondary clarifier are known as waste activated sludge (WAS) in literature, and they must be discarded from the tank. Some proportion of the sludge is about to die, and WAS is used to get rid of death and old sludge content. It is the main operational parameter that controls biomass concentration in the bioreactor. Figure 2.1 illustrates the block flow diagram of a typical activated sludge process.

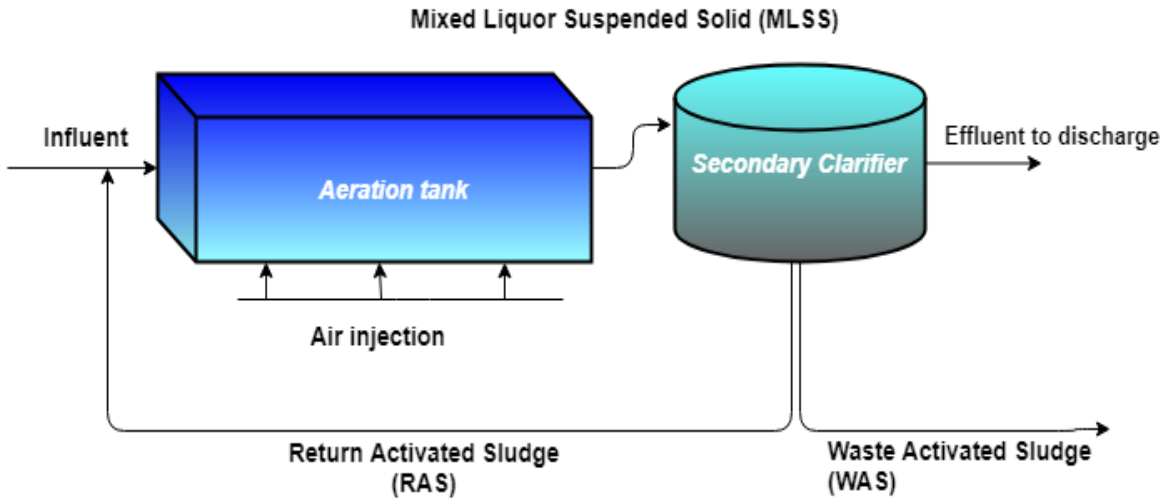

Figure 2.1: Typical activated sludge process.

The biochemical reaction mechanism of the activated sludge process is a core part for understanding the treatment process. The transformation of soluble organic matters into harmless particles form performed by living microorganism inclusion to raw wastewater. These living organisms feed on the soluble organic substances of the incoming wastewater and convert them to cell mass, carbon dioxide, and energy. Many types of living organisms are utilized in the activated sludge process. The microorganisms are mainly composed of aerobic bacteria, together with a substantial amount of fungi, protozoa and some other microbes (Bhargava, 2016). Microorganisms are divided into five main groups in the aeration tank (Theobald, 2014).

1. Bacteria
2. Protozoa
3. Filamentous bacteria

4. Metazoa
5. Fungi and algae

The population of microorganisms mainly consist of **aerobic bacteria**. Bacteria is a kind of organism that has a single cell, and it reproduces by the division of a single cell to the two new cells. They feed on organic nutrients in wastewater, and this process occurs with the presence of oxygen. The growth rate of bacteria in wastewater decreases with food consumption. **Protozoa** generally need oxygen to remove suspended particles and dispersed bacteria. However, some types of protozoa perform treatment process without an oxygen supply. This group of microorganisms helps to clarify the wastewater effluent. Also, five types of protozoa are known, and Figure 2.2 indicates them.

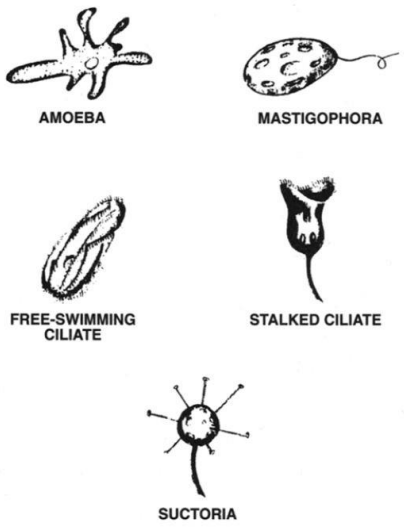

Figure 2.2: Types of Protozoa
(Pennsylvania Department of Environmental Protection, 2014).

Filamentous bacteria forms filaments that can be classified as long and short. It is a specific kind of bacterial growth in the activated sludge process. The operational condition has a considerable impact on filamentous bacteria development. Long filaments support the flocculation of bacteria to a certain extent. However, an excess number of filaments lead to bulking sludge creation. This bulking sludge is the reason for poor settling and turbidity in the tank.

On the other hand, short filaments can cause foaming in the aeration basin. **Metazoa** does not have an essential contribution to wastewater treatment. Metazoa consist of many cells, and they help to clarify effluent. **Fungi and algae** might affect the pH of

wastewater, but they usually do not create any problem in the activated sludge process.

The mixture of microorganisms characterized as activated sludge and “active” term comes from the living organism content of the sludge. The biochemical conversion of pollutants occurs in three distinct steps (State of Maine Department of Environmental Protection, 2009).

1. Transfer step
2. Conversion step
3. Flocculation step

Figure 2.3 illustrates the transformation of particles into several end products by means of a bacteria cell. Initially, the pollutants or food particles for bacterial cells contact with the slime layer. This layer is also called as a protection layer of the cell. After passing through the protection layer, the food particles reach the cell membrane. The absorption of soluble organic particles into a bacterial cell takes place by the use of cell membrane, and they are the source of direct food. On the other hand, some insoluble organic matters are not able to directly pass through the cell membrane. These matters are adsorbed onto the cell membrane and broken into pieces. In order to transport the non-diffusible particulate into the cell, an enzyme is produced by the cell. The enzyme moves through the cell membrane and attached to the particulate. The solubilized particulate can be easily transported into the cell.

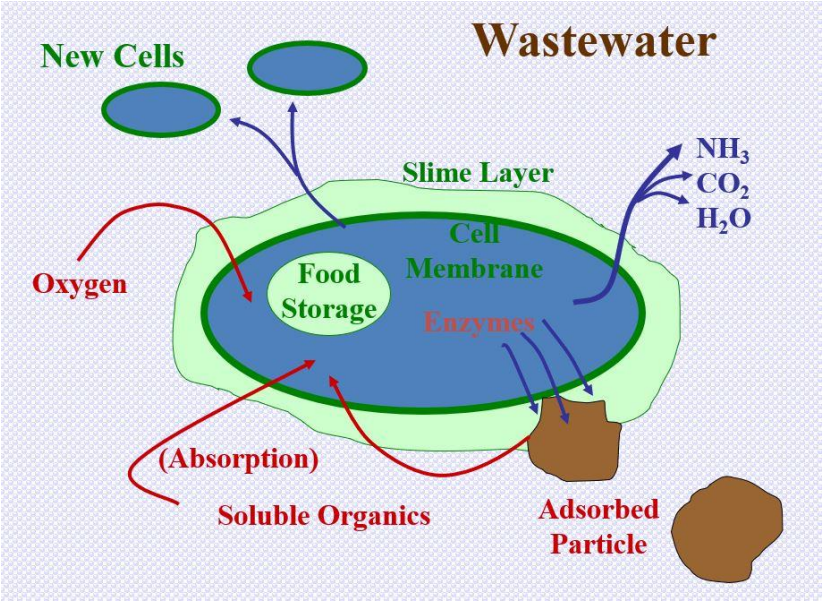

Figure 2.3: Biochemical transformation pathways in a bacterial cell (State of Maine Department of Environmental Protection, 2009).

The enzyme treats like a catalyst and detaches the food in the interior of the cell. Then, it continues to the same process for remaining particulates on the cell membrane. Finally, the transfer step is completed.

Afterward, all the foods that are inside the cell converted to end products in the conversion step. The process in the second step is also known as the metabolic process. Metabolism is a process in which some molecules are broken while others are formed with several series reactions. Since two types of processes obtain the products, metabolism is divided into two parts. The first one, anabolism, describes the synthesis process of compounds. The latter reaction, so-called catabolism, involves the breaking of compounds. Accordingly, the metabolic process contains oxidation and synthesis reactions.

The energy supply and carbon are two necessary factors for the reproduction and growth of a cell. Bacteria can store energy in the chemical bonds of the compounds. Respiration is a process that produces utilizable energy from high energy compounds. The redox reaction mechanism occurs during the respiration process. Some portions of the organic matters are oxidized to supply the process with an energy source. Also, some of them are synthesized to new cells, and these cells take part in a subsequent oxidation reaction.

Oxidation

$$\underset{\text{matter}}{\text{Organic}} + O_2 \xrightarrow{\text{microorganisms}} CO_2 + H_2O + NH_3 + \text{energy} + \underset{\text{end products}}{\text{other}}$$

Synthesis

$$\underset{\text{matter}}{\text{Organic}} + O_2 + \text{nutrients} \xrightarrow{\text{microorganisms}} \underset{\text{bacterial cell}}{\text{new}} + CO_2 + H_2O + \underset{\text{end products}}{\text{other}}$$

Endogenous Respiration

$$\underset{\text{bacterial cell}}{\text{new}} + O_2 \xrightarrow{\text{microorganisms}} CO_2 + H_2O + \text{nutrients} + \text{energy}$$

After completing the conversion step, the flocculation, which is the third step of biochemical transformation, occurs. A single bacterium behaves like colloidal solids and is suspended in the wastewater treatment tank. One of the primary desired characteristics of bacteria is to create solid form residues inside wastewater. They are known as floc-forming bacteria in the literature (Grady, et al., 1999). These solid particles or flocs make the separation process more convenient by settling out and

allow achieving high-quality effluent at the end of the third step. The flocculation occurs when individual bacteria cells contact one another during the mixing process. Slime layer of each cell is the promoter for the flocculation process which enables the sticking of microorganisms. Aging and death are common characteristics of living organisms that play an essential role in the treatment process. Aging of a cell in the sludge is the reason for the break-up of flocs and abundance of old cells obstructs the floc-forming process. A new cell attaches to the floc when the death one detaches. In order to achieve the required effluent quality, the proportion of floc-forming and filamentous bacteria must be carefully controlled.

On the other hand, bacteria grow fast in a low age sludge which means that the surface area of bacteria develops continuously. It prevents the formation of a good slime layer to cover a cell and a low-density floc is formed. The density and size of the floc are very useful factors for efficient treatment.

Extended aeration activated sludge (EAAS) plants used to remove wastes that come from both domestic and industrial applications. High treatment efficiency is one of the main advantages of the EAAS process. The majority of pollutants are aerobically digested via an extended aeration period. Hence, the waste activated sludge disposal sections are generally neglected in this plant (Mc.Carty & Brodersen, 1962). Air supply duration to the wastewater is more than 18 hours in the aeration basin. Also, the primary sedimentation tank is omitted due to longer aeration time. The solid retention time (SRT) is typically between the range of 20 - 30 days (Grady, et al., 1999). Since solid retention time is too much, large bioreactors are more suitable for the extended aeration process. However, to achieve a well-mixing condition in a large bioreactor is quite difficult for the EAAS plant. Air may be injected by the surface or diffusion aeration methods. Mechanical mixing is necessary to maintain uniform distribution of MLSS concentration throughout the aeration tank. Energy consumption is high in comparison with other variations of activated sludge processes. Closed-loop reactors replace the EAAS large bioreactors to cope with mixing limitations. This configuration is another effective variation of the AS process. This variation is known as the oxidation ditch activated sludge process.

Sequencing batch reactors (SBR) is known as a fill-and-draw activated sludge system (EPA, 1999). All the sequences of treatment steps are performed in a single tank. These steps involve equalization, aeration, and clarification processes. The influent fed to the operation tank in which harmful components are removed, treated and effluent is discharged. The same processes occur in SBR and conventional activated

sludge in principle. However, all unit processes of conventional activated sludge plants are carried out in separate operation tanks.

There are five treatment process steps in a single tank of SBR system. Figure 2.4 describes all these steps in a regular turn.

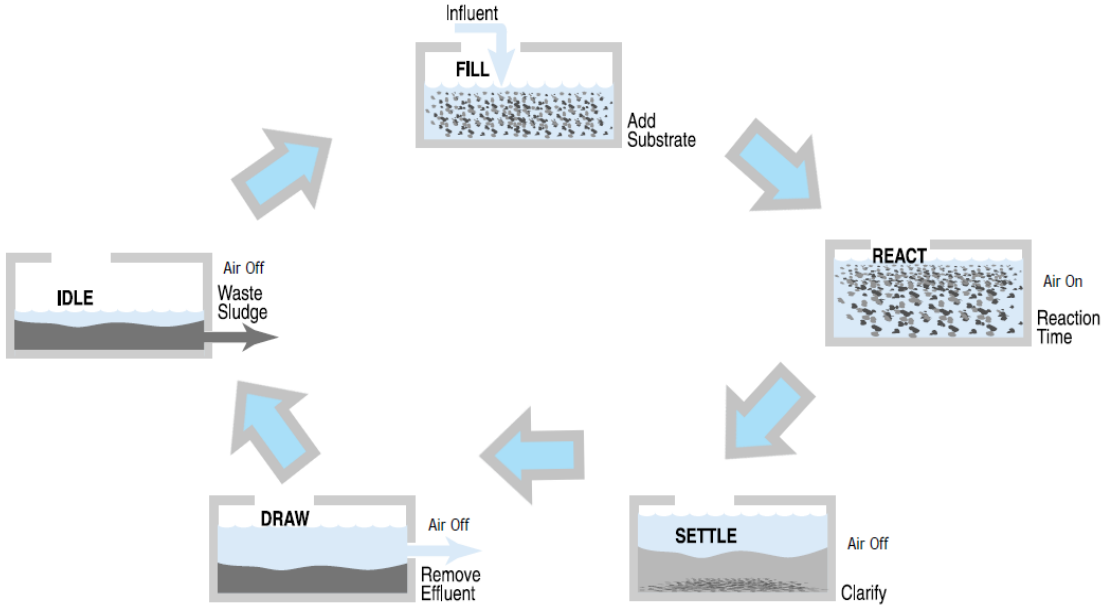

Figure 2.4: Typical SBR process cycle.

The SBR tank receives influent wastewater in the first step. Air supply and mechanical agitation are usually omitted during the fill phase. However, mixing-fill phase and aerated-fill phase options are performed due to carry out different treatment purposes. For example, the tank is in an anoxic environment during the mixing-fill phase, and this option is favorable for denitrification process. In the reaction step, air supply and mixers are active. Wastewater does not anymore enter the basin. The biochemical conversion mechanism occurs in this phase, and the majority of pollutants are removed. In the settle phase, mechanical mixing and aeration operation remain off. Also, there is no inflow to the tank. Flocculants settle to the bottom of tanks and distinctive interphase formed. This step is followed by the draw or decant phase in which the discharge valve is open and clear effluent is removed from the basin. During the idle phase, a small amount of WAS is pumped out of the system, and a new operation cycle starts.

High purity oxygen Activated Sludge (HPOAC) is a process in which oxygen is used instead of air with approximately 98% purity. High purity oxygen supply improves the

performance of the oxygen transfer rate in the bioreactor and oxygen transfer rate performance is better than other systems with air supply. Furthermore, the bioreactor is composed of different stages, and influents are added to the system with a co-current flow configuration. Oxygen, RAS, and wastewater are only added to the first stage in which efficient mixing operation occurs. The number of steps is flexible and the typical range is between 3 or 4, but up to 6 stages are possible in the industry (Grady, et al., 1999). Well-mixing is a necessary part of each stage and a variety of options are used to enhance the mixing process. Mechanical equipment, such as surface submerged propeller or slow speed surface aerators are typical mixing devices for the HPOAC process. Retention time is 1 or 2 days, but the quality of the wastewater might affect the treatment process and long retention time must be provided. The system requires not too large bioreactor because of the higher volumetric oxygen transfer rate in the process. Figure 2.5 shows a simplified schematic of the HPO activated sludge process.

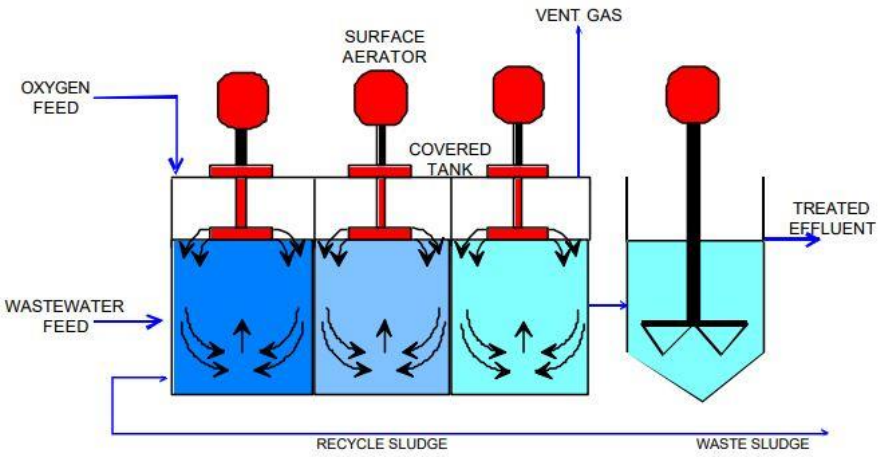

Figure 2.5: Typical HPO activated sludge process with three stages (Morin & Gilligan).

The last stage of bioreactor vented out the gaseous substances from the system. The composition of the vent stream is unreacted oxygen, carbon dioxide, etc. The secondary clarifier required to accomplish treatment operation as usual. The latest generation of HPO activated sludge process is able to incorporate the anoxic stage for denitrification and anaerobic stage for phosphorous removal.

2.2.2 Oxidation Ditch Process

Oxidation ditch (OD) process is the special form of extended aeration activated sludge process and it is one of the most useful biological purification methods with relatively low capital costs. The process has been developed in the middle of the last century and was initially designed for small scale purposes (Nelsen, et al., 1984). Afterward, the OD process has evolved worldwide because of lower construction costs, consistently high effluent quality, and relatively inexpensive maintenance costs. However, the application of the OD process for larger municipal and industrial wastewater treatment purposes brought some problems like ineffective aeration, insufficient mixed liquor velocity, and detention time. In order to overcome these challenges, a variety of ways has been developed. OD processes are classified into two types due to the shape of oxidation basins, Pasveer- and Carrousel-type (Sperling, 2007). Figure 2.6 a) and b) shows both types of oxidation ditches, Pasveer- and Carrousel-type, respectively.

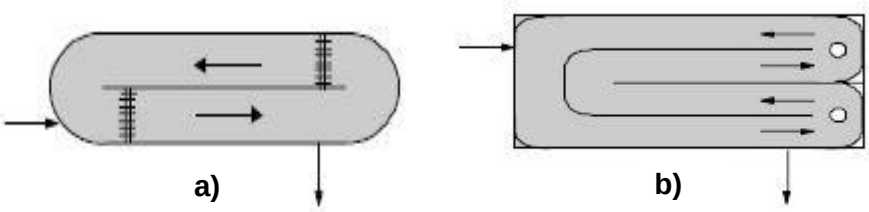

Figure 2.6: a) Pasveer-type oxidation ditch b) Carrousel-type oxidation ditch (Sperling, 2007).

The Pasveer-type oxidation ditch is an oblong-shaped basin in which mixed liquor circulates with relatively high speed. The wall divides the basin into two channels that look like in appearance to a racetrack. Different aeration devices are known for oxidation ditches. Horizontal shaft aerators, such as “brush rotor” aerators used not only for aeration purposes but also to provide horizontal liquid velocity throughout Pasveer-type oxidation ditches (Jern, 2006).

On the other hand, the Carrousel system is another type of oxidation ditch and consists of concrete tanks designed one inside the others. It uses vertical shaft aeration devices differently from the Pasveer-type system. The geometrical shape of both systems contributes to the developing flow pattern of mixed liquor. As a result, wastewater treatment efficiency is increasing. Mostly, oxidation basins are closed-loop bioreactors with various shapes such as circular, square, and oblong. Oval

shaped tanks are industrially preferred since they help the circulation of flow and maintain the solid particles in suspension.

Meanwhile, the multi-channel configuration of the tank helps to obtain the required bulk flow conditions. As a result, the microorganisms in mixed liquor are contacted with the incoming flow through the circulation process. Also, semi-circular inner walls are applied around the internal wall for further improvement of geometry. They are slightly decentralized relative to the interior wall for developing mixed liquor velocity. A wide part of the semi-circular wall accepts more liquid while narrow one discharge liquid with high speed. This kind of configuration cause to effective circulation process. Moreover, the circulation process entrains oxygen bubbles and stimulate biochemical reactions in the whole tank. Typically, when “brush rotor” aeration device is used, shallow liquid depth is preferential to avoid non-aerated zones at the bottom of a basin.

In general, the OD system is operated as a continuous or intermittent process. The factors that affect the operation type are the inflow rate, tank capacity, and unfavorable environmental temperature (Portella, 2013). The mixing regime in the oxidation ditches characterized as plug-flow and complete-mix behavior (Sperling, 2007). The complete-mix behavior pertains to most of the variables, such as suspended solids and biochemical oxygen demand (BOD), whereas the plug-flow behavior observed for a variable with a fast dynamic. For example, dissolved oxygen has a concentration gradient when the mixed liquor circulates along the ditch. The concentration of dissolved oxygen is high in the aeration zone and starts to quick decrease when the mixed liquor flows away from the aeration region. It shows that oxygen is rapidly consumed due to fast reaction kinetics up to reach another aeration one. Regarding the variables with slow dynamics, the concentration profile is more or less same along the oxidation ditch. Accordingly, hydraulic behavior approaches to the complete-mix regime in this condition.

The performance of OD system depends to a great extent on the overall flow pattern. In order to achieve an effective biological wastewater treatment, mixing and aeration play a significant role in the oxidation ditches.

Aeration Process: The main aeration devices in the aerobic processes are mechanical surface aerators, diffused-air systems, and high-purity oxygen diffusers. In principle, a mechanical aeration system contains brushes or discs mounted on the shaft, and mechanical agitation of wastewater splashes liquid droplets to surrounding

where these droplets contacted with air from the atmosphere. On the other hand, for the diffuser system, air is supplied through blowers and piping system to the bottom of basins where diffusers are located. Diffused-air system includes blowers, supply pipes, and particular types of diffusers, while mechanical aeration system is a simple device with brushes mounted on the horizontal or vertical shaft.

Mechanical aerators are divided into two groups based on their design and features (Tchobanoglous, et al., 2006). They are aerators with a horizontal and vertical axis. Both take air from the atmosphere by splashing liquid in the ditches. Surface aerators with the horizontal axis are usually used in the oblong shape oxidation ditches. There are two kinds of surface aerators which are based on their configuration. The brush-type aeration devices, also known as a Kessener brush, are composed of numerous bristles which are mounted on a horizontal cylinder. This device is partially submerged in the wastewater. An electric motor drive used to rotate a horizontal cylinder with a certain speed, and the bristles spray liquid droplets above the liquid surface. Nowadays, blades and discs are used instead of bristles as well. The brush-type and disc aerators are illustrated in Figure 2.7.

Figure 2.7: Brush aerator (left) and Disc aerator (right) (wateronline.com).

Apart from the aeration process, mechanical surface aerators promote to circulation process across the tank to keep solid particles suspended in the mixed liquor. In addition, the circulation of liquid with certain velocity entrains air in the wastewater. It helps to distribute oxygen molecules in the ditches uniformly.

The diffused-air system is classified according to the physical characteristics of diffusers which produce bubbles with different diameters. The diffusers are submerged in the liquid and air bubbles can be introduced to the wastewater as fine bubbles or coarse bubbles (Tchobanoglous, et al., 2006).

The air diffusion systems are divided into three groups according to the porosity of the diffusers and produced bubble size (Sperling, 2007):

- porous diffusers
- non-porous diffusers
- other diffusion devices: jet aerators, aspirating aerators and U-tube aerators.

The porous diffusers, also known as fine bubble and medium bubble diffusers, have various forms that are used in the aeration process. They are disc, dome, membrane, and plate type air diffusers. The materials used in the manufacture of the porous diffusers are ceramics, flexible membranes, or plastics. Apart from plate-type diffusers, all other three types of diffusers are more preferred in recent years since plates are relatively expensive and difficult to maintain. Disc and dome diffusers are typically installed in a grid pattern on the bottom of oxidation ditches to provide uniform aeration. They are mounted on air manifolds which run the length of the tanks. It is quite essential to supply air manifolds with clean compressed air which avoids clogging of tiny pores of diffusers. The clean air supply protects not only the diffusers but also improves the performance of the aerobic treatment process.

Regarding the diameters of the bubbles, Table 2.1 shows the appropriate sizes for fine, medium, and coarse bubble terms.

Table 2.1: Bubble diameters (Sperling, 2007).

Fine bubble	diameter less than 3 mm
Medium bubble	diameter between 3 mm and 6 mm
Coarse bubble	diameter greater than 6 mm

There are several types of non-porous diffusers used to aerate the basins. The non-porous diffusers produce greater bubbles than porous diffusers. The maintenance cost of the non-porous diffusers is lower than the porous one in which tiny pores have a tendency to clog. The orifice and tube diffusers are the two main forms of the non-porous diffusion system that applied in aeration tanks. The main forms of both types of diffusers are shown below in Figure 2.8.

Figure 2.8: Porous (a,b) and non-porous(c) diffusers (xylem.com).

The other air diffusion systems are available in the industry, such as jet aerators, aspirator aerators, and U-tube aerators. A jet aeration system is mainly used for deep aeration tanks in which liquid depth is greater than 8 m (Tchobanoglous, et al., 2006). The working principle of the device based on the pumping of the liquid with air diffusion. The pumping process circulates the fluid in the aeration tank with compressed air.

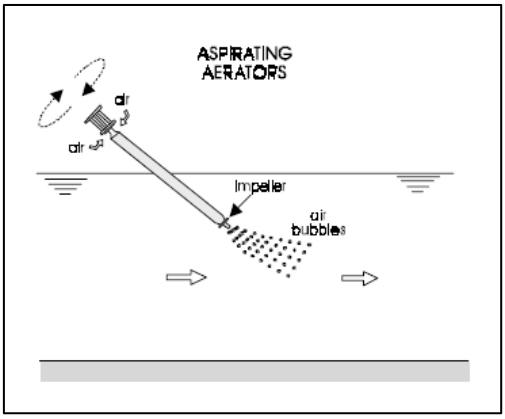

Figure 2.9: Air diffusion by aspirating aerator.

The aspirator aerators have an electric-driven motor that rotates outside of the liquid, and air is drawn through a hollow tube via pumps and injected into the system. The injected air is diffused by means of propellers and circulates along the aeration basin. The schematic of air diffusion by aspirator aerator is presented in Figure 2.9.

The efficiency of aeration process plays a vital role in wastewater treatment plants from many aspects. From an energy consumption point of view, the aeration system consumes approximately 50 to 65 percent of the total energy requirement of the activated sludge process plant (Pipeline, 2003). Apart from energy expenses, oxygen transfer efficiency is significant in achieving effective wastewater treatment. The type, shape, and size of aerator devices influence the efficiency of oxygen transfer. Meanwhile, many other factors, including wastewater characteristics, wastewater

depth, the geometry of oxidation ditches, and the rate of air inflow must be considered for efficient oxygen transfer. As an example, mechanical aerators are not recommended for processes where liquid depth is high. Since the bottom of the tank is not uniformly aerated in this case. Therefore, air injection from the bottom of the tank is more beneficial. The term oxygen transfer efficiency (OTE) is defined as the ratio between the amount of oxygen transferred from air bubbles to mixed liquor and the total amount of oxygen supplied to the aeration device. In order to compare the performance of different aeration devices, OTE is measured under standard conditions. The oxygen transfer measured under standard conditions is referred to as standard oxygen transfer efficiency (SOTE). The comparison of standard conditions and operating conditions in the aeration process are summarized in Table 2.2.

Table 2.2: Standard and Operating conditions (Sperling, 2007).

Standard Conditions	Operating conditions
clean water	wastewater
liquid temperature; $T_L = 20℃$	real liquid temperature
altitude; $h = 0\ m$ (sea level)	real altitude of the plant
aeration system installed in a test tank	aeration system installed in a real tank

In a diffused-air system, internal clogging occurs when compressed air impurities pass through the filter. Internal clogging is another reason for low OTE in the oxidation ditches. Also, external fouling happens due to the inorganic precipitants and the growth of bacteria on the surface of porous media. Regular maintenance required to keep the aeration efficiency high.

The term that gives an idea regarding energy consumption is standard aeration efficiency (SAE) or oxygenation efficiency. The standard aeration efficiency is the standard oxygen transfer rate (SOTR) (kg O_2/h) per unit power consumed (kW). The expression in equation 2.2.1 with the unit of kg O_2/kWh (Sperling, 2007).

$$\mathrm{SAE} = \frac{\mathrm{SOTR}}{\mathrm{Power}} \tag{2.2.1}$$

In general, the oxygen transfer efficiency is higher for fine bubble diffusers. By decreasing the size of bubbles, the number of bubbles and also the total surface area for gas transfer is increasing which means greater oxygen transfer. Also, quite high air flowrate may decrease the oxygen transfer rate by increasing circulating velocities.

Besides, spiral flows are observed in the basin and cause short residence time of air bubbles which is undesired from an efficiency point of view. The various types of aeration devices and their efficiency ranges are given in Table 2.3.

Table 2.3: Aeration devices and SAE ranges (Tchobanoglous, et al., 2006).

Type	SAE ($\mathbf{kg\ O_2/kWh}$)
Low-speed surface aerators	1.5 - 2.1
High-speed surface aerators	1.1 - 1.4
Jet aerators	0.9 – 1.4
Fine bubble diffusers (Disc-type)	2 - 7

The efficiency of oxygen transfer in fine bubble diffusers may vary depending on some factors. The main three factors that have a considerable impact on the efficiency term are:

- liquid depth
- density of diffusers
- flux of diffusers

The retention time of air bubbles is increasing in the fine bubble system with liquid depth. As a result, higher oxygen transfer efficiency is obtained by keeping air bubbles longer time in the liquid. Bubble retention time is not only the function of liquid depth. The spiral flows have a negative effect on it, and this kind of flow is almost observed in all fine bubble systems. In order to alleviate the spiral flow effects, diffuser density on the floor of the tank must be increased. The density of diffusers is mathematically defined as the ratio of floor area covered with diffusers to the whole floor area of a tank. For the sake of clarity, Figure 2.10 describes the difference between the densely installed diffuser and sparse configuration.

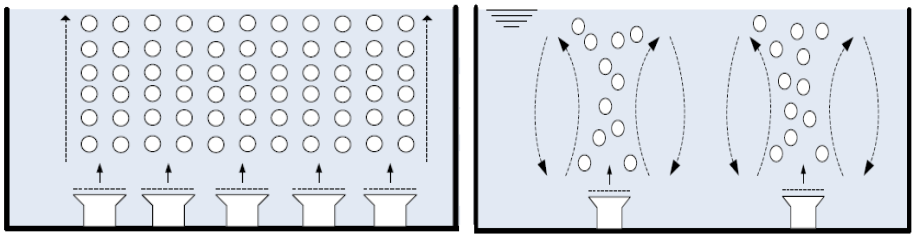

Figure 2.10: High density (left) and low density (right) fine bubble diffuser configuration (John Lindam, 2014).

Low-density diffuser configuration is the primary reason for spiral flows in the aeration basins as illustrated in the scheme. Air bubbles quickly rise within reactors and affect the overall process efficiency as well.

The third one, diffuser flux, is related to the density of the diffuser system in the oxidation ditches. Diffuser flux is the ratio of the amount of flow that passes from unit membrane area. If high-density diffusers installed on the bottom of the tank, the diffuser flux is relatively low. Accordingly, using densely connected fine bubble diffusers improve oxygen transfer rate, and also decrease flux term. It means that the rising velocity of air bubbles is slower in the liquid media. Meanwhile, the development of the efficiency term allows optimizing air flowrate to keep the desired value for oxygen concentration. According to the study in 1982, total air requirements decrease by 40% when the coarse bubble diffusers replaced with the fine bubble diffusers in the wastewater treatment plant (EPA, 1999). The relationship between all these parameters ends up with lower energy consumption which is the main target in the biological wastewater treatment plants.

Mixing process: Besides of aeration process in the oxidation ditches, the completely mixed condition is another requirement for biochemical reactions. Typically, the layout of a diffused-air system does not fully cover the floor of large oblong-shaped tanks, and air bubbles are not uniformly distributed in the non-aeration zone. Application of low speed submerged mixing devices generates thrust which pushes the fluid and circulating it throughout the tank. These mixing devices are commonly known as agitators or flowmakers in wastewater treatment plants. Agitators can be horizontally or vertically oriented in the aeration basins. For rectangular tanks with rounded ends, a horizontal configuration is applied. Therefore, the primary advantage of the flowmaker is to produce horizontal bulk flow with a certain velocity. The typical horizontal flow velocity is approximately 0.3 m/s to keep the mixed liquor in a homogeneous mixture (Grady, et al., 1999). Also, air bubbles considerably contribute to maintaining the liquid as suspension. However, air bubbles create a circulation zone which has a detrimental effect on the operation by reducing bubble retention time. Another benefit of submerged flowmakers is to defeat spiral flows by creating sufficient horizontal bulk flow. The performance of agitators must be carefully monitored to extend equipment life. The correct positioning of mixing devices and liquid forces on the blades are some critical parameters that need more attention in process design. When the agitator position is not chosen correctly, mechanical damage to the equipment is unavoidable because of forces on the blades, backflow, etc.

High-density fine bubble diffusers not only improve the efficiency of oxygen transfer and aeration process but also promote to use the flowmakers with lower thrust requirements. It is related to the amount of air flowrate that enters the system. When a higher amount of air supplied, bubble plumes become a barrier for agitator and quite high thrust values required to ensure certain horizontal flow velocity. It states that power consumption will be quite high in this condition.

On the other hand, oxidation ditches with mechanical aeration devices take advantage of them to generate bulk flow and obtain minimum horizontal circulation velocity. However, maintenance costs for the mechanical parts are relatively high when it is compared to diffused-air systems.

Operation: The organic components that must be removed in wastewater are various forms of phosphorus and nitrogen compounds. Some of the primary compounds are organic nitrogen, ammonia or ammonium, nitrite, and nitrate. In order to remove all these contaminants, the oxidation ditches can be operated in numerous conditions. The operation principles of an oxidation ditch system may vary because of the characteristics of pollutants in wastewater. Depending on the type of organic components needs to be removed, treatment zones are classified as:

- Anaerobic
- Anoxic
- Aerobic

There is an additional small rectangular tank attached to the oxidation ditches. The anaerobic biochemical process occurs in this tank which also accepts return activated sludge from secondary clarifiers. Anaerobic condition refers to that no free oxygen molecules present in the tank environment. Therefore, bacteria consume the organic substances in which oxygen is found. The removal of phosphorous happens in this tank. Phosphorous-oxygen components are feed for hungry bacteria, and they start to release phosphorous while keeping oxygen molecules into their cells because of oxygen deficit. By this mechanism, the removal of phosphorus content realized.
Both anoxic and aerobic processes may take place within the oxidation ditches. Otherwise, particular wastewater basins are used for anoxic process purposes. The most abundant nitrogen-based compound is usually ammonia or ammonium and organic nitrogen in wastewater. Ammonia often ionized to ammonium in aqueous solution. However, in wastewater treatment pH value is a significant parameter that

defines ammonia and ammonium content. Ammonium is favored in acidic solutions, and typical wastewater pH range between 6 and 9 (Peng & Zhu, 2006).
For this reason, approximately all of ammonium gases present in an ionized form in wastewater. Aeration process is necessary to transform ammonia into nitrogen and hydrogen molecules. This is called the nitrification process. The sequence of the nitrification process is represented below.

$$\underbrace{NH_4^+}_{\text{Ammonium}} \rightarrow \underbrace{NO_2^-}_{\text{Nitrite}} \rightarrow \underbrace{NO_3^-}_{\text{Nitrate}}$$

The nitrification steps are accomplished by particular autotrophic bacteria. Autotrophic and heterotrophic are two kinds of bacteria. Autotrophs usually consume inorganic substances while heterotrophs take organic materials as food. Autotrophic bacteria are also known as nitrifiers. Nitrifiers eat up dissolved oxygen to achieve nitrification. The growth rate of autotrophs is increasing at a warm temperature and high dissolved oxygen concentrations. If dissolved oxygen is not enough in wastewater, nitrifiers become inactive which means an unsuccessful nitrification process. The following reaction mechanisms describe the nitrification process (Sperling, 2007):

$$NH_4^+ + O_2 + \text{nitrifying bacteria} \rightarrow H^+ + H_2O + NO_2^- + \text{energy}$$

$$NO_2^- + O_2 + \text{nitrifying bacteria} \rightarrow NO_3^- + \text{energy}$$

In general, oxidation ditches are aerobic basins, but the process is operated as an anoxic condition by simply turning off air injection. Also, the multi-channel configuration of ditches allows working in aerobic and anoxic environments because of the fast consumption rate of dissolved oxygen. It is called anoxic because the number of free oxygen molecules is too low. When mixed liquor flows to the non-aerated zone, dissolved oxygen concentration decreases quickly. In contradiction to nitrification, the process in the anoxic zone known as denitrification. Denitrification mechanism is shown below.

$$BOD + NO_3^- + \text{denitrifying bacteria} \rightarrow N_2 + OH^- + \text{energy}$$

The mechanism is related to extract oxygen molecules of nitrites or nitrates and convert them into free nitrogen gases employing heterotrophic bacteria. Then, nitrogen is released to the atmosphere as a byproduct.

Chapter 3

Computational Fluid Dynamics

3.1 Fundamentals of CFD

Computational Fluid Dynamics is a computer-based tool that solves the governing equations of fluid flow for simulating hydrodynamic behavior of a system. The motion of a fluid is described by a set of five partial differential equations that represent the mathematical statement of conservation law of physics (Versteeg & Malalasekera, 2007).

Conservation of mass equation: The derivation of the equation is based on the mass balance in a fluid element and described as the equality between the rate of increase of mass in fluid element and the net rate of flow of mass into fluid element.

$$\frac{\partial \rho}{\partial t} + \frac{\partial (\rho u_i)}{\partial x_i} = 0 \qquad (3.1.1)$$

or without Cartesian tensor notation,

$$\frac{\partial \rho}{\partial t} + \frac{\partial (\rho u)}{\partial x} + \frac{\partial (\rho v)}{\partial y} + \frac{\partial (\rho w)}{\partial z} = 0. \qquad (3.1.2)$$

Conservation of momentum equation: Newton's second law states that the rate of change of momentum of a fluid particle equals the sum of the forces on the particle.

$$\frac{\partial \rho u_j}{\partial t} + \frac{\partial (\rho u_i u_j)}{\partial x_i} = \frac{\partial \tau_{ij}}{\partial x_i} + \rho B_j \quad i, j = 1,2,3 \qquad (3.1.3)$$

The right-hand side of equation (3.1.3) is expressed as a contribution of two kinds of forces on a fluid element, surface forces and body forces. Both forces are the representative of source term for momentum balance equation based on Newton's second law. (L.S.Caretto, 2009)

Conservation of energy equation: The energy equation is derived from the first law of thermodynamics, which states that the rate of change of energy of a fluid particle is equal to the rate of heat addition to the fluid particle plus the rate of work done on the particle:

$$\frac{\partial (\rho e)}{\partial t} + \frac{\partial (\rho u_i e)}{\partial x_i} = -\frac{\partial q_i}{\partial x_i} + \frac{\partial u_i \tau_{ij}}{\partial x_i} + \rho u_i B_j. \qquad (3.1.4)$$

All these equations have a similar form and can be generalized as

$$\frac{\partial(\rho\varphi)}{\partial t} + \mathrm{div}(\rho\varphi u) = \mathrm{div}(\Gamma\nabla\varphi) + S_{\varphi} \qquad (3.1.5)$$

or in Cartesian tensor form

$$\underbrace{\frac{\partial(\rho\varphi)}{\partial t}}_{\text{Accumulation term}} + \underbrace{\frac{\partial(\rho\varphi u_i)}{\partial x_i}}_{\text{Convective term}} = \underbrace{\frac{\partial}{\partial x_i}\left(\Gamma\frac{\partial\varphi}{\partial x_i}\right)}_{\text{Diffusive term}} + \underbrace{S}_{\text{Source term}} \qquad (3.1.6)$$

where t is time [s], ρ is the density of a fluid $[kg/m^3]$, x_i is the length in dimension i, u_i is the velocity [m/s] in the direction i, and φ is the variable of flow. The quantities Γ and S represent the diffusion coefficient and the source term, respectively.

Equation (3.1.6) is comprised of four different terms, and this equation is known as a general differential equation for the property φ. The dependent variable φ represents the velocities of the momentum equation (u, v, w) or the temperature (T) of the energy equation. Mass conservation equation is obtained from the general differential equation by applying φ=1. All these are non-linear differential equations and cannot be solved analytically. These equations are linearized and solved in numerous small control volumes by means of advanced numerical tools.

The surface forces on a fluid particle are distinguished two types, pressure and viscous forces. In order to obtain the most useful form of momentum conservation equation for fluid flows, introducing a suitable model for viscous stresses is necessary. The resultant conservation equations are known as Navier-Stokes equations.

$$\frac{\partial\rho u_j}{\partial t} + \frac{\partial(\rho u_i u_j)}{\partial x_i} = -\frac{\partial P}{\partial x_j} + \frac{\partial}{\partial x_i}\left(\mu\frac{\partial u_i}{\partial x_i}\right) + \rho B_j \qquad (3.1.7)$$

For an incompressible fluid, the governing equations without Cartesian tensor can be summarized as follow:

Continuity

$$\frac{\partial u}{\partial x} + \frac{\partial v}{\partial y} + \frac{\partial w}{\partial z} = 0 \qquad (3.1.8)$$

Momentum

$$\rho\left(\frac{\partial u}{\partial t}+u\frac{\partial u}{\partial x}+v\frac{\partial u}{\partial y}+w\frac{\partial u}{\partial z}\right)=-\frac{\partial P}{\partial x}+\mu\left(\frac{\partial^2 u}{\partial x^2}+\frac{\partial^2 u}{\partial y^2}+\frac{\partial^2 u}{\partial z^2}\right)+\rho B_x$$
$$\rho\left(\frac{\partial v}{\partial t}+u\frac{\partial v}{\partial x}+v\frac{\partial v}{\partial y}+w\frac{\partial v}{\partial z}\right)=-\frac{\partial P}{\partial x}+\mu\left(\frac{\partial^2 v}{\partial x^2}+\frac{\partial^2 v}{\partial y^2}+\frac{\partial^2 v}{\partial z^2}\right)+\rho B_y \qquad (3.1.9)$$
$$\rho\left(\frac{\partial w}{\partial t}+u\frac{\partial w}{\partial x}+v\frac{\partial w}{\partial y}+w\frac{\partial w}{\partial z}\right)=-\frac{\partial P}{\partial x}+\mu\left(\frac{\partial^2 w}{\partial x^2}+\frac{\partial^2 w}{\partial y^2}+\frac{\partial^2 w}{\partial z^2}\right)+\rho B_z$$

Energy

Equation (3.1.4) is the total energy balance equation that comprises of internal and kinetic energy. Many different forms of the energy equation are exist and used in practice by substituting other thermodynamic properties such as enthalpy and temperature instead of internal energy (L.S.Caretto, 2009). However, the energy equation must be considered if any thermal interaction is available in an examined system. In this study, the variation of temperature is quite small, and heat transfer is not a point of interest.

3.2 Turbulence Modelling

Turbulent flow is more common to see in many industrial applications because it intensifies mass and heat transfer rates. The chaotic behavior and irregularity are the main features of turbulent flow. As a consequence, a wide range of length scale, velocity scale and timescales of turbulence are observed. Turbulence eddies encountered in turbulent motions due to irregular and unstable flow characteristics. The instability of the flow leads to fluctuating of instantaneous velocity with high frequency. The identification of complete turbulent flow is only possible by capturing all velocity fluctuations. It means that a considerable amount of data must be considered in turbulent flow description. As a result, turbulence simulation with a deterministic approach is a hugely challenging issue, especially on a large-scale problem (Andersson, et al., 2012). The cost of computation reduced by implementing the statistical approach in turbulence simulation. In this approach, mean flow values of turbulent flow properties used instead of all actual values in space and time.

The instantaneous flow properties decomposed to averaging and fluctuating components in the statistical approach. The instantaneous velocity decomposition into averaging and fluctuating parts described below, respectively.

$$u_i = \langle u_i \rangle + u_i' \qquad (3.2.1)$$

The average indicates mean velocity while the fluctuating one is used as a representative of turbulence. As has already been mentioned, chaotic flow behavior induces large and small turbulence eddies. During the measurement of instantaneous velocity, the fluctuation observed with high amplitude and low frequency is the result of large eddies. However, small eddies have low amplitude and high frequency. Instead of capturing small-scale high-frequency values of flow properties, they are neglected by manipulating governing equations. This method allows for reducing computation costs significantly. As a result of manipulation, additional unknown variables introduced to the governing equations. In order to define these variables, turbulence modelling is a crucial part of CFD simulation.

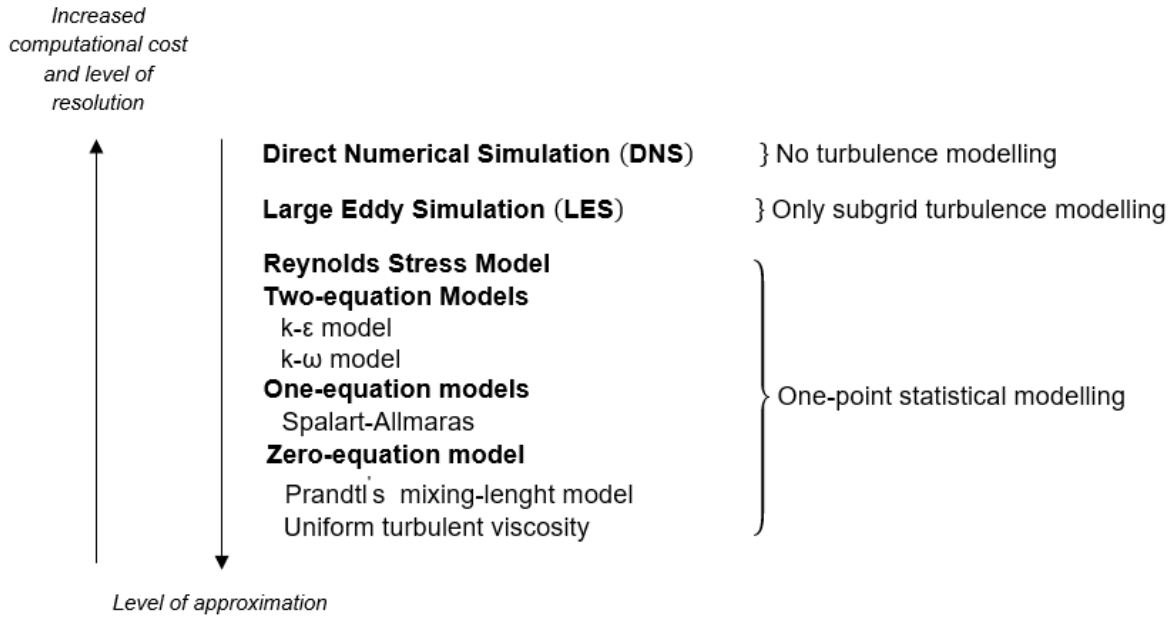

Figure 3.1 A schematic overview of turbulence modelling (Andersson, et al., 2012).

Several turbulence models exist with different level of approximations and limitations. The accuracy of turbulence simulation is inversely proportional to the approximation level.

Turbulence model with a high-level of approximation is computationally cost-effective and they are reliable models in the preliminary designing of engineering applications. The general scheme of conventional turbulence models is illustrated in Figure 3.1.

The unsteady Navier – Stokes equations are solved directly by Direct numerical simulations (DNS). Turbulence model is not a requirement for DNS. It means that all

the flow properties are considered without simplification. It is crucial to use sufficiently fine cells in computational geometry with small time steps in order to resolve all the scales of turbulence. High-Reynolds-number turbulent flows have fluctuations with a wide range of turbulence scales and complicate the direct solution of the problem. DNS implementation is limited in industrial applications, and large computational resources need to realize this simulation.

Large-eddy simulation (LES) is a relatively simple form of DNS in which small length and velocity scales of turbulent flow are not considered in the direct solution. It allows decreasing the need for excessive computational power since the smallest turbulence scales remain unsolved. The large eddies are directly resolved in the calculation, while the ones which are smaller than the cell neglected. Furthermore, LES used in engineering applications with high-Reynolds-numbers flows. The unresolved small turbulence scales modelled with subgrid stress models.

Both DNS and LES are computationally expensive and limited. Although their solutions are more precise, they are still not a common choice for routine simulations. Besides small turbulence scales, intermediate and also large ones must be filtered out to realize routine simulations. Therefore, turbulent flow modelling become simpler and favorable. A variety of turbulence models exist for routine simulations. They are based on the Reynold decomposition concept in which the statistical determination of flow property is the key point. The general illustration of the Reynold decomposition concepts for parameter φ given below.

$$\varphi = \langle\varphi\rangle + \varphi' \tag{3.2.2}$$

In equation (3.2.2) instantaneous flow properties described as a mean part and a fluctuating part, respectively. By applying this concept, turbulence fluctuations are separated in the governing equations, and different models exist to solve them.
The continuity equation for incompressible flow is

$$\frac{\partial u_i}{\partial x_i} = 0 \tag{3.2.3}$$

and the Navier-Stokes equations are

$$\frac{\partial u_i}{\partial t} + u_j \frac{\partial u_i}{\partial x_j} = -\frac{1}{\rho}\frac{\partial P}{\partial x_i} + \nu \frac{\partial^2 u_i}{\partial x_j \, \partial x_j}. \tag{3.2.4}$$

By substituting the instantaneous parameters with its components as defined in Reynold decomposition concept, and time-averaging of them result in Reynolds averaged Navier-Stokes equations.

Equation (3.2.3) and (3.2.4) can be re-written after modification as

$$\frac{\partial \langle u_i \rangle}{\partial x_i} = 0 \tag{3.2.5}$$

and

$$\frac{\partial \langle u_i \rangle}{\partial t} + \langle u_j \rangle \frac{\partial \langle u_i \rangle}{\partial x_j} = -\frac{1}{\rho}\frac{\partial \langle P \rangle}{\partial x_i} + \nu \frac{\partial^2 \langle u_i \rangle}{\partial x_j^2} - \frac{\partial \langle u_i' u_j' \rangle}{\partial x_j}. \tag{3.2.6}$$

Equation (3.2.6) is known as the general form of RANS equation. It is also written as

$$\frac{\partial \langle u_i \rangle}{\partial t} + \langle u_j \rangle \frac{\partial \langle u_i \rangle}{\partial x_j} = -\frac{1}{\rho}\frac{\partial}{\partial x_j}\left\{ \langle P \rangle \delta_{ij} + \mu \left(\frac{\partial \langle u_i \rangle}{\partial x_j} + \frac{\partial \langle u_j \rangle}{\partial x_i} \right) - \rho \langle u_i u_j \rangle \right\}. \tag{3.2.7}$$

Equation (3.2.7) looks like the original Navier-Stokes equation. There is only a difference which is the term $-\rho\langle u_i u_j \rangle$. This term is called as Reynolds stresses. By introducing Reynolds stresses into the governing equation, the total number of unknown terms increases. Thus, modelling of Reynolds stresses required to solve the RANS equations.

Figure 3.2 shows the velocity-time plot of turbulent flow and compares the turbulence models. It is clear that DNS resolves all scales in the calculation. However, LES removes small eddies and resolves large ones while the RANS approach computes mean velocities and fluctuating components must be modelled.

The concept of turbulent eddy viscosity is the method used to model Reynolds stresses. It is based on the Boussinesq approximation and eddy viscosity, ν_T, must be defined for turbulence modelling.

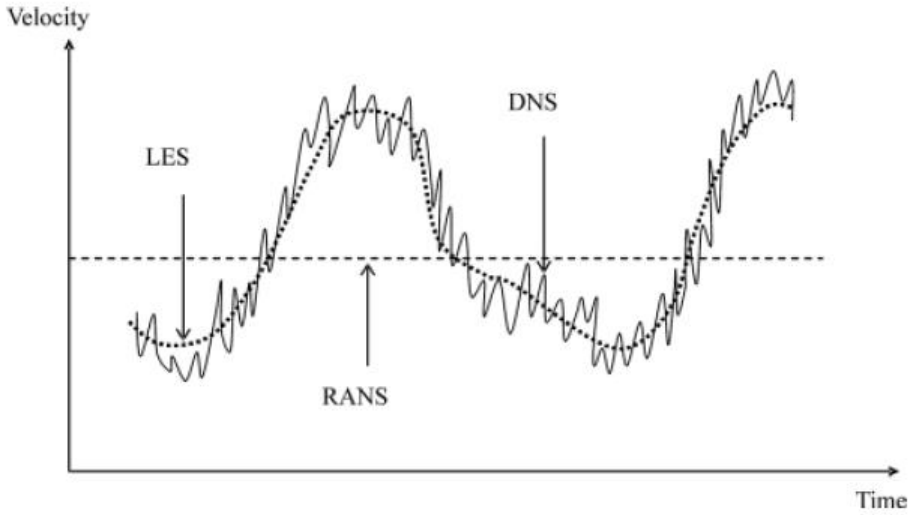

Figure 3.2: Resolved turbulence scales in a steady turbulent flow (Andersson, et al., 2012).

Turbulent eddy viscosity determined by the velocity, u, and length scales, l, of turbulence and the following expression used to compute it.

$$\nu_T = C_\nu ul \tag{3.2.8}$$

Turbulence models are classified based on the number of equations used to determine length and velocity scales of turbulent flow. In engineering applications, two-equation models are considered as the complete models in which both length and velocity scales defined by two partial differential equations (PDE). The degree of accuracy to capture turbulence related to the assumptions used in the modelling. Typically, velocity scale modelled by solving the k equation, which is the turbulent kinetic energy per unit mass, and l equation for the length scale. Also, instead of the length scale, other flow properties used. They are turbulence energy dissipation rate, ε, specific dissipation rate, ω, and frequency scale, f. All of these properties can be explicitly determined from the length scale equation.

Standard $k-\varepsilon$ model

Turbulent viscosity as a function of k and ε defined as

$$\nu_T = C_\nu \frac{k^2}{\varepsilon}. \tag{3.2.9}$$

The transport equation for turbulence kinetic energy, k, can be calculated by the following equation.

$$\frac{\partial k}{\partial t} + \langle u_j \rangle \frac{\partial k}{\partial x_j} = \nu_T \left[\left(\frac{\partial \langle u_i \rangle}{\partial x_j} + \frac{\partial \langle u_j \rangle}{\partial x_i} \right) \frac{\partial \langle u_i \rangle}{\partial x_j} \right] - \varepsilon + \frac{\partial}{\partial x_j} \left[\left(\nu + \frac{\nu_T}{\sigma_k} \right) \frac{\partial k}{\partial x_j} \right] \qquad (3.2.10)$$

σ_k is known as Prandtl-Schmidt number. Energy dissipation rate of turbulent kinetic energy must be defined to close the k transport equation. The general form of transport equation for the energy dissipation rate shown in equation (3.2.11).

$$\underbrace{\frac{\partial \varepsilon}{\partial t}}_{I} + \underbrace{\langle u_j \rangle \frac{\partial \varepsilon}{\partial x_j}}_{II} = \underbrace{C_{\varepsilon 1} \nu_T \frac{\varepsilon}{k} \left[\left(\frac{\partial \langle u_i \rangle}{\partial x_j} + \frac{\partial \langle u_j \rangle}{\partial x_i} \right) \frac{\partial \langle u_i \rangle}{\partial x_j} \right]}_{III} - \underbrace{C_{\varepsilon 2} \frac{\varepsilon^2}{k}}_{IV} + \underbrace{\frac{\partial}{\partial x_j} \left[\left(\nu + \frac{\nu_T}{\sigma_\varepsilon} \right) \frac{\partial \varepsilon}{\partial x_j} \right]}_{V} \qquad (3.2.11)$$

The terms in the equation 3.2.11 can be interpreted as follows.

I. Accumulation of ε.
II. Convection of ε via mean velocity.
III. Production of ε.
IV. Dissipation of ε.
V. Diffusion of ε.

The coefficients of above-mentioned equations are assumed to be universal and their values are given in Table 3.1

Table 3.1: Standard $k - \varepsilon$ model constants (Andersson, et al., 2012).

C_ν	$C_{\varepsilon 1}$	$C_{\varepsilon 2}$	σ_k	σ_ε
0.09	1.44	1.92	1.00	1.30

RNG $k - \varepsilon$ model

Renormalization group analysis of the transport equations is the basis of RNG $k - \varepsilon$ model. The formulation of the dissipation rate equation is different from the standard $k - \varepsilon$ model. The only physical difference is an additional source term, S_e, and the modified equation is

$$\frac{\partial \varepsilon}{\partial t} + \langle u_j \rangle \frac{\partial \varepsilon}{\partial x_j} = C_{\varepsilon 1} \nu_T \frac{\varepsilon}{k} \left[\left(\frac{\partial \langle u_i \rangle}{\partial x_j} + \frac{\partial \langle u_j \rangle}{\partial x_i} \right) \frac{\partial \langle u_i \rangle}{\partial x_j} \right] - C_{\varepsilon 2} \frac{\varepsilon^2}{k} + \frac{\partial}{\partial x_j} \left[\left(\nu + \frac{\nu_T}{\sigma_\varepsilon} \right) \frac{\partial \varepsilon}{\partial x_j} \right] - S_e \qquad (3.2.12)$$

in which the source term, S_e, is expressed as

$$S_e = 2\,\nu S_{ij}\,\langle\frac{\partial u_l}{\partial x_j} + \frac{\partial u_l}{\partial x_i}\rangle. \qquad (3.2.13)$$

Accuracy and reliability of the RNG $k-\varepsilon$ model for various class of flows are better than the standard $k-\varepsilon$ model, and it consumes more computational time due to the additional terms (ANSYS Inc., 2017).

Realizable $k-\varepsilon$ model

This model ensures positive normal stresses in all flow conditions. Neither standard nor RNG $k-\varepsilon$ model is realizable. The normal stress components can be written as follows.

$$\langle u_i u_i\rangle = \sum_i \langle {u_i}^2\rangle = \frac{2}{3}k - 2\nu_T\frac{\partial\langle u_i\rangle}{\partial x_j} \qquad (3.2.14)$$

It is clear from Equation (3.2.14) if the strain is larger, the normal stresses become negative. However, it is not possible by definition since the sum of square cannot be negative. Therefore, the realizable $k-\varepsilon$ model always predicts positive values for normal stresses.

Also, energy dissipation rate equation has an additional term which is called production term. It is not found in the other two $k-\varepsilon$ models.

$k-\omega$ model

It is another two-equation model used in turbulence modelling. Instead of dissipation rate, ε, there is a new parameter which is called a specific dissipation rate and denoted by ω. It can be thought of as the ratio of ε to k.

Specific dissipation rate used as the length determining quantity in $k-\omega$ model. The modelled k and ω transport equations are

$$\frac{\partial k}{\partial t} + \langle u_j\rangle\frac{\partial k}{\partial x_j} = \nu_T\left[\left(\frac{\partial\langle u_i\rangle}{\partial x_j} + \frac{\partial\langle u_j\rangle}{\partial x_i}\right)\frac{\partial\langle u_i\rangle}{\partial x_j}\right] - \beta k\omega + \frac{\partial}{\partial x_j}\left[\left(\nu + \frac{\nu_T}{\sigma_k}\right)\frac{\partial k}{\partial x_j}\right], \qquad (3.2.15)$$

$$\frac{\partial \omega}{\partial t} + \langle u_j \rangle \frac{\partial \omega}{\partial x_j} = \alpha \frac{\omega}{k} \nu_T \left[\left(\frac{\partial \langle u_i \rangle}{\partial x_j} + \frac{\partial \langle u_j \rangle}{\partial x_i} \right) \frac{\partial \langle u_i \rangle}{\partial x_j} \right] - \beta^* \omega^2 + \frac{\partial}{\partial x_j} \left[\left(\nu + \frac{\nu_T}{\sigma_\omega} \right) \frac{\partial \omega}{\partial x_j} \right]. \quad (3.2.16)$$

Turbulent viscosity, ν_T, is expressed as

$$\nu_T = \frac{k}{\omega}. \quad (3.2.17)$$

In wall-bounded flows, the $k - \varepsilon$ models need the application of wall functions. It is not a requirement for $k - \omega$ model, and law of the wall can be precisely predicted in viscous sublayer. In order to predict the law of the wall, it is necessary to create very fine mesh elements close to the wall. Both $k - \varepsilon$ and $k - \omega$ models give the right prediction in constant pressure boundary layer flows while the $k - \omega$ model is the best for boundary layers with pressure gradients (Andersson, et al., 2012).

Shear Stress Transport (SST) Model

SST model is the combination of $k - \varepsilon$ and $k - \omega$ models which predicts adverse pressure gradients and separating flows with high accuracy. The $k - \varepsilon$ model is used in the free stream while the $k - \omega$ models in wall-bounded regions. As a first choice, the SST model is recommended instead of the $k - \varepsilon$ model in many applications (Andersson, et al., 2012).

Reynold Stress Models (RSMs)

Eddy viscosity turbulence models do not give correct predictions to the solution of complex flows and fail. Therefore, the RSMs do not use the eddy viscosity hypothesis. All the components of the Reynolds stress tensor are solved with their specific transport equations. Algebraic equations solved in algebraic Reynolds stress models and differential transport equations for the differential Reynolds stress models (ANSYS, Inc., 2009). The implementation of the RSMs is computationally expensive due to the number of transport equations resolved.

3.3 Near-wall Modelling

The velocity of fluid is zero at a solid wall and it is known as the “no-slip condition”. The relative velocity between the fluid and the wall increases toward the free stream by moving away from a wall. It happens in the wall layer which is also defined as a turbulent boundary layer. Turbulent boundary layers are divided into an inner region and outer region. The inner region can also be divided into sub-layers. The relative magnitude of the viscous and turbulent stresses identifies these sub-layers. The total shear stress, τ_{xy}, is the summation of the viscous and turbulent components as shown below, respectively.

$$\tau_{xy} = \rho\nu \frac{d\langle u_x \rangle}{dy} + \rho\langle u_x' u_y' \rangle \tag{3.3.1}$$

Viscous stress dominates the momentum transfer in the innermost layer and this layer is referred to as the viscous sub-layer. In this region, the total shear stress is completely based on viscous shear and mathematically described as

$$\tau_w = \rho\nu \frac{d\langle u_x \rangle}{dy}\bigg|_{y=0}. \tag{3.3.2}$$

Viscous and turbulent stresses dominate the total shear stress equally at a certain distance from the wall and this region is called as buffer sub-layer. Turbulent stress becomes effective further away from the wall. In this case, the sub-layer is referred to as fully turbulent. The profiles of the flow parameters vary with a logarithmic function in this region.

The characteristic velocity scale, which is also known as the wall friction velocity, u_*, and length scale, l_*, for the sub-layers are used in the non-dimensional analysis of near-wall modelling. They are defined as

$$u_* = \sqrt{\frac{\tau_w}{\rho}} \tag{3.3.3}$$

and

$$l_* = \frac{\nu}{u_*}. \tag{3.3.4}$$

Thus, two dimensionless quantity can be expressed based on the definitions of the characteristic scales. Both are calculated with the following equations.

A dimensionless length, $$y^+ = \frac{y}{l_*} \tag{3.3.5}$$

and a dimensionless velocity, $$u^+ = \frac{\langle u \rangle}{u_*} \tag{3.3.6}$$

In the viscous sub-layer, the velocity profile with no-slip boundary condition is written as

$$u^+ = y^+ \tag{3.3.7}$$

where the velocity linearly varies with y^+.

However, the relationship between $u^+$and y^+ is expressed with a logarithmic function at larger distances from the wall.

$$u^+ = \frac{1}{\kappa}\ln(y^+) + C \tag{3.3.8}$$

κ is the von Karman constant and C is the log-layer constant which depends on wall roughness. This equation is known as the logarithmic law of the wall.

In order to successfully predict the wall-bounded turbulent flow, the correct modelling of the near-wall region is substantial. Since some well-known turbulence models are only valid in the fully developed turbulent flow, it creates the need for near-wall modelling. There are two possible options used in wall-bounded turbulent flows.

1. The wall function method
2. The Low-Reynolds-Number method

In the wall function method, empirical equations are used and avoid generating dense meshes close to the wall. Therefore, it consumes less computational time. Furthermore, it does not require to resolve the turbulent boundary layer. The concept of wall function is indicated in Figure 3.3. The first grid point, P, placed in the log-law region in which wall function is valid. The viscous sub-layer remains unresolved, and wall function covers the region between the first grid point and the point on the wall itself.

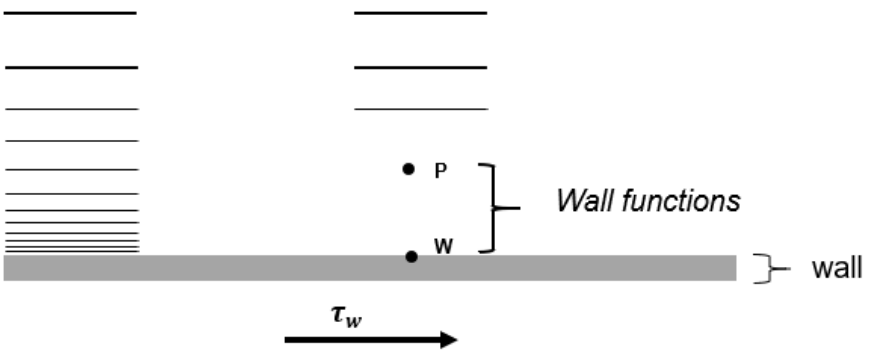

Figure 3.3: Application of wall functions (Andersson, et al., 2012).

The Low-Reynolds-Number method directly resolves the boundary layer details with a very fine mesh close to the wall boundary zone. It significantly increases the need for computational power and time. Turbulence models with ω equation are applicable for the Low-Reynolds-Number method.

The general transport equations for k and ε in Low-Reynolds-Number models are expressed as the following equations, respectively.

$$\frac{\partial k}{\partial t} + \langle u_j \rangle \frac{\partial k}{\partial x_j} = \frac{\partial}{\partial x_j}\left(\left(\nu + \frac{\nu_T}{\sigma_k}\right)\frac{\partial k}{\partial x_j}\right) + \nu_T\left[\left(\frac{\partial \langle u_i \rangle}{\partial x_j} + \frac{\partial \langle u_j \rangle}{\partial x_i}\right)\frac{\partial \langle u_i \rangle}{\partial x_j}\right] - \varepsilon \tag{3.3.9}$$

$$\frac{\partial \tilde{\varepsilon}}{\partial t} + \langle u_j \rangle \frac{\partial \tilde{\varepsilon}}{\partial x_j} = \frac{\partial}{\partial x_j}\left(\left(\nu + \frac{\nu_T}{\sigma_\varepsilon}\right)\frac{\partial \tilde{\varepsilon}}{\partial x_j}\right) + C_{1\varepsilon} f_1 \nu_T \frac{\tilde{\varepsilon}}{k}\left[\left(\frac{\partial \langle u_i \rangle}{\partial x_j} + \frac{\partial \langle u_j \rangle}{\partial x_i}\right)\frac{\partial \langle u_i \rangle}{\partial x_j}\right] - C_{2\varepsilon} f_2 \nu_T \frac{\tilde{\varepsilon}^2}{k} + E \tag{3.3.10}$$

The relationship between energy dissipation, ε, and $\tilde{\varepsilon}$ is

$$\varepsilon = \varepsilon_0 + \tilde{\varepsilon} \tag{3.3.11}$$

where ε_0 is the value of the energy dissipation, ε, at a wall. Also, turbulent viscosity, ν_T, is defined by the following equation.

$$\nu_T = f_\mu C_\mu \frac{k^2}{\tilde{\varepsilon}} \tag{3.3.12}$$

The Low-Reynolds-Number model differs from the standard $k - \varepsilon$ model due to the damping functions f_1 and f_2 in the transport equation of the energy dissipation and the damping function f_μ (Andersson, et al., 2012).

3.4 Multiphase Modelling

In principle, a flow contains two or more phases of matter is referred to as multiphase flow. Multiphase flows are common in our surroundings such as gases in a liquid, liquid in gases or solid particles in liquids. Typically, two-phase flows are categorized due to the distribution of the components. Separated and dispersed two-phase flow categories are encountered in many industrial applications. In a separated flow, there are a few interfaces between two phases. On the contrary, one fluid is considered as a continuous phase while other presents as dispersed particles in a dispersed flow.

Multiphase flow modelling can be done by several models in CFD simulations. The following computational models are quite famous and widely used in CFD applications.

- Euler - Lagrange model
- Euler - Euler model
- Volume of Fluid (VOF) model
- Mixture or algebraic slip model
- Porous - bed model

The Euler - Lagrange model is suitable for the two-phase flows in which discretely distributed particles of dispersed phase tracked in a continuous phase. The trajectories of a particle followed and computed that exchange mass, momentum, and energy with the fluid phase. Individual particle tracking needs for sufficient computational resources. Thus, this model is applicable to a system that possesses a low volume fraction of the dispersed phase. The number of particles in two-phase flow is the main limitation for the Euler - Lagrange model. Examples of dispersed flow observed around us are air bubbles in water, water droplets in a continuous gas phase or solid particles in air. In this kind of flow, each phase computed separately, and discrete particles act to the continuous phase flow by generated source term. It is not preferred to track all existing particles due to the challenges in the computation process. Accordingly, a bundle of particles or representative of individual particles are taken into account in this model. Another requirement for proper usage of the Euler - Lagrange model is the size of dispersed phase particles or bubbles.

They must be smaller than the mesh cells of continuous fluid phase. In this technique, the single-phase Navier-Stokes equation resolved for a continuous phase by individually tracking the particles

$$\frac{\partial(\alpha_f \rho_f)}{\partial t} + \frac{\partial(\alpha_f \rho_f u_{i,f})}{\partial x_i} = S_c, \tag{3.4.1}$$

$$\frac{\partial(\alpha_f \rho_f u_{i,f})}{\partial t} + \frac{\partial(\alpha_f \rho_f u_{i,f} u_{j,f})}{\partial x_i} = -\alpha_f \frac{\partial(P)}{\partial x_i} + \frac{\partial(\alpha_f \tau_{ij,f})}{\partial x_j} + S_{i,p}, \tag{3.4.2}$$

where α_f is the volume fraction of continuous phase and f denotes a continuous phase. There are two source terms, S_c and $S_{i,p}$, the former is a representative of mass transfer between phases, while the latter describes exchange of momentum between the discrete particles and continuous media. The source term, $S_{i,p}$, is the summation of the forces that influence the dispersed particles.

The term, $S_{i,p}$, takes into account forces on the particles which are in a control volume. Therefore, the number of particles in that volume can be defined as

$$\frac{n}{V} = \frac{6\alpha_d}{(\pi D_p^3)} \tag{3.4.3}$$

where particle has a spherical shape and D_p is the diameter.

The Euler - Euler model is also called as a two-fluid model in which two phases are treated mathematically as completely interpenetrating fluids. The principle of modelling based on the volume averaging or ensemble averaging (Andersson, et al., 2012). The model equations are comprised of volume fraction which is an essential quantity in this technique. Regardless of the low volume fraction requirement in the Euler – Lagrangian model, this one is applicable for a wide range of volume fractions. The sum of volume fractions is equal to one and it is mathematically expressed as

$$\sum_{l=1}^{p} \alpha_k = 1. \tag{3.4.4}$$

The Euler -Euler modelling of multiphase flows based on the following mass and momentum conservation equations, respectively.

$$\frac{\partial(\alpha_k \rho_k)}{\partial t} + \frac{\partial(\alpha_k \rho_k u_{i,k})}{\partial x_i} = -\sum_{l=1}^{p} (\dot{m}_{kl} - \dot{m}_{lk}) \tag{3.4.5}$$

$$\frac{\partial(\alpha_k \rho_k u_{i,k})}{\partial x_i} + \frac{\partial(\alpha_k \rho_k u_{i,k} u_{j,k})}{\partial x_i} = -\alpha_k \frac{\partial(P)}{\partial x_i} + \frac{\partial(\alpha_k \tau_{ij,k})}{\partial x_j} + \alpha_k \rho_k g_i + F_{i,k}. \tag{3.4.6}$$

F_k represents the interaction force with the other phases, where index k denotes the corresponding phase. Also, p stands for the total number of phases in the summation term. Mass transport from phase k to phase l indicated by the term $\dot{m}_{kl}$. Two closure models must be used to define τ and F_k. τ used describing rheology of phase and complex closure models must be implemented if the non-Newtonian fluid present in the system. In addition, the variables included in the equations are averaged.

The volume of fluid model is suitable for stratified flow to track the interface of phases. Both Euler-Euler and Euler- Lagrange are not capable of accurate modelling stratified flows. The concept of VOF model is to treat each phase as a sperate fluid. The Navier -Stokes equations for each phase resolves with momentum exchange term. It is usually applied to a flow where the interphase surface is clearly visible. The position of the interface described based on the volume fraction in a grid cell. The momentum equation expressed as:

$$\frac{\partial(\rho u_i)}{\partial t} + u_i \frac{\partial(\rho u_i)}{\partial x_i} = -\frac{\partial \tau_{ij}}{\partial x_j} + \frac{\partial P}{\partial x_i} + \rho g_i + S_{i,s}. \tag{3.4.7}$$

The source term, $S_{i,s}$, contains surface tension force which is a significant variable for stratified flows.

The mixture model is the simplified multiphase flow model and has similarity with the Euler - Euler model. There is a local equilibrium in relative velocities of phases. A set of equations is solved for the mixture, whereas algebraic equations for the relative velocity. The velocity of phases that are different from the mean velocity is referred to as drift velocity. The drift velocity denoted by $u_{i,dr,k}$. The continuity and momentum equations are given as

$$\frac{\partial(\rho_m)}{\partial t} + \frac{\partial(\rho_m u_{i,m})}{\partial x_i} = 0 \tag{3.4.8}$$

$$\frac{\partial(\rho_m u_{i,m})}{\partial t} + \frac{\rho_m \partial(u_{j,m} u_{i,m})}{\partial x_j} = -\frac{\partial P}{\partial x_i} + \frac{\partial \tau_{ij,m}}{\partial x_j} + \rho_m g_i - \frac{\partial \sum_k \alpha_k \rho_k u_{i,dr,k} u_{j,dr,k}}{\partial x_j}. \quad (3.4.9)$$

The subscript m means the mixture and mixture density is expressed as

$$\rho_m = \sum_{k=1}^{p} \alpha_k \rho_k. \quad (3.4.10)$$

where p is the total number of phases. The velocity for the phase k is equal to the sum of the drift velocity and the mean velocity components. Also, some flow properties are defined by the volume fraction and mixture viscosity is an example which is given as

$$\mu_m = \sum_{m} \alpha_k \mu_k. \quad (3.4.11)$$

The porous-bed model is suitable for the flows which are driven by pressure drop over the medium (Andersson, et al., 2012). This kind of flow encountered commonly in fixed bed reactors. The pressure drop and the porous media resistance are two fundamental factors in the governing equations.

3.4.1 Forces on a Single Particle

As it is mentioned in the description of the Euler-Lagrangian and Euler-Euler models, additional source terms used in the momentum equations. These source terms involve the forces on the dispersed particles. The detailed explanation of each of the forces is the main objective of this subsection.

The forces act on a single particle can be described for the equation of motion with a general expression as

$$m_d \frac{du_{i,d}}{dt} = F_{i,Drag} + F_{i,Press} + F_{i,Virt} + F_{i,History} + F_{i,Buoy} + F_{i,Lift} + F_{i,Therm} + F_{i,Turb} + F_{i,Brown.} \quad (3.4.1.1)$$

On the left-hand side of the equation m_d represents the mass of the particle, while $u_{i,d}$ is the linear velocity of the particle. The forces on the right-hand side are as follows:

- $\mathrm{F_{i,Drag}}$: drag force acting on the particle.
- $\mathrm{F_{i,Press}}$: pressure force due to pressure gradient which becomes important if the fluid density varies from that of the particle.
- $\mathrm{F_{i,Virt}}$: virtual mass force which acts to accelerate the virtual mass of fluid occupied by the particle.
- $\mathrm{F_{i,History}}$: history or Basset force. It is taken into account when there is a deviation in flow pattern from a steady-state.
- $\mathrm{F_{i,Buoy}}$: buoyancy force due to gravity.
- $\mathrm{F_{i,Lift}}$: is the Saffman and Magnus lift force. it is effective due to the velocity gradient and particle rotation.
- $\mathrm{F_{i,Therm}}$: the thermophoretic force arises due to a temperature gradient.
- $\mathrm{F_{i,Turb}}$: the force due to turbulence effects.
- $\mathrm{F_{i,Brown}}$: Brownian force due to molecular collisions.

The drag force expression for a single particle is shown in equation (3.4.1.2) and it is valid in dispersed flows with the low volume fraction.

$$\mathrm{F_{i,Drag}} = \frac{1}{2}\mathrm{A_d C_D \rho_f |u_f - u_d|(u_{i,f} - u_{i,d})}. \qquad (3.4.1.2)$$

The terms in the parentheses represent the relative velocity between the phases and this relative velocity is known as slip velocity (ANSYS, Inc., 2009). $\mathrm{A_d}$ stands for the effective particle cross-section, while the drag force coefficient represented by $\mathrm{C_D}$. Moreover, there is a modified form of the drag force equation at high volume fraction of the dispersed phase.

$$\mathrm{F_{i,Drag}} = \frac{1}{2}\mathrm{A_d C_D \rho_f \alpha_f^{-2.65} |u_{i,f} - u_{i,d}|(u_{i,f} - u_{i,d})}. \qquad (3.4.1.3)$$

The drag force coefficient varies based on the dispersed-phase Reynolds number. For a particle in laminar continuous phase, the drag coefficient calculated with an equation that is divided into three different parts. The equation is given as:

$$C_D = \begin{cases} \dfrac{24}{Re_d} & \text{if } Re_d < 0.5 \\ \dfrac{24}{Re_d}\left(1 + 0.15{Re_d}^{0.687}\right) & \text{if } 0.5 < Re_d < 1000 \\ 0.44\alpha_f & \text{if } Re_d > 1000 \end{cases} \quad (3.4.1.4)$$

The experimental analysis of turbulent flows shows that the drag coefficient does not obey the law mentioned above, but its value proportional to the turbulence intensity (Andersson, et al., 2012).

The pressure force is dominant in such circumstance a large pressure gradient exists or density of the particle smaller than that of fluid. The pressure force on the volume of the particle can be described at a constant pressure gradient in the form of

$$F_{i,Press} = V_d\left(-\frac{\partial P}{\partial x_i} + \frac{\partial \tau_{ij}}{\partial x_j}\right). \quad (3.4.1.5)$$

The influence of the virtual mass force increases with the mass of the particle. This force accelerates the surrounding fluid and the following expression used.

$$F_{i,Virt} = -C_{VM}V_d\rho_f\frac{d}{dt}\left(u_{i,d} - u_{i,f}\right) \quad (3.4.1.6)$$

Another significant force is the buoyancy which is mathematically equal to the amount of fluid displaced due to the particles. The buoyancy force acting on the immersed particle and given as

$$F_{i,Buoy} = \left(m_p - m_f\right)g = m_p\left(1 - \frac{\rho_f}{\rho_p}\right)g. \quad (3.4.1.7)$$

3.5 Application of CFD in wastewater treatment plants

The conceptual design of wastewater treatment plant units is generally based on empirical calculations and this method has limited capability to predict the behavior of these units due to the fluid flow phenomena complexity (Rosa, et al., 2017). The use of CFD ensures a more precise prediction of the fluid flow hydrodynamics and deal with design challenges in the treatment facilities.

Various scientists have used CFD simulation for designing and modelling purposes of wastewater treatment processes starting from 1990s. Meanwhile, the evolution of

published studies shows that CFD modelling has been accepted as a more reliable method for investigation of WWTP operations, according to Rosa et al. (2017).

Figure 3.4 indicates the number of various studies in the biological treatment process that was accomplished during the last 50 years. The trend shows numerical techniques are losing its popularity by the development of CFD technique. Nowadays, the CFD technique is more popular and reliable among the several numerical tools in the modelling of biological treatment processes.

The modelling of a secondary clarifier has been accomplished by Brouckaert and Buckley (1999) to examine the hydrodynamics after installation of baffles on the existing treatment unit. Their investigations were performed with a simplified clarifier model, which takes into account axisymmetry of cylindrical geometry, two-dimensional (2D) problem, involving pure water only. Although some simplifications have been considered for this case, the result of CFD simulation was reliable and quite helpful to understand the fluid flow behavior for the modified clarifier.

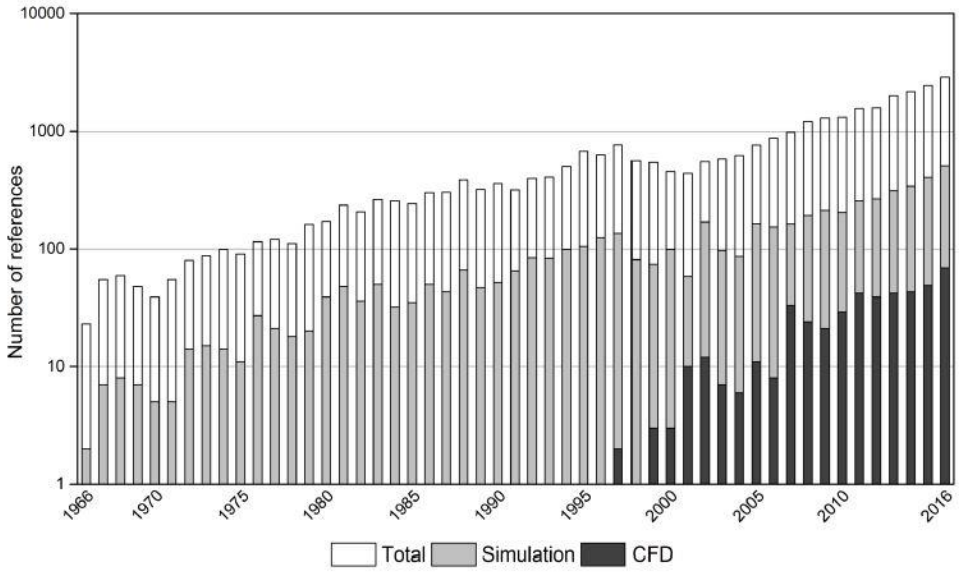

Figure 3.4: Biological treatment process publications over the last 50 years (Rosa, et al., 2017).

On the other hand, the lack of symmetrical configuration and the presence of gas or solid phase in a system make three-dimensional (3D) and multiphase CFD modelling necessary. Karama et al. (1999) simulated a 3D CFD model of the anaerobic zone of activated sludge reactor to predict a dead zone. Furthermore, two experimental tests, the residence time distribution test and oxygen reduction potential test, were conducted and favorable results were obtained at the end of CFD modelling.

The numerical and experimental agreement of the study consolidated CFD as a robust tool in predicting activated sludge reactor hydrodynamics.

In addition, CFD has been proved as an efficient tool to optimize and upgrade aeration systems (Cockx, et al., 1999). The full-scale multiphase study has been investigated in the aeration reactor and mass transfer of dissolved ozone validated by experimental results with negligible inaccuracy.

Recent development and availability of computational resources pave the way for simulating complex WWTP problems and completely characterize fluid flow without doing significant simplifications. There are many samples in literature for this kind of approach, but the only drawback of whole WWTP simulation is the calculation time. Despite the high computing time, CFD simulation of full-scale WWTP using population balance modelling has been successfully analyzed in this year (Climent, et al., 2019). On the one hand, simplifications are still preferred and widespread approach in CFD modelling because it takes less calculation time and is a cost-effective method.

Although there were considerable simplifications in most of the completed studies in wastewater treatment operation, such as reducing the number of phases, uniform characteristics of fluids, and symmetrical geometry approach, CFD modelling has been accepted as a powerful tool to analyze wastewater treatment units. Currently, the development of computational power makes detailed and deep fluid flow modelling more convenient for researchers.

Chapter 4

CFD Model Development

4.1 Simulation Software

CFD simulation of this work was performed by ANSYS CFX 18.2 release. ANSYS CFX is a multi-purpose commercial software that has been successfully used in the simulation of fluid flow for many years. ANSYS CFX 18.2 is able to cope with transient or steady-state modelling of various forms of fluid flows such as multiphase, buoyant, non-Newtonian flows or flows in multiple reference frames (ANSYS Inc., 2017).

It is composed of four software modules and each of them has unique capabilities to perform CFD analysis. Figure 4.1 describes the general analysis sequence of a CFD problem with ANSYS CFX package:

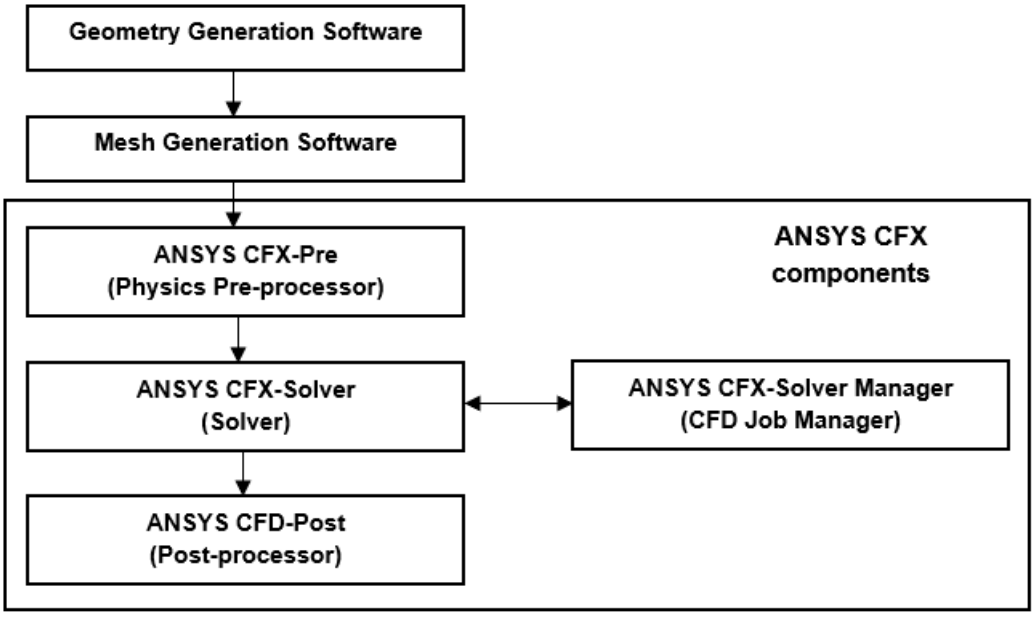

Figure 4.1: ANSYS CFX software modules (ANSYS Inc., 2017).

After geometry and mesh generation, flow physics and boundary conditions are defined in CFX-Pre. Then, CFX-Solver solves all of the solution variables while CFX-Solver Manager allows a user to manage and control CFD problem. CFD-Post is a postprocessing tool which is used to extract and analyze ANSYS CFX simulation results.

ANSYS ICEM CFD is a mesh generation and repair tool that deals with complex geometries in CFD analysis. In this study, ICEM CFD 18.2 release was used to generate meshes for geometries.

4.2 Computational Geometry

A full-scale Pasveer-type oxidation ditch with a total working volume of 7300 m^3 has been chosen for this study. Three-dimensional geometries of the tank and submerged agitators were designed as a representative of the oxidation ditch and implemented in this CFD analysis. However, some considerable simplifications have been done, because of real complex geometries. These simplifications help to reduce computational costs to a great extent. Although oxidation ditches are usually operated in continuous mode, the inlet and outlet of the tank were avoided. The extended hydraulic detention time allows neglecting the tank outlet and inlet. Therefore, the batch process has been chosen.

In reality, fine bubble diffusers ensure oxygen demand to initiate biochemical reactions. A cluster of fine bubble diffusers are located at a certain distance from the bottom of the tank and they are known as a diffuser grid. It has been modelled as a group of rectangular block structures in each aeration channel. There are two aeration channels, and each of them is partially covered with a diffuser grid. Both of them have eight rectangular blocks for the aeration process. Mixing is provided by two submerged agitators which are located before the diffuser grids. The 3D view of the oxidation ditch considered in this work is shown in Figure 4.2.

The dimensions of the tank are 75.0 m x 18.0 m x 6 m. The positioning of diffusers and agitators is based on the best practice guidelines of the manufacturing company. There are two semi-circular guiding walls at each end of the oxidation ditch. They promote horizontal bulk flow. Both diffuser grids are 0.3 m above the tank floor.

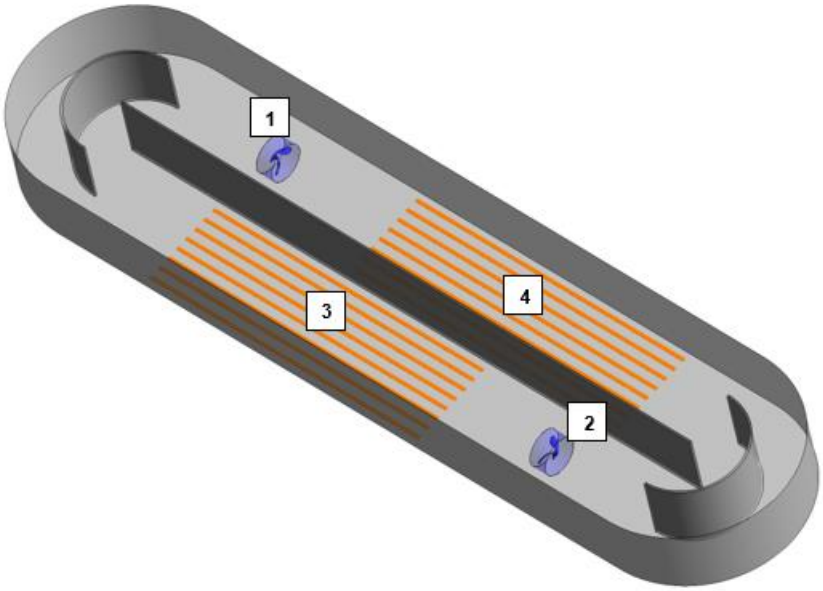

Figure 4.2: 3D view of the full-scale oxidation ditch,
Agitators (1 and 2), Diffuser grids (3 and 4).

The submerged agitators ensure flow circulation in the clockwise direction. The support legs of agitators have been avoided for the sake of simplicity in the geometry designing step. The agitator model defined by the manufacturer for this study. It consists of three blades that generate axial thrust up to 4660 N and propeller speed is 35 rpm. The diameter of the propeller is around 2660 mm. Figure 4.3 shows the computational geometry of the agitator model.

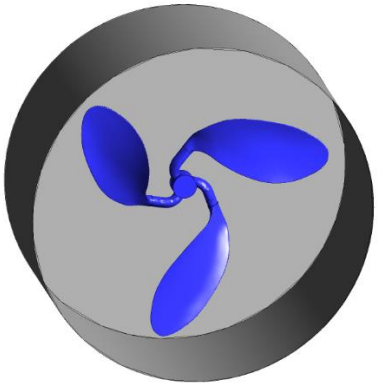

Figure 4.3: 3D view of computational agitator geometry.

4.3 Mesh Generation

Based on the topology of the mesh elements, the mesh generation methodology can be divided into two categories. They are known as structured and unstructured meshes. Structured mesh elements represented by i, j, k indices which are used to locate neighboring cells. It means that a structured mesh follows a uniform pattern while it is not a matter of discussion for an unstructured mesh. In general, the accuracy of the solution is more reliable in structured meshes. Although the structured mesh process allows generating high-quality mesh elements, its application for complex 3D geometries is a complicated task. Generating meshes with structured topology is a time-consuming task for complex geometry, so unstructured meshes are easily applied instead of structured ones. The elements of structured meshes are commonly hexahedrons, while that of unstructured meshes are tetrahedrons. Also, it is possible to make use of the advantages of both structured and unstructured meshes by combining them in a single geometry. This approach is called as hybrid mesh generation in practice. A hybrid mesh allows generating prismatic cells in the viscous region, while the remaining part of geometry meshed with tetrahedral cells.

ANSYS ICEM CFD 18.2 is used to generate both structured and unstructured meshes. Since the computational geometries are quite complex in this study, unstructured mesh generation is preferential. ANSYS ICEM CFD has unique mesh algorithms which are able to generate unstructured meshes with good quality. Based on this feature, unstructured meshing has been implemented for both tank and propeller geometry.

4.3.1 Mesh Generation for the Tank Geometry

Mesh generation is one of the most significant parts of CFD analysis since the result's accuracy depends on the mesh quality. In principle, a correct simulation result is directly proportional to a mesh density. In other words, the accuracy rate of CFD study is increasing by refining the mesh elements. Therefore, it is necessary to obtain the optimal number of mesh elements. At the same time, computational time and processing capacity are another two significant factors that must be considered for CFD study. If the mesh density is too high, it might be a time-consuming simulation which is the commonly undesired situation.

The mesh sensitivity analysis is a method that defines the optimal number of mesh elements for a correct CFD analysis. In literature, there are many published papers regarding the methodology used for mesh sensitivity analysis. Typically, mesh independence study done by generating meshes with different mesh densities for a single geometry. After completing the simulation for each of these meshes, the results are compared. If there is no significant difference, it is more convenient to use the coarse mesh elements because of less computation time. Otherwise, mesh refinement must be carried out up to a certain value in which the compared results are almost the same.

In order to create unstructured meshes, the tetra/mixed volume meshing algorithm has been applied to the tank geometry. The Robust (Octree) is one of these volume meshing methods which allows faster mesh computation. In addition to this, this mesh algorithm refining the mesh elements in necessary locations, while keeping the rest of the mesh elements as large as possible (ANSYS, Inc, 2016). This method does not require any existing surface to start volume meshing since it uses a patch-independent approach.

The curvature/proximity-based refinement option was used to refine mesh elements in some critical regions, such as in the aeration zone, which might affect the result of simulation to a great extent. It ensures automatic mesh refinement based on the curvatures of geometry. Since the tank model is quite large, the generation of too many mesh elements is unavoidable with the Octree method. As a result, the computational time will be relatively high. In order to alleviate this issue, the Delaunay method used to generate volume elements without changing the existing surface meshes. It promotes to reduce mesh density to some extent. On the other hand, Octree tetrahedral cells have sharp transitions, so replacing volume elements with the Delaunay option also avoids these problems.

In order to capture boundary layer flow details, highly refined meshes must be generated. It can be done by refining the existing tetrahedral cells next to wall boundaries. Refining mesh elements lead to a substantial increment of the mesh density. The solution of the problem is to create prism layers near the boundary. The post inflation prism meshing algorithm was used for the following meshing step which extracts tetrahedral cells next to boundary surfaces and fills the subsequent gap with prisms. High-quality tetra-volume mesh and tri-surface mesh is an essential precondition to start the prism meshing process. Accordingly, global mesh smoothing has been applied to reach a pre-specified criterion.

ANSYS ICEM CFD ensures comprehensive control of generated prism layer. If it is necessary, the first layer thickness is easily adjusted or they can split further to provide rationale layer growth respect to the first prism. Three tetra/prism meshes with different densities were generated for the tank geometry. The following table summarizes them with details.

Table 4.1: Mesh specifications.

Mesh parameters	**Mesh A (coarse)**	**Mesh B (medium)**	**Mesh C (fine)**
Total elements (millions)	3.81	7.53	15.87
Tetra quality	min. 0.38 ave. 0.78	min. 0.37 ave. 0.75	min. 0.37 ave. 0.88
Tri quality	min. 0.36 ave. 0.78	min. 0.38 ave. 0.80	min. 0.31 ave. 0.81
Penta quality	min. 0.36 ave. 0.94	min. 0.39 ave. 0.95	min. 0.31 ave. 0.96
Quad quality	min. 0.42 ave. 0.98	min. 0.40 ave. 0.98	min. 0.38 ave. 0.98

Based on the density of cells, meshes have been categorized as a coarse, medium, and fine one. ANSYS ICEM CFD mesh quality indicator varies between 0 and 1. The best quality mesh element indicated with 1, while the worst one is 0.

Figure 4.4 shows the wireframe model of meshes from the top to perceive the difference in mesh density. In this figure, the cylindrical case of agitators removed for the sake of clarity.

a)

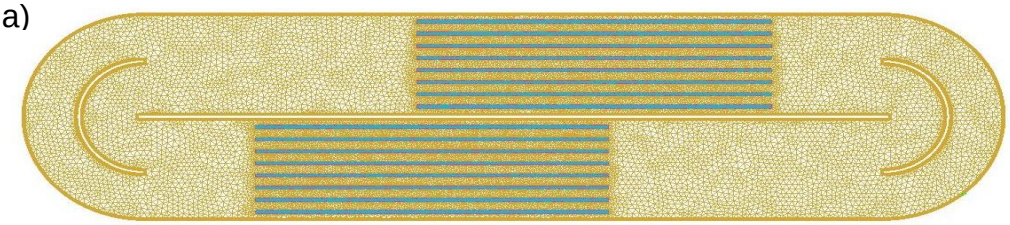

b)

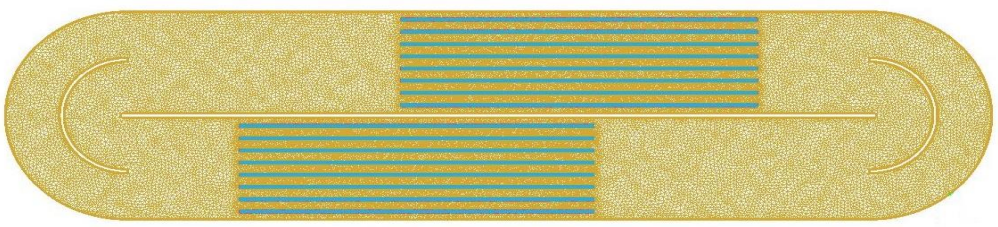

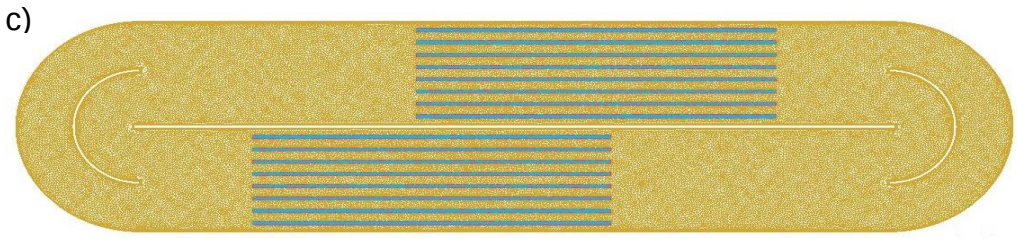

Figure 4.4: Top view of the wireframe mesh model:
a) Mesh A b) Mesh B c) Mesh C

4.3.2 Mesh Generation for the Agitator Geometry

Figure 4.5 indicates the isometric view of the surface cells and front view of fluid volume cells in the computational domain, respectively.

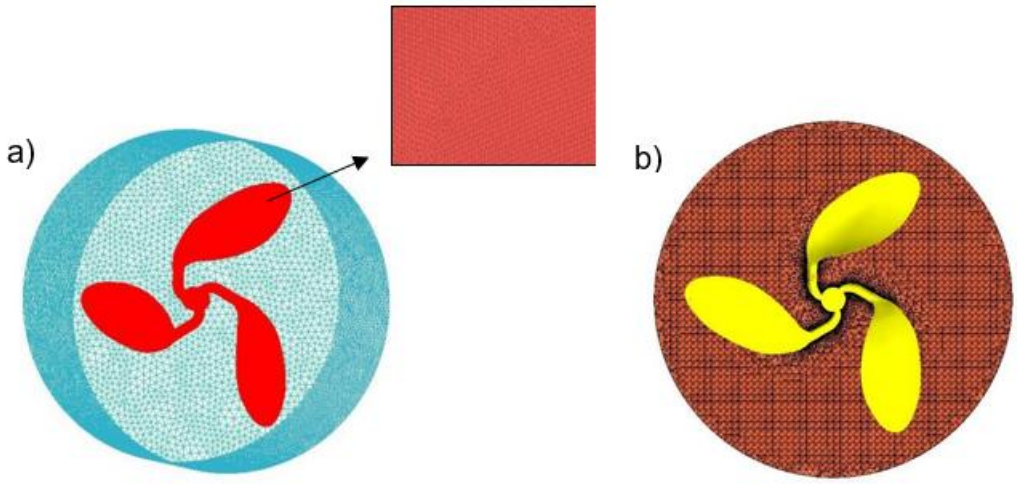

Figure 4.5: Agitator mesh view a) Surface mesh view b) Volume mesh view

The same methodology has been followed as in the tank meshing process to generate cells. However, the cells on the blades need excessive refinement to capture the flow details. That is the reason why the oversimplification of the blade geometry is necessary. Otherwise, the overall number of cells in the domain will be large enough which means more computation time. Accordingly, the blades have been designed as a surface. The real thickness of the blades was not considered, and their extra volume elements avoided.

4.4 Setting Up the Multiphase Flow Model

In general, wastewater flows into the oxidation ditch contains solid particles and liquid media. Air bubbles inserted into the basin by means of aerators in the meantime. Thus, flows in this process are considered as multiphase and multiphase flow modelling is necessary. In order to alleviate the required computational resources, the solid matters present in the system are not considered during the simulation and two-phase flows have been simulated.

A broad range of explanations regarding the multiphase modellings was already given with relevant mathematical expressions in the previous chapter. ANSYS CFX uses two of these models which are the Euler – Lagrange multiphase model and the Euler – Euler multiphase model. In current work, the Euler – Euler multiphase model has been implemented which treats both phases separately as interpenetrating continua. Two distinct sub-models of the Euler – Euler model exists which are given below.

1. The homogeneous model
2. The inhomogeneous model

The inhomogeneous model was chosen in which separate fields of velocity and that of other variables used for each fluid during the computation (ANSYS Inc. , 2009). The only shared field is the pressure field in the inhomogeneous model. This model is also composed of two models. The morphology of each phase defines the model that is used in the inhomogeneous multiphase model (ANSYS Inc. , 2009). For the oxidation ditch process, liquid media is a continuous fluid, while spherical air bubbles are referred to as dispersed fluid. A dispersed fluid distributes in a continuous one discretely. The particle model has been applied which is suitable for systems when a continuous fluid and a dispersed fluid present. It ensures accurate prediction of interfacial momentum, mass, and heat transfers. These transfer terms are strictly dependent on the contact surface area between air bubbles and water. The following expression describes the interfacial area density, A_{lg}, as a function of bubble mean diameter (ANSYS, Inc., 2009).

$$A_{lg} = \frac{6\alpha_g}{D_g} \tag{4.4.1}$$

Mean diameter of an air bubble denoted as D_g, whereas α_g represents the volume fraction of the gas phase.

4.4.1 Interphase Momentum Transfer

Bubbles moving with a certain velocity in water are affected by the drag force. The drag force acts in the opposite direction of the velocity vector. Thus, the influence of drag force must be taken into account when a dispersed phase exists in a system. Since air bubbles exist in the wastewater basin, the interface momentum transfer model is inevitable. The Ishii – Zuber drag law is available for modelling of general fluid particles such as droplets and bubbles. This model was used based on its robustness. The surface tension coefficient and gravity vector must be specified to apply the Ishii – Zuber model. As it has already been written in equation (3.4.1.4), drag force coefficient for spherical particles depends on the Reynolds number. However, the coefficient is independent of the Reynolds number in the distorted particle regime (ANSYS, Inc., 2009). Eotvos number, which is a non-dimensional variable, provides the drag coefficient in this regime.

$$\mathrm{Eo} = \frac{\mathrm{g}\mathrm{D_g}^{2}\Delta\rho}{\sigma} \qquad (4.4.1.1)$$

Equation (4.4.1.1) shows Eotvos expression where σ represents the surface tension coefficient. It is also a function of density difference between the phases. Drag coefficient in distorted regime is equal to

$$\mathrm{C_{D,(dist.regime)}} = \frac{2}{3}\mathrm{Eo}^{1/2}. \qquad (4.4.1.2)$$

The water-air surface tension coefficient has been specified explicitly. It is equal to 0.072 [N/m] (Dean, 1999).

Besides the drag force, the interphase turbulent dispersion force model applied to the multiphase flow settings. The aim of the model is to simulate the dispersion of the air bubbles from high volume fraction regions to low volume fraction regions. Turbulent eddies of the continuous phase and interphase drag are the reason for moving particles from the high to low concentration area.

In order to predict this effect in the multiphase flow, the Favre averaged drag model was chosen. It is based on the Favre or Mass weighted average of the interphase drag force (ANSYS, Inc., 2009). The default value, which is equal to unity, was implemented for the turbulence dispersion coefficient. It is a dimensionless variable.

4.4.2 Buoyant Flow

In multiphase flows, the difference between the density of phases generates a buoyancy force. Buoyancy reference density is a significant parameter for accurate modelling of multiphase flows. ANSYS CFX considers the buoyancy reference density as a density of continuous fluid when a dilute dispersed phase takes part in the flow. According to this, water density specified as a buoyancy reference density.

Density-difference fluid buoyancy model has been applied in the simulation which is also the default option in ANSYS CFX.

4.5 Setting Up the Turbulence Model

ANSYS CFX allows to model turbulence separately for each phase that presents in multiphase flow. In this simulation setup, the SST turbulence model used for the continuous fluid, whereas the Dispersed phase zero equation model applied to the dispersed one.

The SST model combines all the advantages of $k-\varepsilon$ and $k-\omega$ models. A detailed explanation of turbulence models has been already given in the previous chapter. The $k-\omega$ model predicts turbulence eddies more accurate than the $k-\varepsilon$ model close to the wall-bounded regions. In the free shear flows, SST model is the same as the $k-\varepsilon$ model. Automatic wall function used with SST model. The principle of automatic wall function is to switch from the wall function to the Low-Reynolds-Number model when there are remarkable mesh refinements.

On the other hand, the Dispersed phase zero equation model is based on the algebraic expression. The turbulence length scales and mean velocity included in this expression.

4.6 Domains

Fluid flow equations are solved in domains which are specific regions. In this work, multiple domains have been used with a specific domain motion. Tank geometry defined as a stationary which means the domain does not move as compared with absolute reference of frame.

For the geometry of each agitator, one domain has been created. Rotating domain motion specified for them. Both stationary and rotating domains are fluid domains. Since the simulation deals with both types of domain motion, the interfaces between them must be described.

Domain interfaces are necessary to connect a stationary domain with a rotating domain. In the tank geometry, the location of each agitator modelled as a cylindrical case. The fluid-fluid interface type was chosen with the general connection interface model. The general – connection method used to connect the non-matching mesh elements, apply frame change between rotor and stator interface, and utilize transient sliding interfaces (ANSYS Inc. , 2009).

Transient rotor-stator technique was selected in the frame change/mixing model. In this model, transient characteristics of flow interaction predicted accurately between rotational and stationary domain interfaces. During the simulation, sliding meshes continuously change their position relative to the stationary meshes. As a result, interface coordinates updated in each timestep (ANSYS Inc. , 2009). Transient rotor-stator is a time-consuming model. It needs a large disk space and sufficient computer resources.

General Grid Interface (GGI) mesh connection method is capable of connecting the grids of a stationary and a rotating domain when they do not match with each other. It is a robust method applied in the domain interface setup, but the main disadvantage is its memory consumption.

4.7 Boundary Conditions

4.7.1 Air Inlet

Two aeration channels designed for the oxidation ditch process and air flowrate of 1344 Nm^3/h per channel was set for the actual tank dimensions. The longitudinal block structure of air diffusers is not feasible to use inlet boundary conditions for air. In order to model air injection via the 3D structure of air diffusers, the subdomain option is available in ANSYS CFX. Subdomains used when source terms applied in the simulation.

Mass source term is used to introduce a new fluid to the system by means of the continuity equation. Fluid mass source option has been implemented for the air

injection subdomain. Fluid mass source specified as a volumetric quantity which is equal to the ratio of the source term to the volume of the relevant subdomain. The value of air mass source was calculated via an expression which is given as

$$S_{MS}(\text{air}) = \frac{\dot{V}_{\text{air}}\rho_{\text{air}}}{V_{\text{air subdomain}}}. \qquad (4.7.1.1)$$

The variables in the above – mentioned equation are as follows:

- $S_{MS}(\text{air})$ – air mass source term introduced to the continuity equation $\left[\frac{\text{kg}}{\text{m}^3\text{s}}\right]$;
- $\dot{V}_{\text{air}}$ – air volumetric flowrate with units of $\left[\frac{\text{m}^3}{\text{s}}\right]$;
- ρ_{air} – air density $\left[\frac{\text{kg}}{\text{m}^3}\right]$;
- $V_{\text{air subdomain}}$ – volume of the subdomain with unit of $[\text{m}^3]$.

Fluid mass source of 0.071 kg/(m^3s) was specified for air injection subdomain.

4.7.2 Agitator

Apart from the mixing process, submerged agitators with a horizontal rotation axis are also used to generate bulk flow in the oxidation ditch. These agitators are therefore referred to as flowmakers. The model of flowmaker has been selected by the manufacturer, and it is illustrated in Figure 4.6.

Figure 4.6: SFG.50.260.35.5.1B model Grundfos flowmaker (www.grundfos.com)

For characterizing the mixing process, various methods are available (Brannock, 2003). One of them is the transient rotor-stator model or sliding mesh method in which the rotation of blades simulated.

It is the most sophisticated method but predicts more accurate results than others. Also, it is a computationally expensive method since the combination of a stationary and rotary domain must be simulated.

Another one is the momentum source model in which source term applied. This is the simplest model and thrust of real flowmaker used to define momentum source term.

Transient rotor-stator model

Two propeller-type flowmakers were modelled as a rotating fluid domain in the simulation setup. The blades of each flowmaker were set as a wall-type boundary. A no-slip condition for water and a free slip condition for air were selected. The angular velocity of 35 [rev/min] was defined as a propeller speed for transient rotor-stator model. Table 4.2 summarizes the specification of the flowmaker model.

Table 4.2: Technical specifications (www.grundfos.com)

Number of propeller blades	3
Axial thrust force	4660 N
Thrust to power ratio	0.901
Propeller speed	35 [rev/min]
Mean velocity	0.65 [m/s]
Propeller diameter	2660 mm
Tip speed	4.9 [m/s]

Momentum source model

The main advantage of the momentum source method is the simplification of flowmaker geometry. It is not required to use agitators as a rotating domain anymore. Moreover, instead of using the real agitator model, it is modelled as a cylinder and momentum source term applied.

Two cylinders as a representative of real agitators were modelled as a part of the stationary tank domain. Thus, a subdomain is created for each of them, and the general momentum source term in axial direction was set. The general momentum source term was calculated via the following expression.

$$\text{General momentum source} = \frac{\text{Thrust}}{\text{Volume of subdomain}} \qquad (4.7.2.1)$$

Axial thrust value is already shown in Table 4.2, and the volume of both subdomains was taken into account to get the momentum source. Based on equation (4.7.2.1), the momentum source of 387 kg/(m^2s^2) was specified for both subdomains.

4.7.3 Outlet boundary

A degassing boundary condition was used to model the free surface of the oxidation ditch. In principle, it is applicable to the multiphase flows where boundary treated as a free – slip wall by a continuous fluid. The continuous fluid remains inside the domain. On the other hand, the dispersed fluid leaves the boundary since it is an outlet for them. Air bubbles move toward to the atmosphere from the air diffusers because air is considered as a dispersed fluid in the oxidation ditch process. However, water is a continuous fluid, and horizontal circulation of water occurs in the tank.

In the degassing boundary, pressure distribution on the boundary computed to capture surface height variations as in real flow (ANSYS Inc. , 2009).

4.7.4 Wall

The walls and floor of the tank were modelled as a wall boundary condition. The influence of wall boundary on mass and momentum were specified a no-slip wall condition for water. A free slip wall model was chosen for air.

No-slip wall boundary condition predicts that the velocity of fluid near the wall is the same as that of the wall. The default value of the wall velocity is zero. It means that fluids velocity at the wall boundary is zero.

Free slip wall boundary condition was implemented for the dispersed phase since the contact area with the solid boundary is approximately zero. In this condition, shear stress at the solid boundary is zero, and there is no wall friction effect.

4.8 Material Properties

Water and air were used in modelling of a multiphase flow problem. Heat transfer modelling was disabled in this study. Aeration process has been modelled based on the material properties of air at 25℃.

At this temperature air density of 1.185 kg/m^3 used in the calculations. A single air bubble mean diameter was set to 3 mm since fine bubble diffusers have been mounted on the tank floor.

Solid particles in the wastewater were not considered in this study, and wastewater was replaced as pure water. Water density and reference temperature were 997 kg/m^3 and 25℃, respectively.

4.9 Global Initialization

There is not an inlet and outlet for wastewater in the computational geometry of oxidation ditch. As a result, the basin was modelled as full of water initially. Global initialization option allows setting velocity components and volume fractions of each phase independently. Initial value of water volume fraction was set to 1, while that of air was 0. All the velocity components in cartesian coordinates were defined as zero.

4.10 Solution Methodology

Transient analysis has been applied to simulate the multiphase flow in the oxidation ditch. It is used to obtain time-dependent behavior of flows. ANSYS CFX ensures various time-stepping options to the users. Adaptive time-stepping option was implemented among them. The timestep adaptation process varies according to the number of coefficient loops. Minimum number of coefficient loops was chosen 3, whereas the maximum one was equal to 5 for controlling the adaptive time stepping. If the target minimum coefficient loop is less than the actual one, the timestep size is increasing. However, timestep size decreases when the actual number of coefficient loops is greater than the target maximum one. In this study, 10 coefficient loops per timestep were set which is the default option in multiphase flows.

The governing equations are solved by discretizing the computational domain using mesh elements. An element-based finite volume method used in which governing equations converted into algebraic approximations in the finite volumes and solution of relevant quantities obtained by using a numerical method. High-resolution advection scheme was specified with Second-Order Backward Euler transient scheme during solver setting.

Convergence performance is directly related to the residuals. Residuals explain to what extent the result of resolved conservation equations is similar to the exact solution of these equations. There is no exact solution of set of equations in which residuals must be equal to zero. However, the solver uses the iterative solution of the governing equations and the solution accuracy is measured by residuals. If residuals are too low, it shows more accurate results obtained. The equation residuals might be represented as root mean square (RMS) normalized values in ANSYS CFX. RMS option was defined for the convergence criteria. The default value for RMS is 1E-4 and it is used for understanding the flow field in many engineering applications. 1E-4 was set as a residual target in the setup.

4.11 Summary of Modelling method

Table 4.2 represents the summary of simulation parameters, and their values have been specified for the development of CFD model.

Table 4.3: Summary of the simulation setup.

Parameters	Specifications
Analysis type	*Transient*
Domain motion	*Stationary and rotating*
Fluid domain dimensions	*Three dimensional*
Phase	*Two-phase: air and water*
Temperature	*25 ℃*
Reference Pressure	*1 atm*
Gravity	*9.81 m/s^2*
Angular velocity of rotating domain	*35 rev/min*
Timestep	*Adaptive*
Multiphase model	*Euler – Euler*
Turbulence model	*for air: Dispersed Phase Zero Equation* *for water: SST*
Air bubble size	*3 mm*
Convergence criteria	*1E-4*
Advection scheme	*High – Resolution*
Transient scheme	*Second Order Backward Euler*

Chapter 5

Results

5.1 Introduction

CFD simulation of mixing and aeration processes in a full-scale oxidation ditch has been performed with numerous scenarios and different types of analysis. There are four different scenarios, and they involve a modelling of agitator, coupling of rotating and stationary computational domains, air injection effects on mixing performance by removing agitator application, and arrangement of the flowmaker positions in the oxidation ditch. Also, mesh independency study has been done to obtain an accurate result with the optimal number of mesh elements. Some critical variables were monitored during the simulation period to assess the performance of processes that occur in the oxidation ditch. The objectives and results of the following scenarios will be discussed in detail in the next subchapters.

- Scenario 1 – Modelling of the flowmakers
- Scenario 2 – Transient Rotor-Stator approach
- Scenario 3 – Positioning of the flowmakers
- Scenario 4 – Aeration process contribution to the mixing process without flowmakers.

5.2 Mesh Independence Study

The effect of the mesh density of the computational geometry on the simulation result was carried out with three different meshes as mentioned in Figure 4.4. The details of generated meshes are shown in Table 4.1. The result of numerical simulations of the fluid flow field is dependent on the mesh density. The results predicted accurately by decreasing the size of mesh elements or in other words, high mesh density used in computational geometry (Karcz & Kacperski, 2012).

On the other hand, the computational resource availability is of capital importance to realize the numerical simulations. Computation time rises by the number of mesh elements, and it does not make sense to spend an excessive amount of time for numerical simulations in many research and engineering applications. Accordingly, it

is possible to overcome this challenge by keeping the number of mesh elements in an optimal range for each problem. Mesh independence study must be done to obtain the optimal mesh density.

In this work, the sensitivity of mesh has been analyzed based on the air volume fraction values in transient solution. The following figure was obtained.

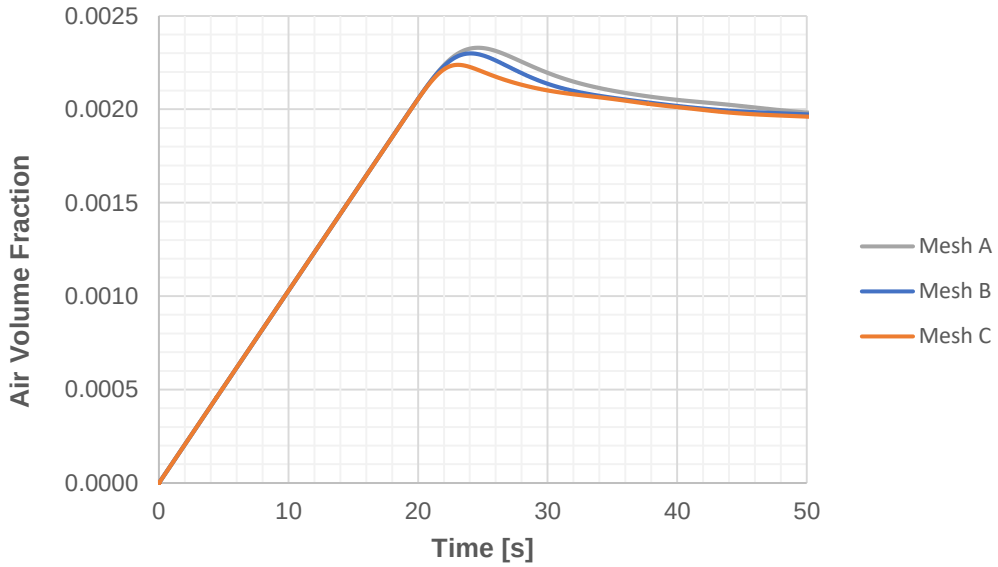

Figure 5.1: Air Holdup Comparison

As it is clear from the plot of air volume fraction, Mesh A has a slightly high volume fraction compared to others. It contains the coarsest mesh elements. Mesh C is composed of the finest mesh elements. Table 5.1 shows the mesh densities of Mesh A, Mesh B, and Mesh C.

Mesh B trend overlaps with that of Mesh C starting from 30 s. Despite the fact that the finest mesh elements must be used for accurate results, the computational effort is too much. Therefore, Mesh B was considered as an optimum choice for simulation purposes. Also, the computation time required for Mesh C is almost twofold of Mesh B, and the obtained simulation results are similar.

Table 5.1: Mesh densities

Mesh independence study	Total number of elements (millions)
Mesh A	3.81
Mesh B	7.53
Mesh C	15.87

5.3 Scenarios

5.3.1 Scenario 1

Modelling of flowmakers

One of the limitations of CFD simulation is the availability of computational resources. The complex computational geometries and flows are in need of high CPU requirements. Therefore, it is possible to alleviate a numerical simulation by means of some validated approaches.

Momentum source term approach is used for replacing rotational domains, such as propellers. Momentum source term approach has a similar result with the sliding mesh method if it is modelled accurately. The developed model of the momentum source term has been applied by Huang, et al. (2013) and the prediction results have a good agreement with the experimental one.

In this scenario, each of flowmakers modelled as a cylinder and thrust value was taken in momentum source term calculations as illustrated in equation (4.7.2.1). The computation speed increases to a great extent with this model. Thrust of 4660 N was specified to calculate the momentum source for both cylinders.

The transient simulation was ended at time 225 s and the comprehensive analysis of the fluid flow field in the oxidation ditch has been done. Two main criterions for assessment of the solution are the velocity of water and air bubble distribution throughout the oxidation ditch.

Figure 5.2 represents the top view of water velocity contours and their vector plots at five different positions. They are horizontal slices with the water velocity scale between 0 m/s and 0.3 m/s. The velocity of 0.3 m/s is the recommended value for keeping the solid matters suspended in liquid media. Thus, in order to analyze mixing quality in the wastewater basin fluid flow with 0.3 m/s was chosen in the velocity scale of Figure 5.2. In general, water circulation with a velocity of 0.3 m/s almost covers most of the regions with some exceptions. It can be easily seen from the water velocity plots that recirculation zones exist at 0.5 m and 1.83 m. Velocity values are lower than the recommended one in the recirculation zones. Recirculation zones at 0.5 m are near the end of aeration regions in the circulation direction. Also, the semi-circular internal walls and rounded corners of the oxidation ditch make a significant contribution to the water circulation speed.

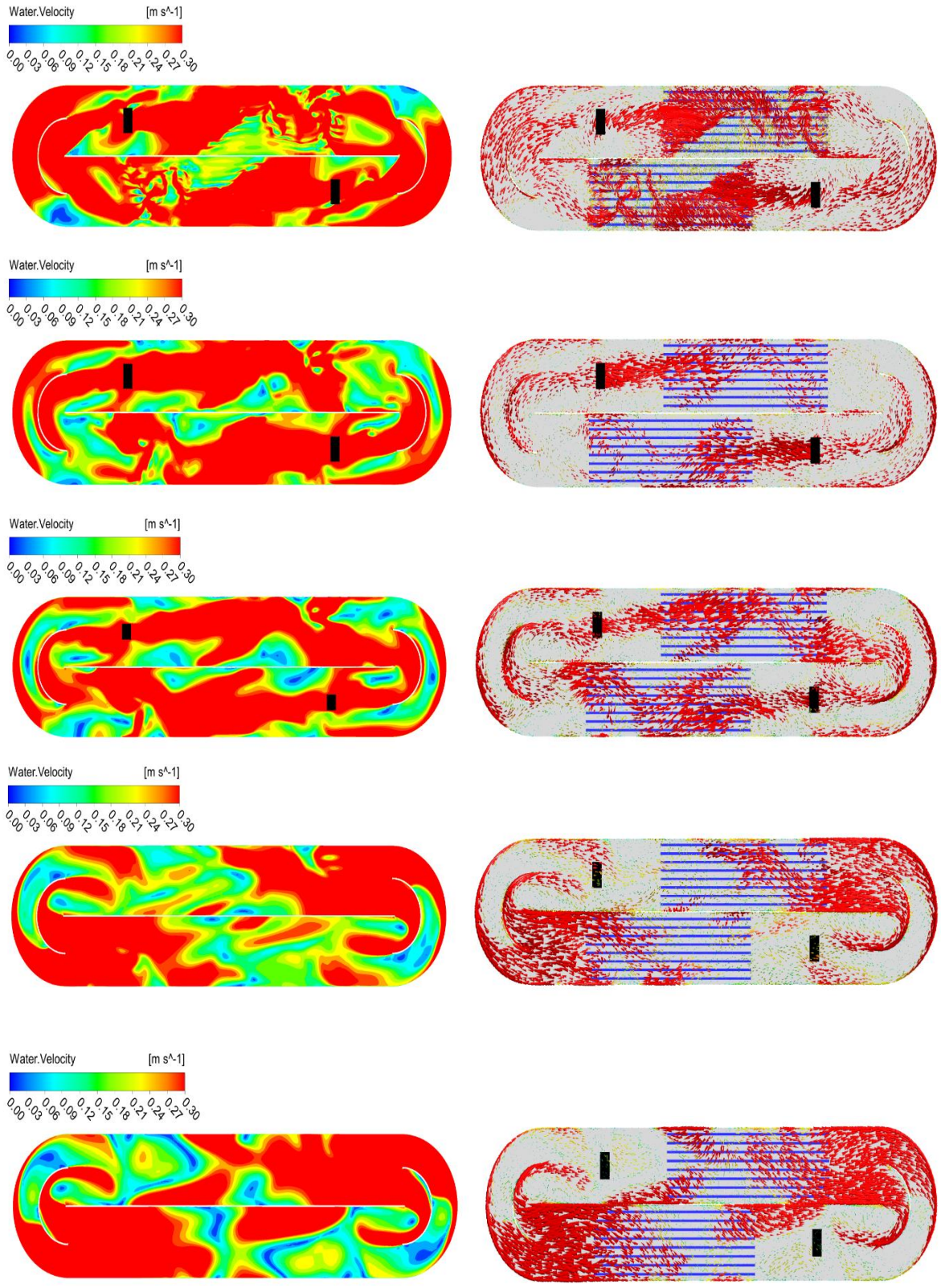

Figure 5.2: Water velocity contour (left) and its vectorial representation (right) on a horizontal plane at 0.5 m, 1.83 m, 3 m, 4.5 m, and 6 m (from top to bottom) above the tank floor.

Although high aeration rates are the reason for recirculation and prevent effective bulk flow, its positive impact on the mixing process observed at water surface. Water velocity is high enough for the efficient mixing process between the end of each aeration zone and its adjacent curve due to air bubbles distribution.

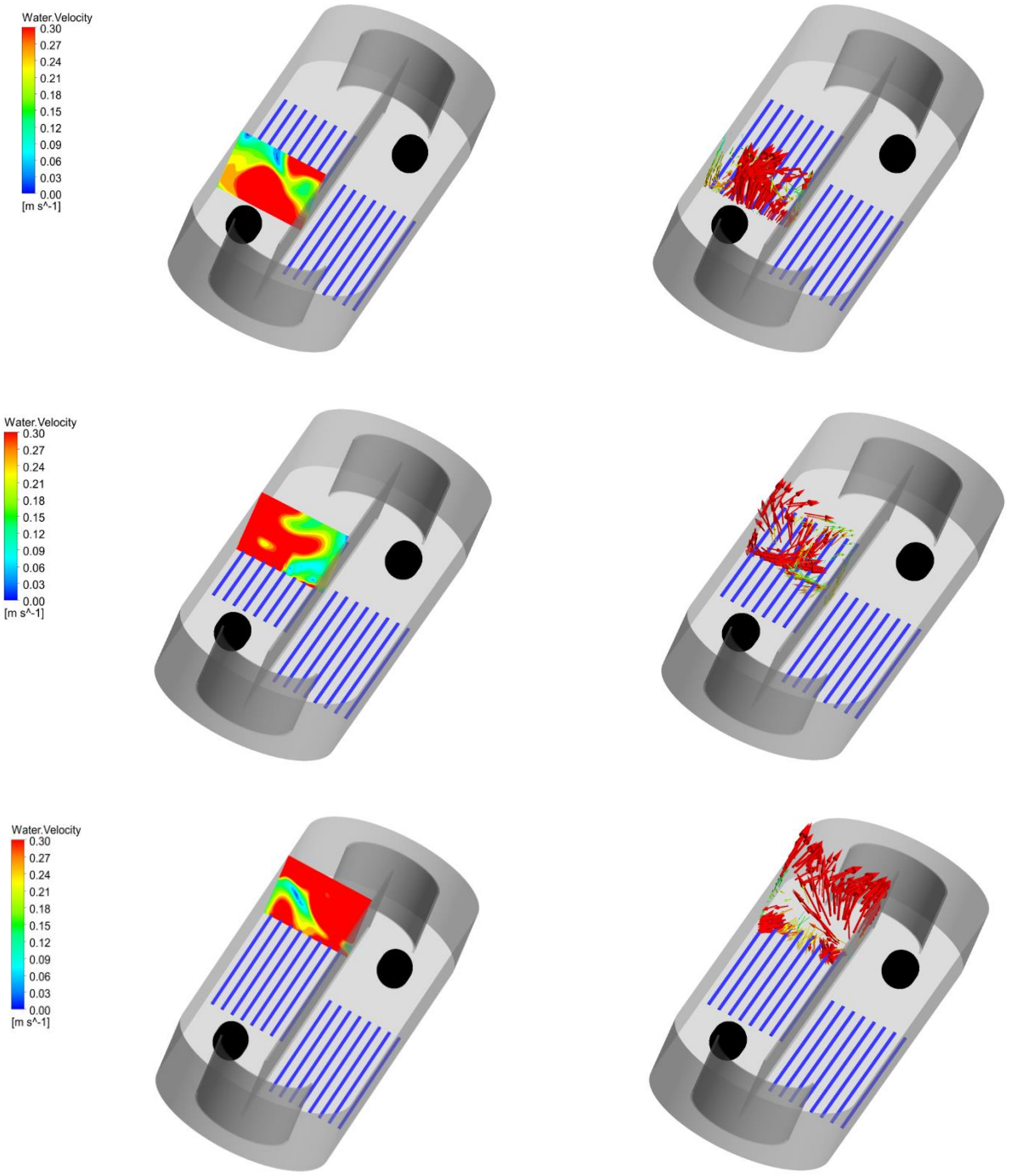

Figure 5.3: Vertical slices of water velocity contour (left) and water velocity vector (right) on the aeration zone.

Vertical slices of water velocity are shown in Figure 5.3 to analyze the mixing process in some critical regions. The water velocity scale also varies between 0 m/s and 0.3 m/s. The positions of vertical slices were chosen at three different points in the aeration zone. Slices vertically cut the beginning, middle, and end of the aeration zone, respectively. This sequence was described from top to bottom in Figure 5.3. The vectorial representation of water velocity shows the recirculation zone generated by air injection.

Longitudinal vertical slice of water velocity contour is shown in Figure 5.4. Also, the water velocity vector on that contour is given.

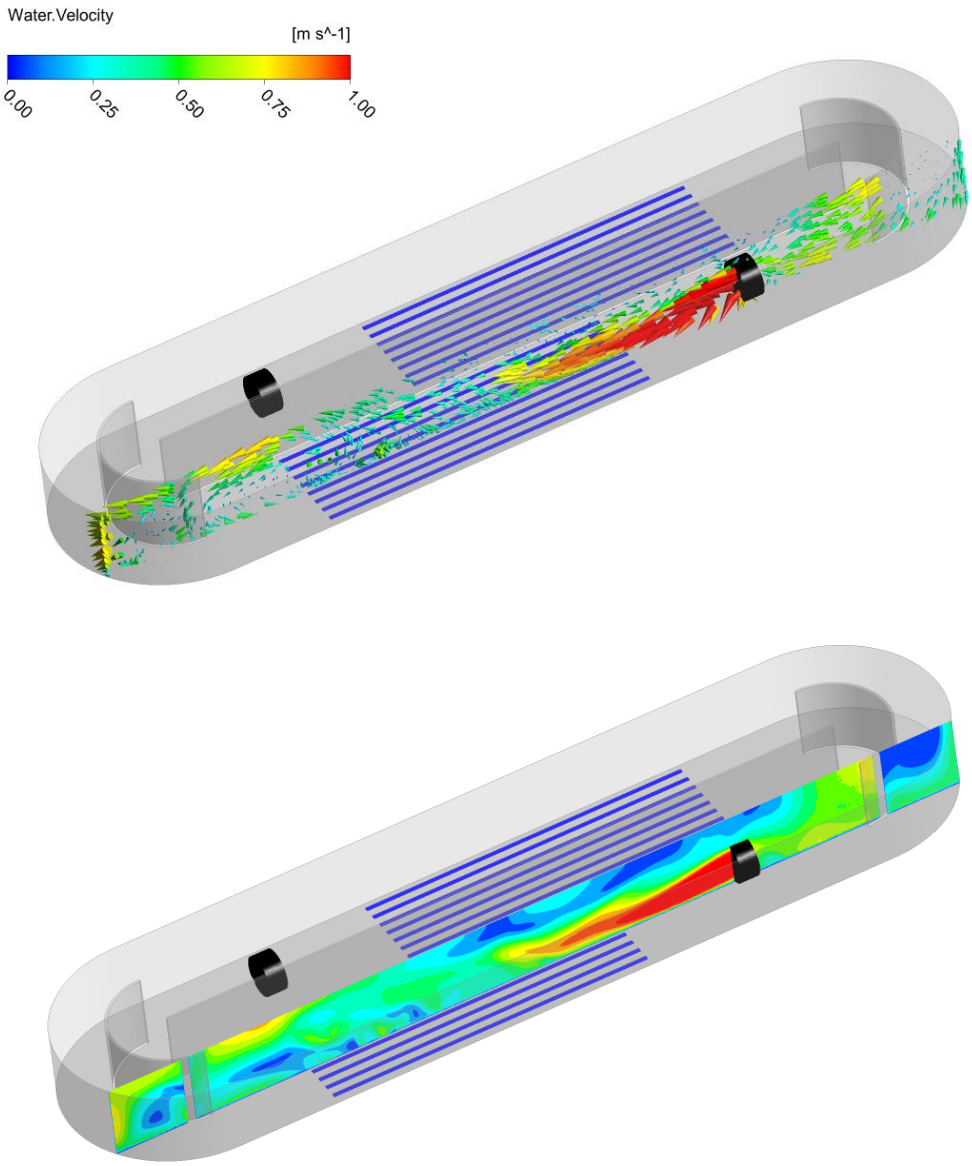

Figure 5.4: Water velocity vector (up) and water velocity contour (down) plots.

The velocity scale varies in the range of 0 m/s and 1 m/s. Since only one-dimensional momentum source term was specified, the swirl effect of modelled flowmakers cannot be observed. Therefore, vectorial illustration differs from real flowmaker behavior. It is possible to obtain the same effect of the propellers in the momentum source term approach if tangential velocity components or tangential forces used instead of axial thrust value.

Huang et al. (2013) applied improved momentum source term approach successfully in which propelling force in the tangential direction and frictional force in radial direction included. The absence of a swirl effect can be seen via streamline plots. Figure 5.5 indicates water streamlines and vectors throughout the tank with a velocity scale varies from 0 m/s to 0.5 m/s.

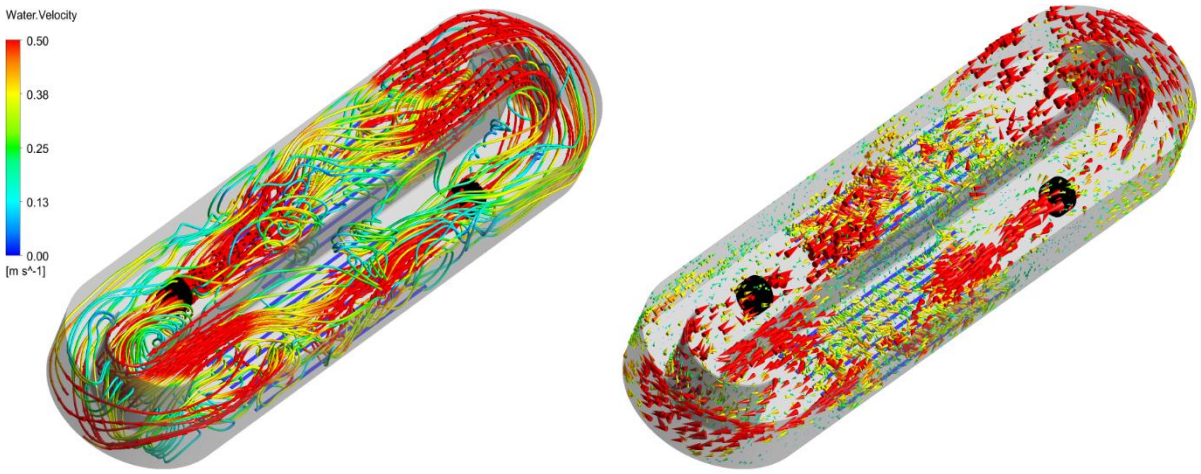

Figure 5.5: Water velocity streamline (left) and water velocity vector (right) at the tank domain.

The deformation of streamlines is observed on the aeration zones, while they are smooth around the non-aerated zone. It occurs due to the recirculation zones which cause a flow blockage of the bulk flow.

Water velocity has been monitored in the tank during the simulation run and it is represented in Figure 5.6. Average water velocity is equal to 0.33 m/s at the end of the simulation run. It is sufficient to obtain good mixing quality. Also, the trend shows that average water velocity is above 0.3 m/s after 55 s. It means that thrust value is enough to create bulk flow and break the flow blockage at the specified aeration rate to keep solid particles in suspension.

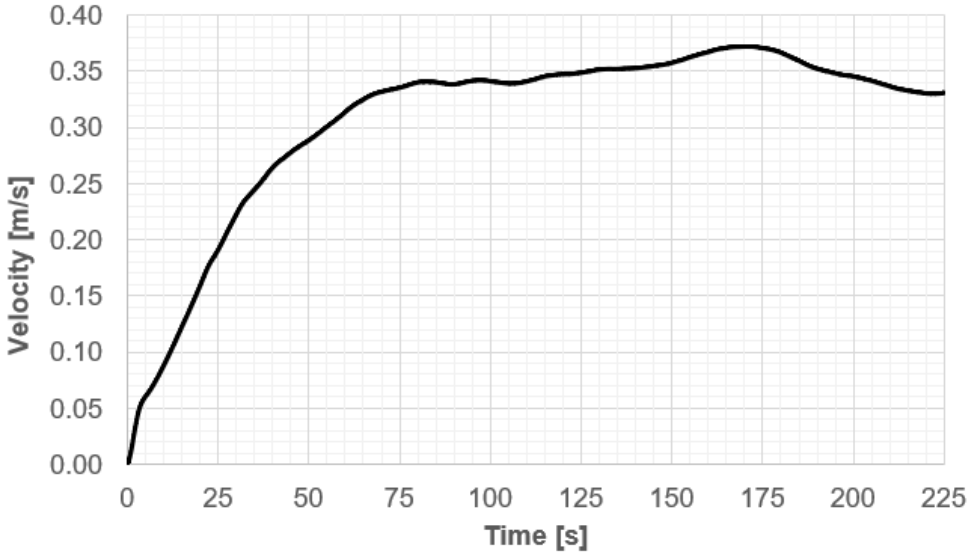

Figure 5.6: Average water velocity plot

Air holdup was also monitored to understand air bubble distribution in computational geometry. The uniform distribution of air bubbles in the tank is not expected due to the fact that diffusers are not completely cover the tank floor. Air holdup trend starts to rise up to 25 s, and then the trend is fluctuating around the value of 0.0020, as shown in Figure 5.7. At the end of the simulation run, air holdup in the tank was measured as 0.0022.

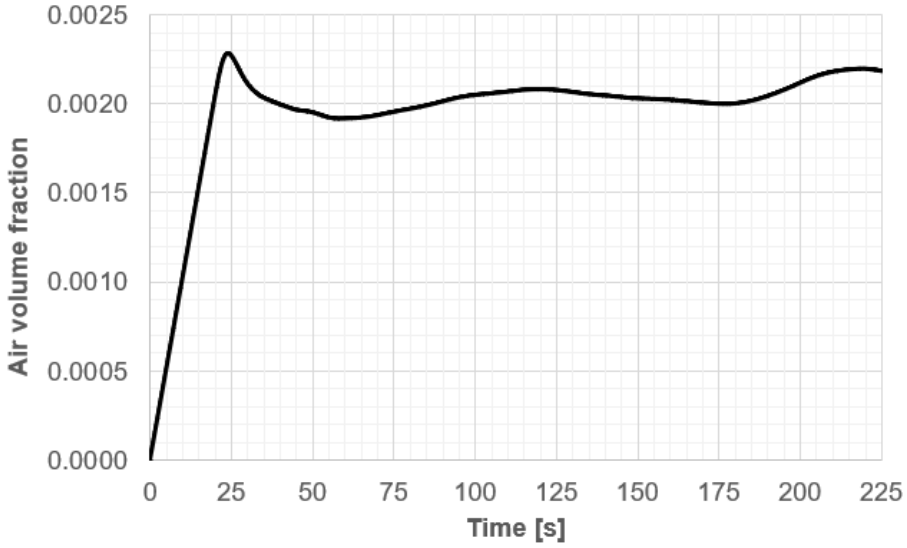

Figure 5.7: Air holdup plot

The air volume fraction isosurface representation gives an impression about air bubbles distribution across the oxidation ditch in Figure 5.8. The volume fraction of 0.0022 was set. The isosurface view was created at time 225 s. Furthermore, air velocity vectors on both aeration zones were given in Figure 5.9. Air velocity vectors in front of each modelled flowmaker gravitated toward the water circulation direction due to the influence of thrust applied to the air plume.

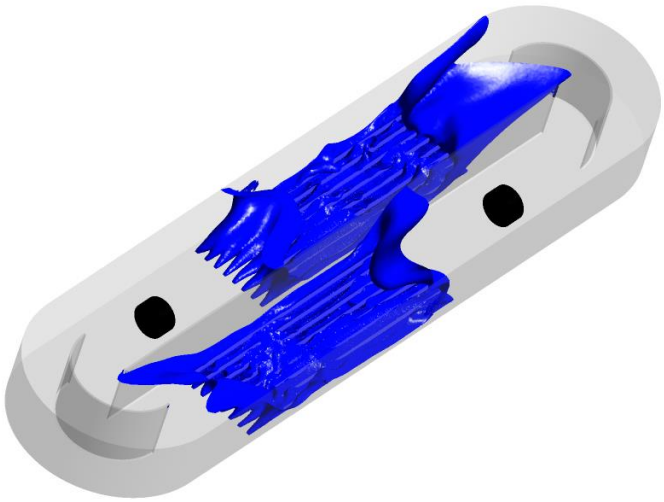

Figure 5.8: Air volume fraction isosurface at 225 s.

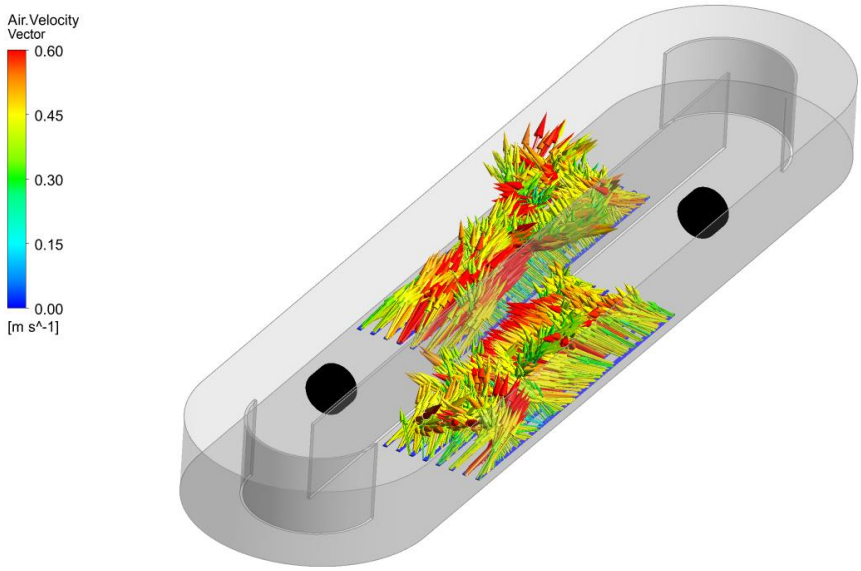

Figure 5.9: Air velocity vectors on the air diffusers.

5.3.2 Scenario 2

Transient Rotor – Stator Model

Scenario 2 is a complicated simulation method which involves the computational geometries of both flowmakers and oxidation ditch tank. In general, it is the most reliable model in order to get the closest results as in the in-situ operations. There is only a disadvantage of the high computation time requirement.

Water velocity field contours are shown on the horizontal planes in Figure 5.10. There are five different height cross-sections for contours. Water velocity vectors are shown for each of the contours to understand the fluid direction. The velocity scale was chosen in the range of 0 m/s and 0.3 m/s in order to analyze mixing quality in the tank. The simulation run was ended at time 225 s. Therefore, all the pictures belong to the velocity profile at 225 s in Figure 5.11.

Backflow is observed near the internal semi-circular walls at 0.5 m high velocity plots. Also, recirculation zones, which are the reason for backflow, can be seen on the diffusers grids. In addition to this, the aggregation of vectors with a velocity of 0.3 m/s is visible at the beginning of aeration zones in the fluid direction. It arises from the influence of generated thrust by flowmakers. The horizontal rotation axis of propellers is 1.83 m above the tank floor. According to this, the fluid flow pattern represented via both velocity contour and vector plots.

The homogenous flow field exists in the rounded ends of the tank. Water moves toward the circulation direction in front of each flowmaker at 6 m high water velocity plots. Water – air interactions cause backward flow in this region.

Since the water velocity is equal to or above 0.3 m/s to a great extent, good mixing quality was obtained at the end of the simulation. Although air injection prevents homogeneous fluid flow, it helps the mixing process by increasing liquid velocity on the aeration regions. The water velocity of 0.3 m/s almost surrounds all the aeration zone at 0.5 m high, while it gradually disappears by moving toward the water surface.

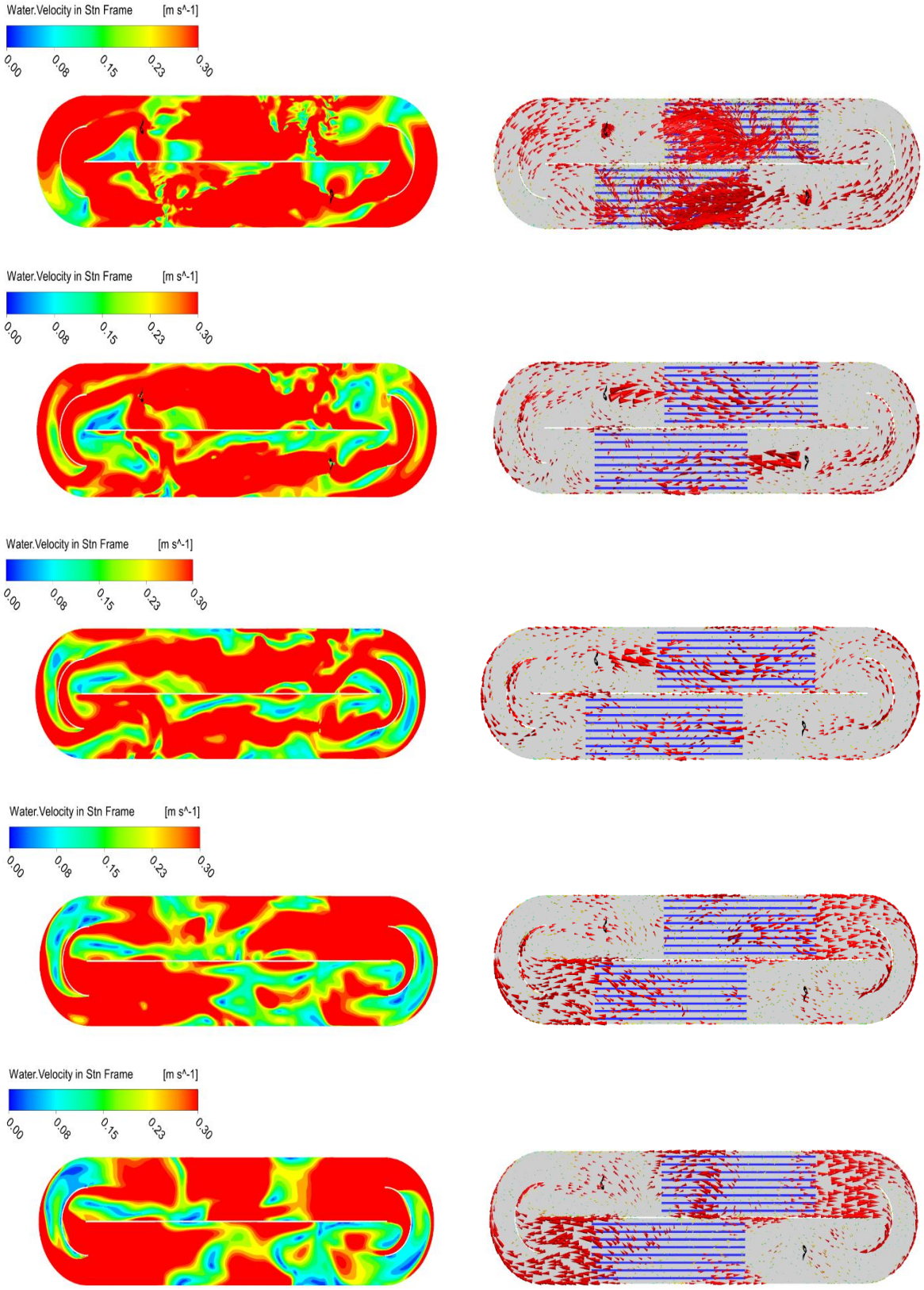

Figure 5.10: Water velocity contour (left) and water velocity vectors (right) on a horizontal plane at 0.5 m, 1.83 m, 3 m, 4.5 m and 6 m (from top to bottom) above the tank floor.

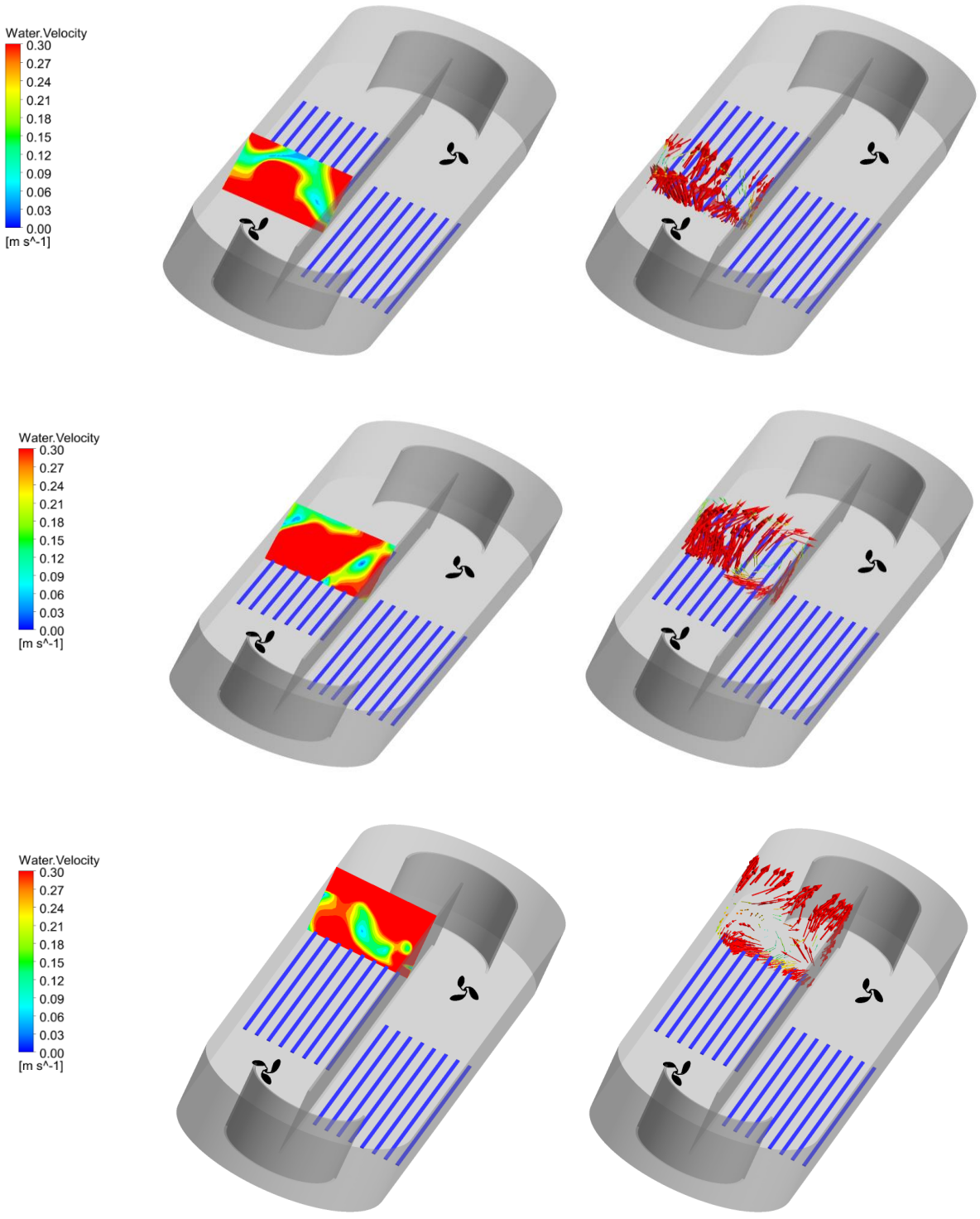

Figure 5.11: Vertical Slices: Water velocity contours (right) and water velocity vectors (left) on the aeration zone.

Recirculation regions stand as a wall and block the fluid flow as shown in Figure 5.11. The vertical slices are placed at the beginning, middle, and end of a diffuser grid from top to bottom.

Another vertical slice in the longitudinal direction is indicated in the following figure. Water velocity vector and contour are given. The velocity scale is between 0 m/s and 1 m/s. The propellers push water with 1 m/s velocity up to the beginning of the diffuser grid uniformly. Then, air injection deforms the uniform flow field.

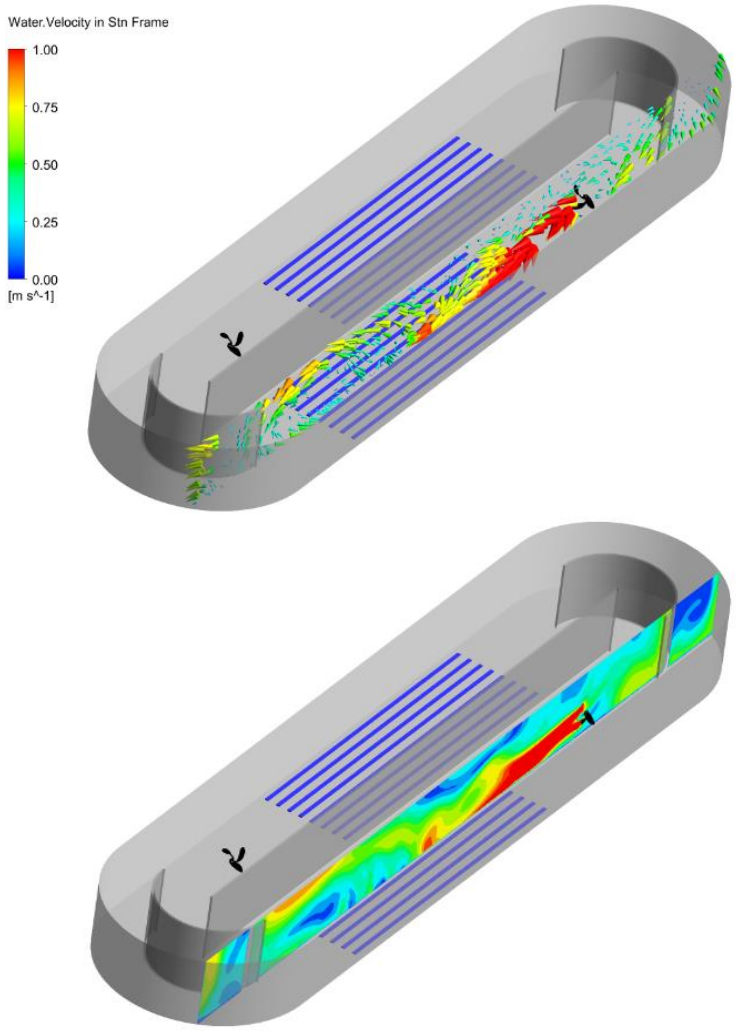

Figure 5.12: Longitudinal vertical slices: Water velocity vector (up) and water velocity contour (down)

Water velocity streamlines are very helpful in order to detect the water circulation, recirculation effect on flow fields, and the swirl effect induced by propellers. So, the streamlines along the oxidation ditch are given in Figure 5.13. Water velocity streamlines are in the range of 0 m/s and 1 m/s. There are specific low-velocity fields near the right-hand side of each propeller in the fluid flow direction.

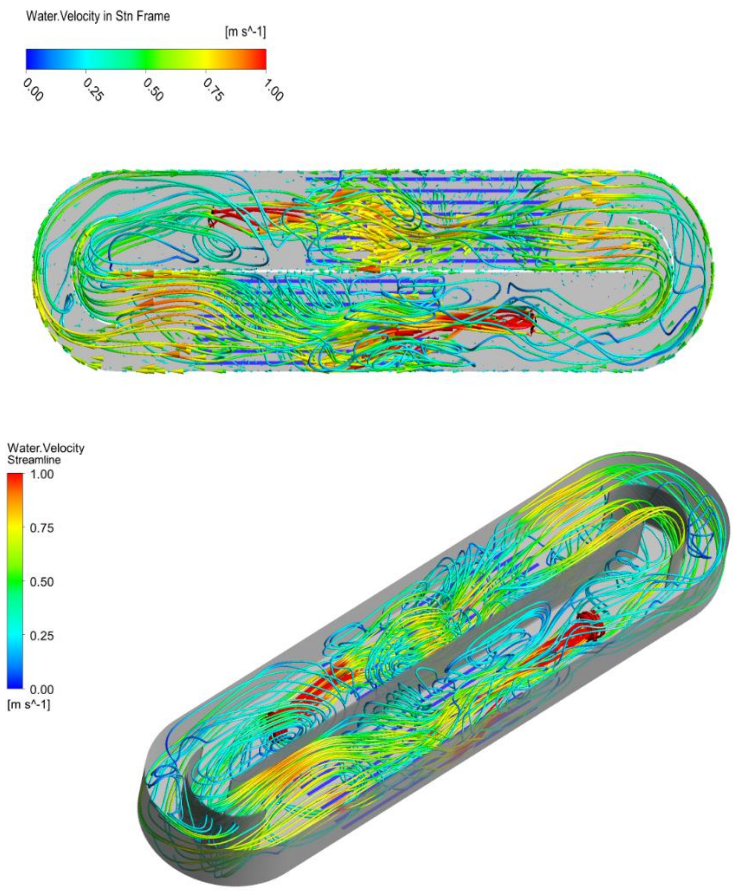

Figure 5.13: Top view (up) and 3D view (down) of water velocity streamlines.

Monitored average water velocity has been plotted in Figure 5.14. Water velocity passes over 0.3 m/s after 45 s, while it is 0.27 m/s at the same time in the momentum source term approach. At the end of the simulation, 0.4 m/s was recorded as average water velocity in the tank. It even increases up to 0.42 m/s with transient rotor-stator model.

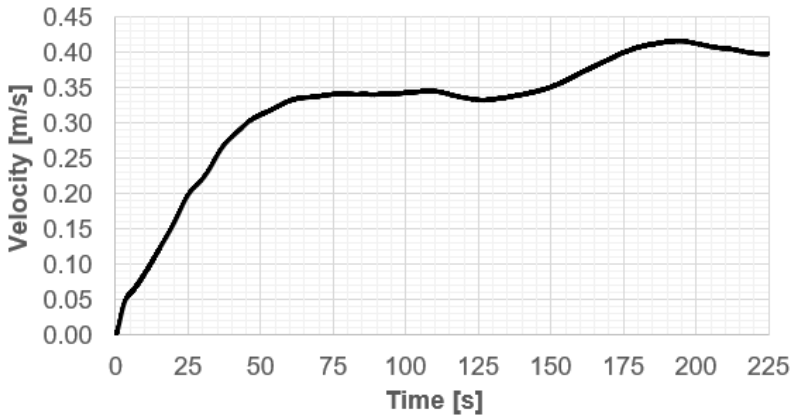

Figure 5.14: Average water velocity profile

Air holdup profile rises to 0.023 at 24 s, and then it has a stable trend line around air volume fraction of 0.002. Air holdup profile is given in Figure 5.15.

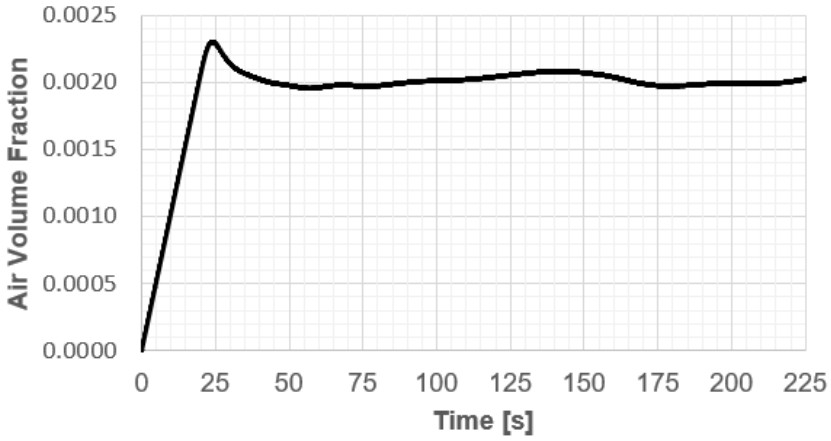

Figure 5.15: Air holdup profile

Also, air volume fraction isosurface in the tank and air velocity vector plots on diffuser grids are shown in Figure 5.16. Air volume fraction value of 0.002 was specified. For air velocity vectors on the diffusers, the velocity scale range varies between 0 m/s and 1 m/s.

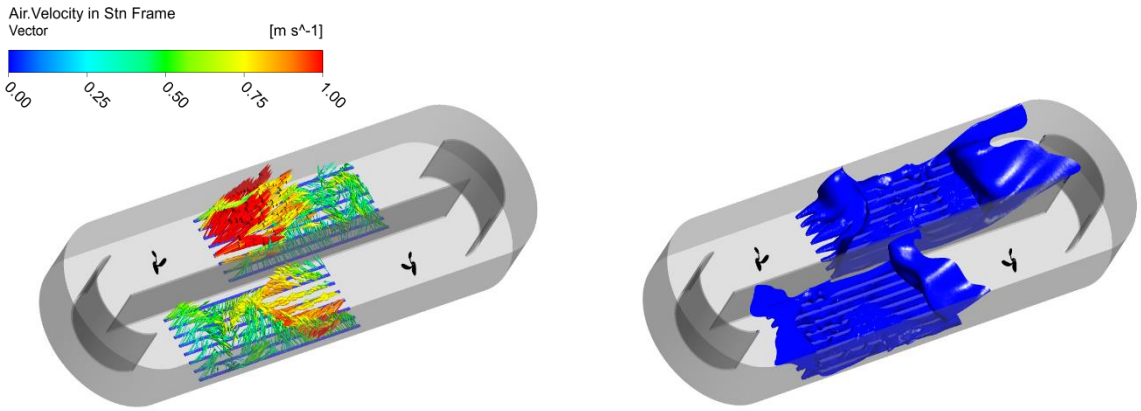

Figure 5.16: Air velocity vectors (right) and air volume fraction isosurface (left).

Forces applied to the blades of the propellers must be within the allowed range in order to protect them from any mechanical damage and extend equipment life. Therefore, it is crucial to analyze the influence of normal force on flowmakers. Transient rotor-stator model has an advantage of monitoring forces during the simulation run. Forces normal to both propellers have been monitored in X, Y, Z directions. The coordinate frame is shown in the following figure.

Blue arrow indicates axial (Z) direction, while red and green ones show radial directions X and Y, respectively. The origin of the coordinate frame located on the hub of flowmaker which is referred to herein as flowmaker 1. Another one is flowmaker 2.

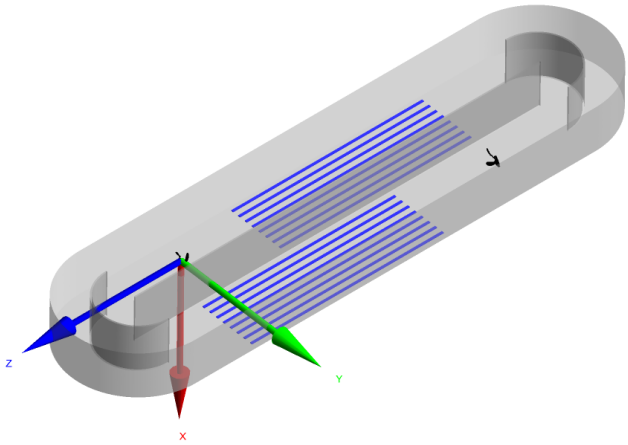

Figure 5.17: Coordinate frame

The result of force monitoring was plotted in Figure 5.18. In X direction, the magnitude of change of absolute force is between 700 N and 800N for the flowmaker 1, while the same for flowmaker 2 passes over 800 N within a timeframe of 100 s to 125 s. A similar trend is observed for flowmaker 1 in the Y direction in comparison with the X direction plot. However, normal forces, which are parallel to Y-axis, increases up to 1000 N on the blades of flowmaker 2. In general, transient behavior is common for the plots of X and Y direction, but there are some exceptions as mentioned above.

Absolute values of normal force were represented for both flowmakers in the Z direction. Flowmaker 1 trend differs from that of flowmaker 2 to a great extent. The oscillation of variable is mainly in the range of 4000 N and 5000 N. if we compare the plots of flowmaker 1 and flowmaker 2, it is possible to claim that normal force fluctuations have the same shape until 75 s. This can be explained by one reason. Since the water is initially stagnant in the oxidation ditch, flowmakers need a fair amount of time to start the circulation process at the tank. Thus, the fluid acts to both flowmakers with the same magnitude of force in that period. After that time, they follow a distinct style of fluctuations up to the end of the simulation.

Higher fluctuation of force on the propeller has a detrimental effect on its performance. The incorrect position of flowmaker may cause fluctuations and decrease mixing performance in a tank.

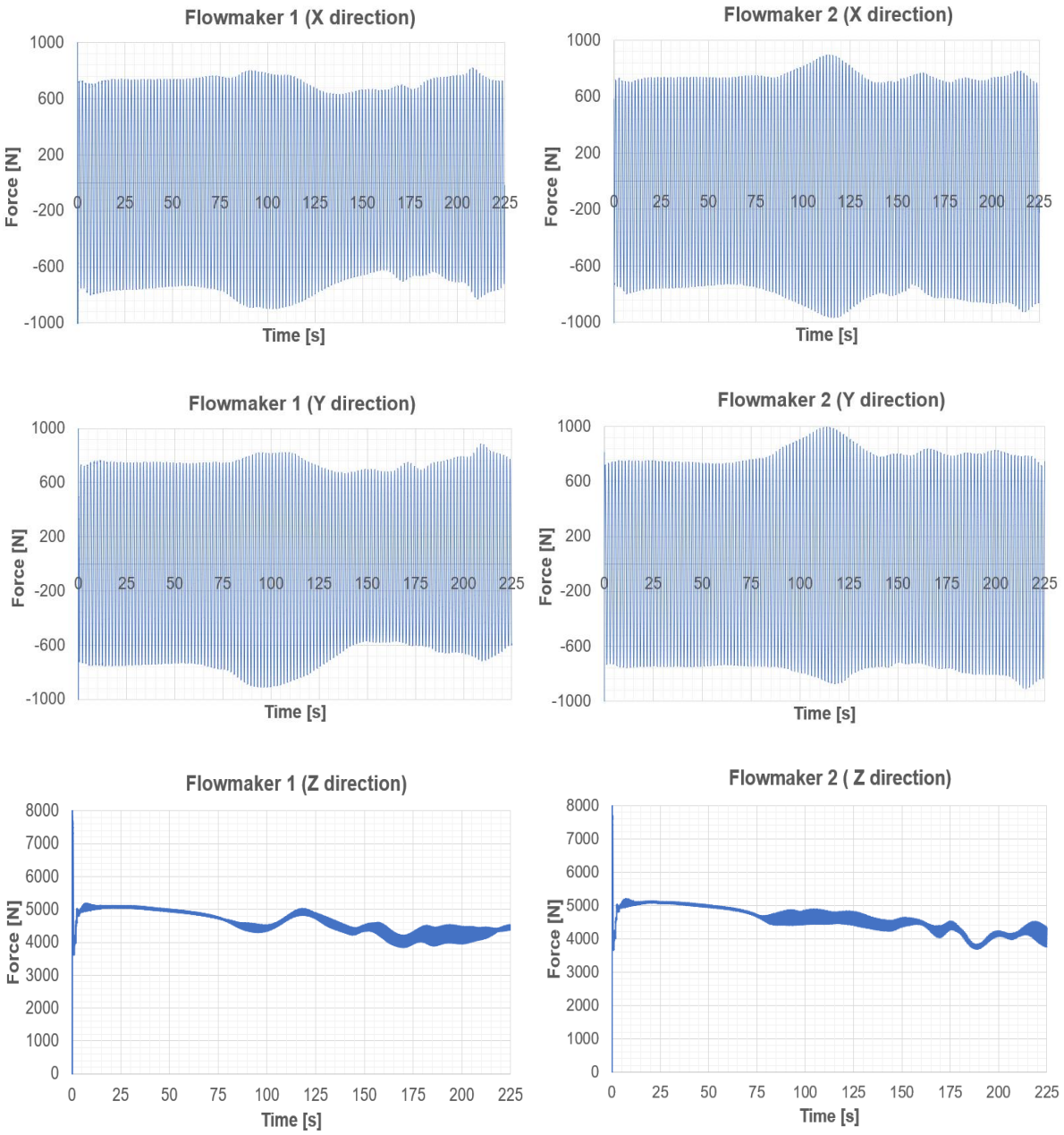

Figure 5.18: Normal force on the blades of flowmakers in axial (Z) and radial (X and Y) direction.

The variation of normal forces was also monitored by considering the effect of aeration process without mixing. Angular velocity of flowmakers was set to 0 rev/min starting from 225 s. The simulation run time is 400 s. Normal force in axial and radial directions was followed. The result of the simulation is given in Figure 5.19.

In axial (Z) direction, the magnitude of force approaches to zero in flowmaker 1 and flowmaker 2 plots. Absolute values were taken into account in this direction. Also, forces are negligible in the X direction.

Normal force in radial (Y) direction is almost stable around the value of 750 N in the first flowmaker, whereas it is about -750 N in the second flowmaker. It arises from the fact that the position of flowmakers is close to the internal semi-circular walls. These walls boost fluid circulation. Therefore, the magnitude of force does not approach zero in the Y direction.

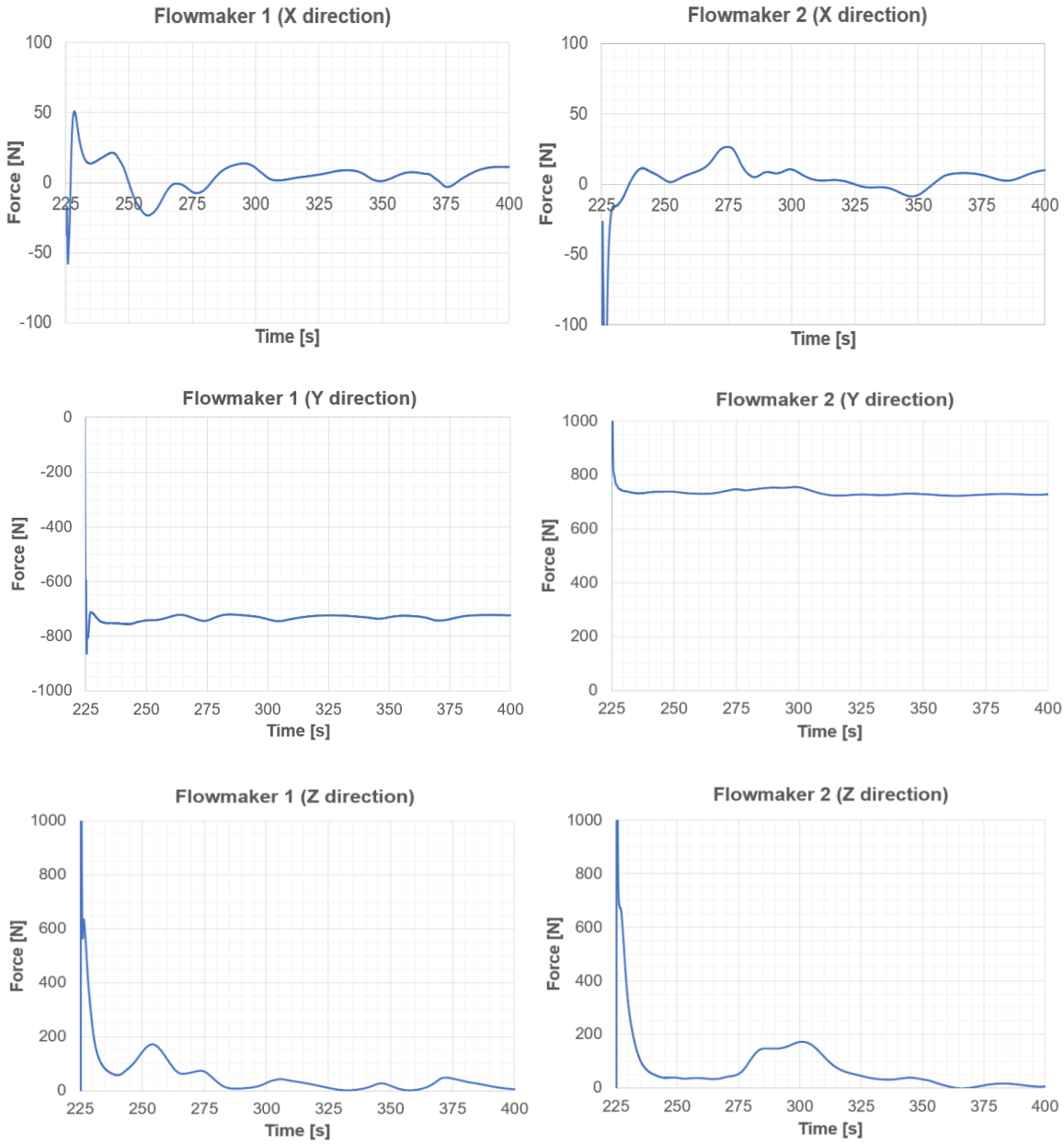

Figure 5.19: Normal force on the blades with aeration process at 0 rev/min.

5.3.3 Scenario 3

Positioning of the flowmakers

One of the significant design steps is to find the optimal place for submersed flowmakers in oxidation ditches. Correct positioning helps to get minimum required horizontal flow velocity and protect blades or other parts of flowmakers from any serious mechanical damage as well. Grundfos is the manufacturer of flowmakers used in this study, and they have basic principles for designing of oxidation ditch system. Positioning rules were taken from the Grundfos best practice guidelines for wastewater treatment tanks and successfully implemented in this CFD simulation.

The main objective of scenario 3 is to monitor thrust values by changing the position of flowmakers rather than analyzing general mixing and aeration process. Therefore, two different positions have been chosen, and simulation was completed for two different cases. They are referred to as case 1 and case 2. Before going into the detail of each case, the rules are given to understand unknown terms.

In the positioning of a submerged flowmaker, there are some crucial factors. One of them is associated with the effect of tank curves since water velocities are distributed unsteadily. The parameter which keeps the rear clearance of propeller in a safe zone is indicated as **C**. Another one is clearance, $\mathbf{C_f}$, which describes the distance between a flowmaker and the first row of the air diffuser grid. In addition to them, it is crucial to keep minimum distance, $\mathbf{C_M}$, between the last row of a diffuser grid and the beginning of the following tank curve.

The positioning rules in oxidation ditch are as follows:

- $C \geq W$ and h_w
- $C_f \geq W$ and h_w
- $C_M \geq h_w$

W and h_w represent the channel width and the water depth, respectively.

Case 1 and case 2 were designed based on the rules mentioned above. The channel width is 8.91, while the water depth is 6 m for the tank. Thus, the position of flowmakers was only modified in the allowable range, and all other values kept as in the actual layout. Figure 5.20 shows case 1 and case 2 layouts. L_C indicates the length of the channel which is 55.26 m.

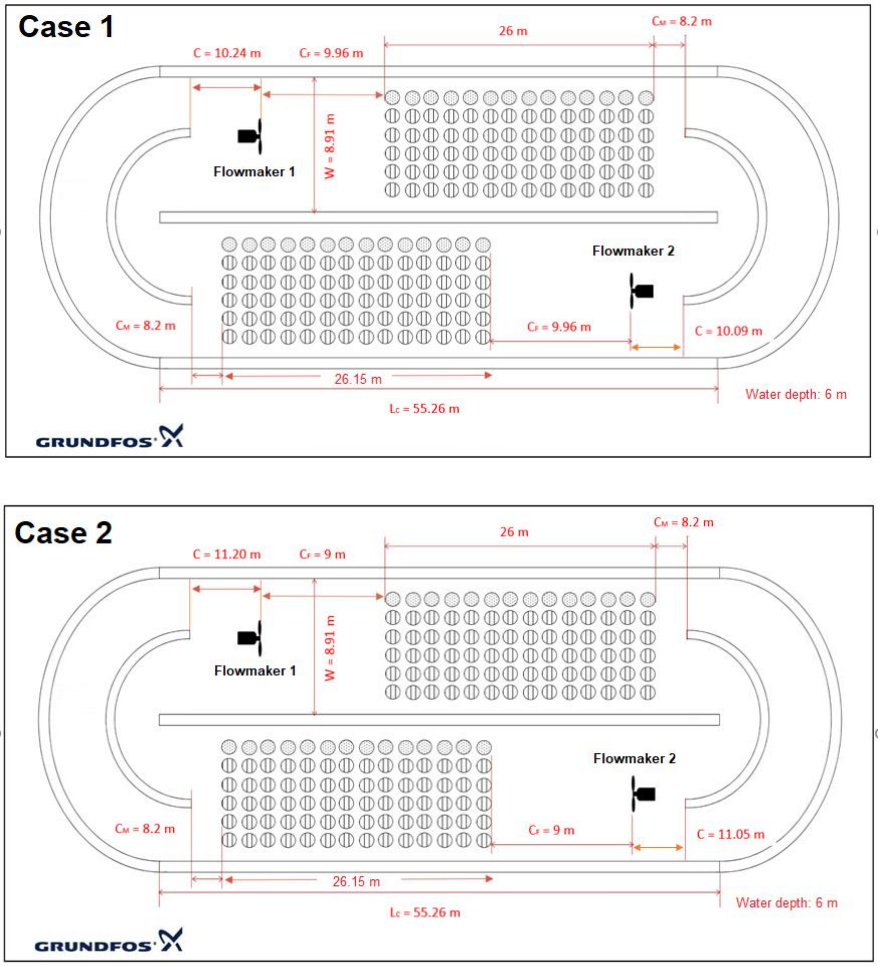

Figure 5.20: Oxidation ditch plan for Case 1 (up) and Case 2 (down)

The value of C_f was 9.26 m for both flowmakers in the original layout, while C was 10.94 m and 10.79 m for flowmaker 1 and flowmaker 2, respectively. Therefore, clearance, C_f, was shifted 0.7 m back in case 1 compared to the original one as shown in the scheme. On the contrary, the distance between the flowmakers and the first row of air diffusers decreased to 9 m. Modified parameters are summed up below.

Table 5.2: Positioning of flowmakers in Case1 and Case 2

Parameters	Case 1		Case 2	
	Flowmaker 1	Flowmaker 2	Flowmaker 1	Flowmaker 2
C_f	9.96 m	9.96 m	9 m	9 m
C	10.24 m	10.09 m	11.20 m	11.05 m

Total simulation time was set 225 s as in the previous scenarios. In order to alleviate the computational effort, the momentum source term approach was used instead of flowmaker 2. Accordingly, normal force on the blade of flowmaker 1 has been monitored in both cases.

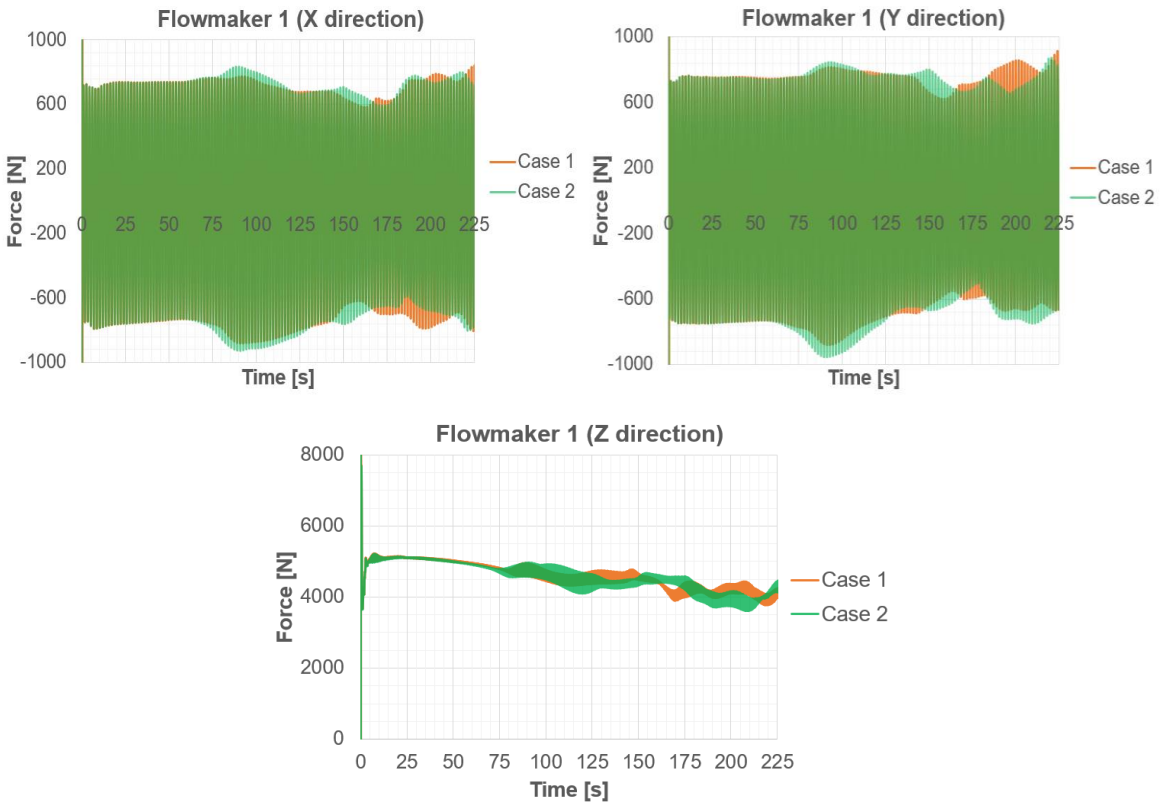

Figure 5.21: Normal force plots of flowmaker 1 for Case 1(orange) and Case 2 (green).

The graphs of X and Y directions show that normal force oscillations increase when propellers are located close to the air diffusers. Since normal forces were measured as the liquid force on the blades, it can also be referred to as thrust. Higher thrust fluctuations damage to the blades to a great extent. Furthermore, it does not only lead to low performance of flowmaker but also wastes more energy during the operation.

In axial (Z) direction, the magnitude of fluctuations in Case 2 is higher than that of Case 1 within the range of 0 to 125 s. It happens because air bubbles stand like a wall in front of flowmakers and drag liquid toward the propeller. After 125 s, transient behavior is observed in both cases. Meanwhile, higher oscillations can be seen in Case 2. it arises from the fact that rear clearance, C, is shorter, and unbalanced upstream flow might be dangerous for propellers.

Backflow can happen due to the air barrier rising from the diffusers when the flowmaker is very close to the air injection system. Therefore, it is recommended to choose an optimal position that increases flowmaker life and generates required horizontal flow velocity as well. Unevenly velocity distribution due to the tank curve must be considered during positioning steps.

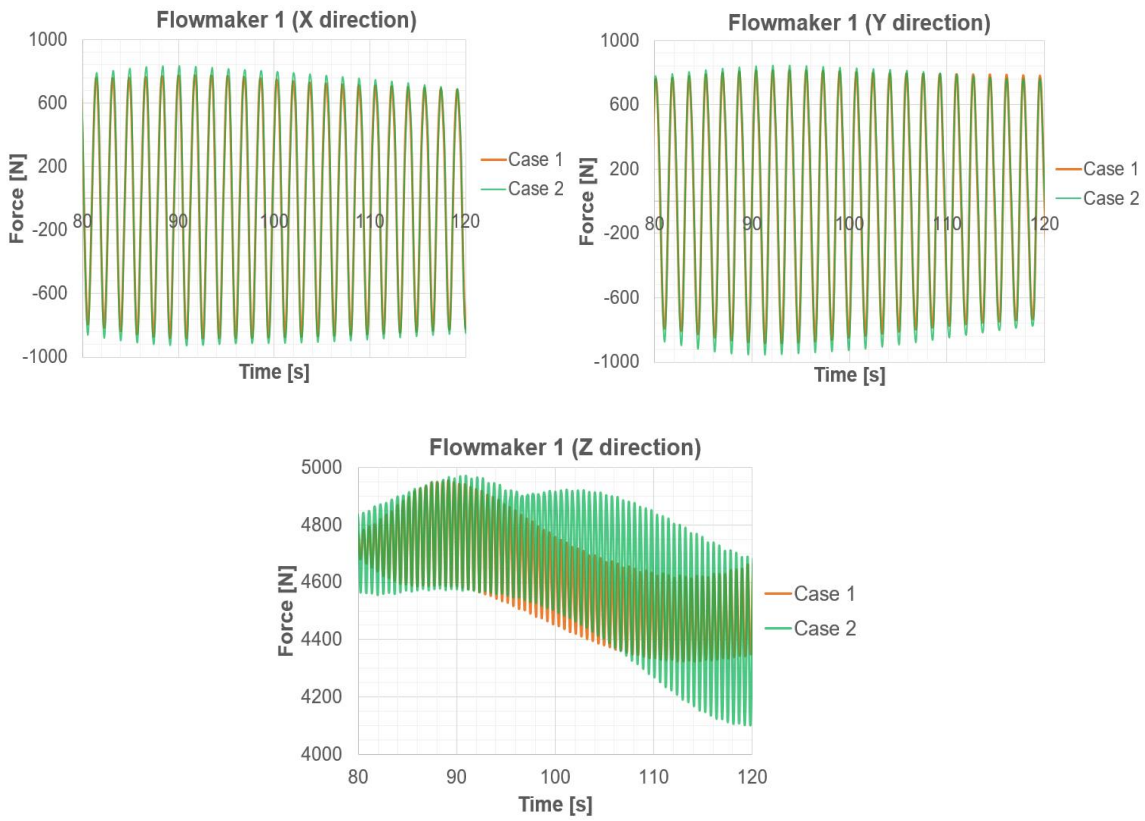

Figure 5.22: Normal force plots between 80 s and 120 s.

In order to understand the importance of positioning rules, the graphs are shown in Figure 5.22 within the specified timeframe. The fluctuations of thrust values are more visible in radial and axial directions as discussed in the previous page.

Air volume fraction isosurface with the influence of the flowmaker was given in Figure 5.23. It shows that the required thrust is generated, and backflow, which arises from air bubbles, is eliminated. Vectors represent the magnitude of water velocity.

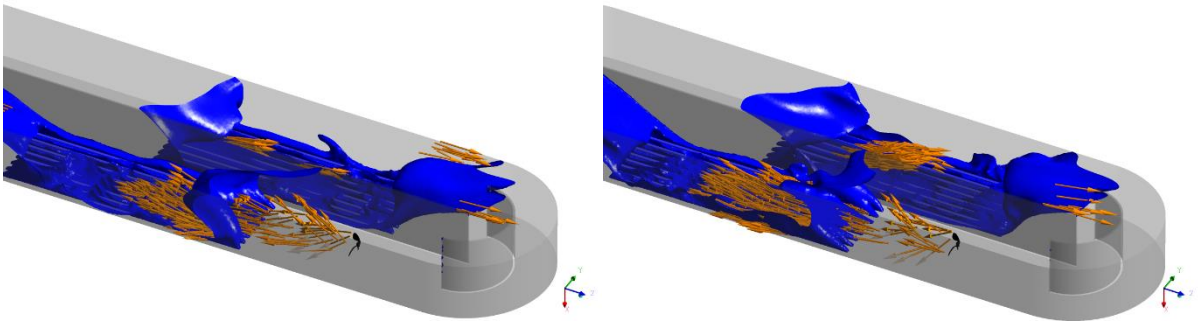

Figure 5. 23 Air volume fraction isosurface for Case 1 (left) and Case 2 (right).

5.3.4 Scenario 4

Aeration process contribution to the mixing process without flowmakers.

The aim of this scenario is to observe how the predefined air flowrate effect on the mixing and circulation process throughout the tank. It is known that the tanks with completely covered air diffusers promote mixing performance considerably. However, the air supply contribution is not clear for a partially covered tank floor. Therefore, this CFD simulation allows analyzing the hydrodynamic behavior of liquid by means of air injection.

If the aeration process makes a significant contribution to mixing performance, it would also be possible to stop the flowmaker during the operation. Thus, energy consumption can be reduced. Besides the energy saving, it helps to extend the equipment life as well.

Both flowmakers were removed from the computational geometry in this scenario. Aeration rate was set to 1344 m^3/h for each of the channels. Total time of CFD simulation was specified as 275 s.

Figure 5.24 shows the water velocity contours and their vectorial schemes in the horizontal plane at five different positions at 275 s. They are at a depth of 0.5 m, 2 m, 3 m, 4.5 m, and 6 m. The velocity scale varies from 0 m/s to 0.3 m/s. Air bubbles drift the fluid toward to middle of aeration channel from each side at 0.5 m high. Non-homogeneous water velocity distribution can be observed on the aeration system due to the chaotic motion of the air bubbles. The recirculation effects are visible between the ends of diffuser grids and the following internal semi-circular wall at 3 m high which corresponds to the middle of water depth.

It is possible to see that the liquid moves with a velocity of 0.3 m/s around only the aeration zones. If we take into account one of the aeration channels, it can be detected that the direction of water velocity vectors is opposite to each other close to the free surface. As a result of this, fluid circulation becomes less efficient or prevented. Furthermore, the fluid in one channel flows against to other and collide at the end of the baffle at 6 m high. One of the most critical points is the velocity of water in rounded-ends of the oxidation ditch tank. For these areas, water velocity is below 0.1 m/s at five different horizontal planes in Figure 5.24.

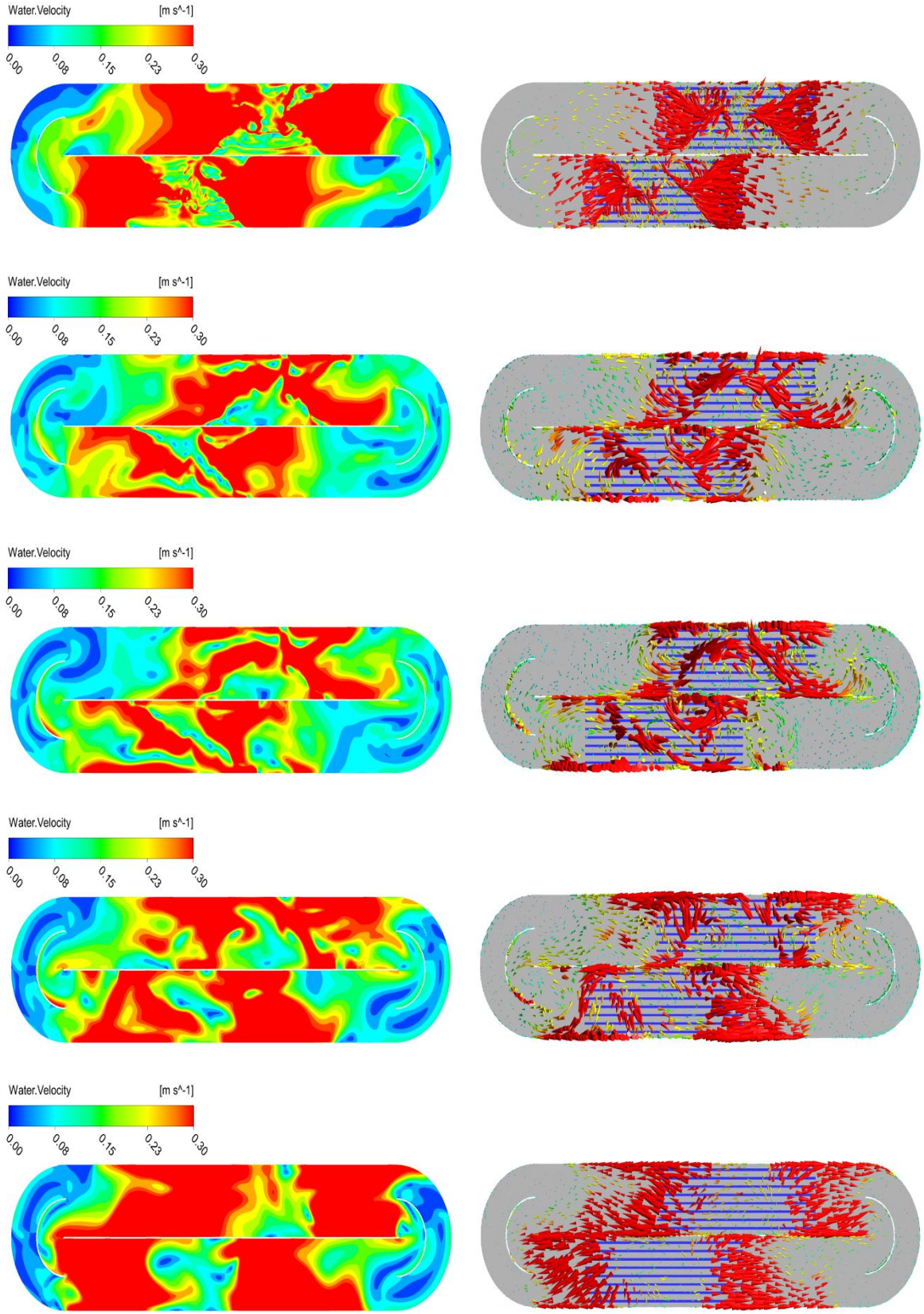

Figure 5. 24: Water velocity contour (left) and water velocity vectors (right) on a horizontal plane at 0.5 m, 2 m, 3 m, 4.5 m and 6 m (from top to bottom) above the tank floor.

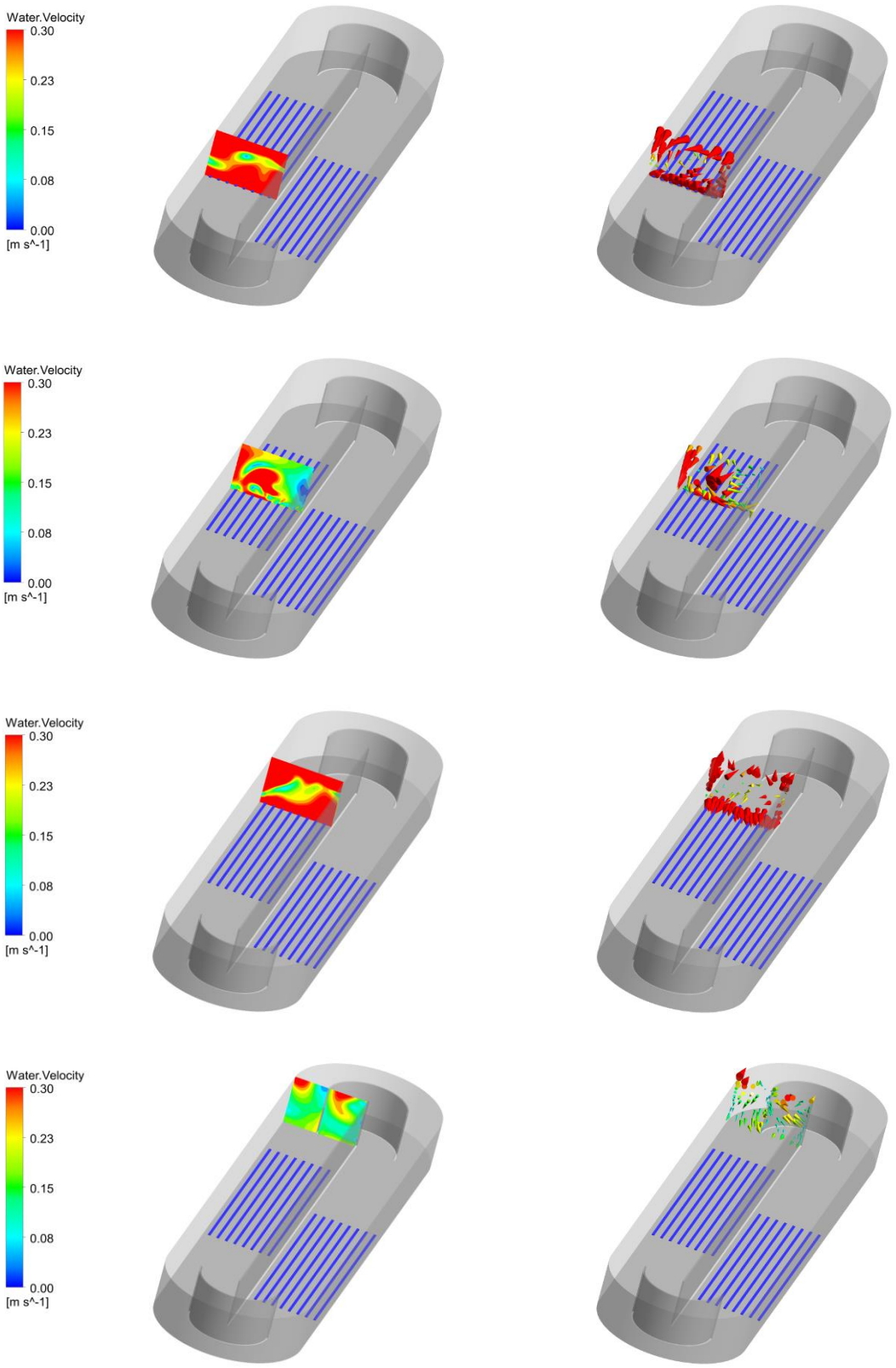

Figure 5.25: Vertical slices of water velocity contours (right) and water velocity vectors (left).

The latitudinal vertical slices have been represented for water velocity contour and vector in Figure 5.25. On the one hand, water velocity vectors move toward each other at the bottom of the tank in the first and last row of diffuser grids. They are oriented in reverse direction at the top of the tank in the same position. Low-velocity fields exist in the middle of the diffuser grid and near the tank curve.

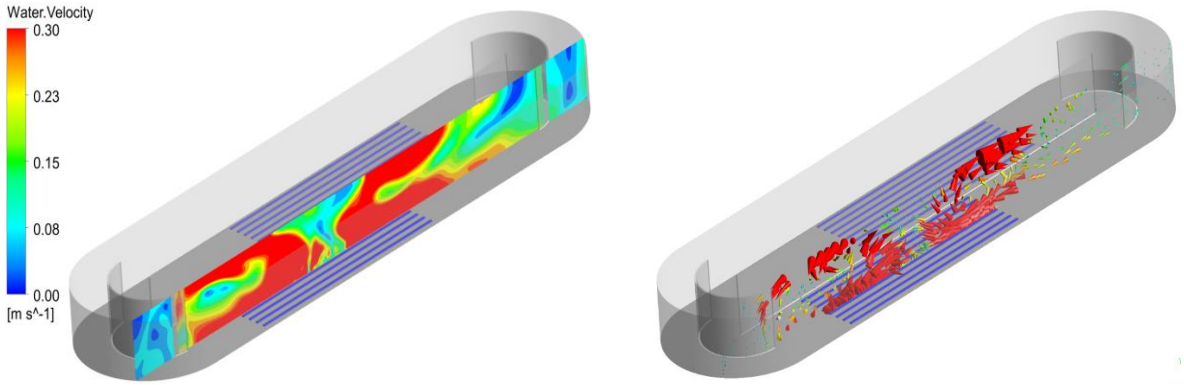

Figure 5.26: Longitudinal vertical slices of water velocity contour (right) and water velocity vector (left).

The longitudinal vertical plane gives more impression about the recirculation effect as indicated in Figure 5.26. In the middle of the aeration zone, the velocity value is below 0.1 m/s which is not enough for homogenization of the fluid and particle mixture.

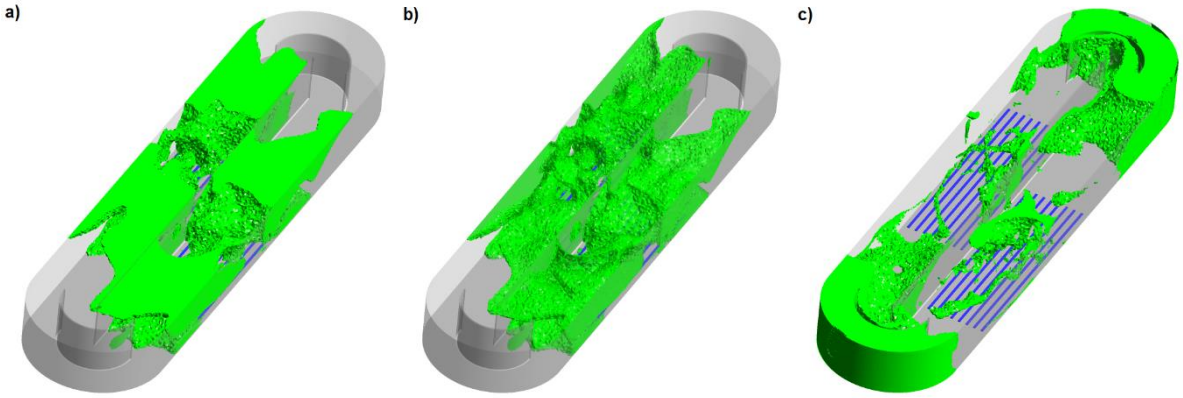

Figure 5. 27: Water velocity isovolumes.
a) above 0.3 m/s b) 0.3 m/s c) below 0.1 m/s

Mixing performance with an air injection system can be more efficiently analyzed when we look at the water velocity isovolumes. This is shown in Figure 5.27. In the first scheme from the left-hand side, water velocity is greater than 0.3 m/s for the occupied volume. The middle one represents the isosurface at 0.3 m/s. Since the velocity of 0.3 m/s is taken as a reference velocity for this study, it can be said that the overall performance of the mixing process is not enough to keep particles suspended in the

liquid. The well-mixing fields are around the aeration zones. The picture on the right-hand side illustrates the volume region in which water velocity is lower than 0.1 m/s. It helps to define the low mixing regions. The channel between the rounded ends and the internal tank curve has a low-velocity field. Therefore, an inefficient wastewater treatment process will happen there. This simulation result describes that required horizontal flow cannot be obtained via the aeration process without running the flowmakers.

Chapter 6

Conclusions and Recommendations

6.1 Conclusions

CFD simulation of mixing and aeration processes in a full-scale oxidation ditch has been completed successfully in this work. The research objectives were achieved through:

- the effective mesh construction for the computational geometry,
- the CFD model development of the oxidation ditch system, including two-phase fluid flow,
- a comprehensive analysis of the mixing and aeration performance with different simulation scenarios,
- the validation of CFD model.

Heuristic techniques have been applied in the designing of oxidation ditch for many years. It is not an efficient method to understand hydraulic behavior properly in the tank. Therefore, an accurate CFD model allows users to analyze the variation of fluid velocity and fluid-fluid interaction at different locations of the oxidation ditch.

The commercial CFD package ANSYS CFX was used to build the two-phase flow model in this study. Since the project focused on a full-scale oxidation tank, considerably simplification was done for computational geometry, especially for the diffuser system. Four different simulation scenarios were accomplished as described in the previous chapter.

The momentum source term approach has been implemented in numerous CFD studies of wastewater treatment plants (Brannock, 2003; Wang, 2010). Based on the model validity and reliability, it was also implemented in this project. The model needs low computational resources, and high computing speed is another advantage. The result shows that the model helps predict fluid flow patterns through the tank. Furthermore, the effect of the geometrical shapes such as semi-circular inner walls, rounded ends, and internal baffle on the hydrodynamics can be analyzed successfully with this method. Since the momentum source term approach does not include the swirl effect of propellers, the difference between the results of this method and the

transient rotor-stator one was observed. Therefore, the momentum source term approach gives a comprehensive insight regarding the fluid motion across the tank.

Transient rotor-stator model allowed a more accurate prediction of fluid flow patterns and simulated the oxidation ditch process as in reality. However, it is application computationally limited. It has a high CPU requirement and consumes excessive memory. Thus, transient analysis with this method is quite expensive. The model of flowmakers has been chosen for the project are capable of generating the required thrust in order to obtain sufficient bulk flow. In addition to this, minimum horizontal flow velocity was achieved to avoid solid matter sedimentation. Apart from comprehensive hydrodynamic analysis, the flowmaker positioning tests were done. Grundfos best practice guidelines were taken into account for the correct positioning and normal force analysis acting on the blades. Monitoring results show that force acting on the blades of propeller is in the allowed range. Also, two different positions were chosen for the propellers. Higher thrust fluctuations were determined when the propeller position was close to the diffuser grids. On the contrary, it was less for the case in which propeller positions were far away from the diffusers. The results correspond to the experimental axial thrust measurements which were accomplished by Fayolle, et al. (2011). In the experiment, the reaction force of the liquid on the propeller was measured for the axial thrust determination. The same methodology was used in this CFD simulation.

The contribution of the aeration process to the mixing performance was also investigated by removing the flowmakers. Inadequate mixing process was monitored throughout the tank due to the recirculation zones. There were dead zones around the rounded ends of the oxidation ditch. Also, it can be said that the diffuser grid arrangement is not suitable to get excellent mixing performance without flowmakers. Therefore, it is necessary to use flowmakers with higher thrust input to break the recirculation effects in aeration zones.

Mesh independence study was done for the validation of CFD model. The sludge rheology was not taken into consideration due to the computational challenges. Hence, it can be concluded that CFD is a reliable technique to investigate the fluid flow variations and the effect of internal configurations in a full-scale oxidation ditch study. Despite excessive computing resource requirements, CFD can be used for the optimization of fluid parameters and the flowmaker model identification successfully.

6.2 Recommendations

The detailed analysis of hydrodynamics in a full-scale oxidation ditch using Computational Fluid Dynamics is limited. However, there is an increase in the number of studies in recent years. During the development of CFD model for this project, some simplifications have been done. In order to further improvement of CFD analysis, future recommendations can be given.

In reality, disc-type fine bubble diffusers or short plate-type diffusers are widely used for the aeration system. Despite the complex geometry of diffusers, it would be helpful to consider the real shape of diffusers in CFD study. It will allow analyzing the recirculation effect of air injection accurately. Also, a comprehensive analysis of air bubble hydrodynamics, coalescence and break-up impacts can be studied by Population Balance Model (PBM). Constant bubble size was used in this research.

Oxidation ditch is a continuous process in which mixed liquor inlet and outlet exist. It would be recommended to consider the tank inlet and outlet for computational geometry in the future. Besides that, the mixed liquor contains solid particles that were skipped and pure water used in the CFD model development. Therefore, CFD investigation by using sludge rheology will predict more precise spatial variations of fluid flow.

References

Andersson, B. et al., 2012. Computational Fluid Dynamics for Engineers. New York: Cambridge University Press.

ANSYS Inc., 2009. ANSYS CFX-Solver Modelling Guide, Pennsylvania.

ANSYS Inc., 2017. ANSYS Help: Overview of ANSYS CFX 18.2.

ANSYS, Inc., 2009. ANSYS CFX-Solver Theory Guide, Canonsburg.

ANSYS, Inc, 2016. ANSYS ICEM CFD Help Manual.

Bhargava, A., 2016. Activated sludge treatment process - concept and system design. International Journal of Engineering Development and Research, 4(2), pp. 890-896.

Brannock, M., 2003. Computational Fluid Dynamics tools for the design of Mixed Anoxic Wastewater Treatment Vessels.

Brouckaert, C. J. & Buckley, C. A., 1999. The use of computational fluid dynamics for improving the design and operation of water and wastewater treatment plants.

Climent, J. et al., 2019. A comprehensive hydrodynamic analysis of full-scale oxidation ditch using population balance modelling in CFD simulation. Chemical Engineering Journal, pp. 760-775.

Cockx, A., Do-Quang, Z., Line, A. & Roustan, M., 1999. Use of computational fluid dynamics for simulating hydrodynamics and mass transfer in industrial ozonation towers. Chemical Engineering Science.

Dean, J. A., 1999. Lange's Handbook of Chemistry. 15th ed.

EPA, 1999. Wastewater Technology Fact Sheet - Fine Bubble Aeration, Washington.

EPA, 1999. Wastewater Technology Fact Sheet - Sequencing batch reactors, Washington.

Fayolle, Y. et al., 2007. Oxygen transfer prediction in aeration tanks using CFD. Chemical Engineering Science, pp. 7163-7171.

Fayolle, Y. et al., 2011. Aeration and Mixing in Loop Reactors Equipped with Fine Bubble Diffusers and Slow Speed Mixers: A Full-Scale Study.

Grady, L., Daigger & Lim, 1999. Biological Wastewater Treatment.

Huang, W., Li, K., Wang, G. & Wang, Y., 2013. Computational Fluid Dynamics Simulation of Flows in an Oxidation Ditch Driven by a New Surface Aerator. Environmental Engineering Science, pp. 663-671.

Jern, N. W., 2006. Industrial wastewater treatment. World Scientific Pub Co Inc.

John Lindam, 2014. www.xyleminc.com. [Online]
Available at: https://www.xylem.com/siteassets/support/case-studies/case-studies-pdf/wp-aeration-efficiency-in-oxidation-ditches-2014.pdf

Karama, A. B., Onyejekwe, O. O., Brouckaert, C. J. & Buckley, C. A., 1999. The use of computational fluid dynamics (CFD) technique for evaluating the efficiency of an activated sludge reactor. Water Science and Technology, Volume 39, pp. 329-332.

Karcz, J. & Kacperski, L., 2012. An effect of the grid quality on the result of numerical simulations of the fluid flow field in an agitated vessel, Szczecin.

Karpinska, A. M. & John, B., 2015. CFD-aided modelling of activated sludge systems - A critical review. Water Research, pp. 861-879.

L.S.Caretto, 2009. Computational Fluid Dynamics, California State University Northridge.

Mc.Carty, P. L. & Brodersen, C. F., 1962. Theory of Extended Aeration Activated Sludge. Water Pollution Control Federation, Volume 34, pp. 1095-1103.

Morin, A. L. & Gilligan, T. P., High purity oxygen biological nutrient removal.

Nelsen, D., Carnegie, J. W. & Hardin, P., 1984. Biological Treatment Process Control, Albany.

Peng, Y. & Zhu, G., 2006. Biological nitrogen removal with nitrification. Applied Microbiology and Biotechnology.

Pennsylvania Department of Environmental Protection, 2014. The Activated Sludge Process.

Pipeline- Explaining the Activated Sludge Process, 2003. http://www.nesc.wvu.edu. [Online]
Available at: http://www.nesc.wvu.edu/pdf/WW/publications/pipline/PL_SP03.pdf

Portella, A. M. K., 2013. New Design Tools for Activated Sludge Process.

Rosa, L. M., Koerich, D. M. & Giustina, S. V., 2017. The use of CFD in design and optimization of wastewater treatment units: A review.

Sperling, M. v., 2007. Aeration. In: Biological Wastewater Treatment Series - Basic Principles of Wastewater Treatment, pp. 161-191.

Sperling, M. v., 2007. Biological Wastewater Treatment Series-Volume five. IWA publishing.

State of Maine Department of Environmental Protection, 2009. Notes on activated sludge process control.

Tchobanoglous, G., Burton, F. L. & Stensel, H. D., 2006. Wastewater Engineering: Treatment and Reuse. 4th ed.

Theobald, D., 2014. Water Technology. [Online]
Available at: https://www.watertechonline.com/microorganisms-in-activated-sludge/

UNESCO, 2019. The United Nations World Water Development Report 2019-Leaving no one behind, Paris: United Nations Educational, Scientific and Cultural Organization (UNESCO).

Versteeg, H. & Malalasekera, M., 2007. An Introduction to Computational Fluid Dynamics. 2nd ed. Pearson Education Limited.

Wang, Y., 2010. Evaluation of Membrane Bioreactor Mixing Performance via Computational Fluid Dynamics Modelling, Sydney.

wateronline.com, wateronline.com. [Online]
Available at: https://www.wateronline.com/doc/disc-aerators-replace-adding-capacity-performance-0001

xylem.com.
Available at: https://www.xylem.com/siteassets/brand-specific-content-including-catalog/sanitaire/sanitaire-resources/aeration-products-for-energy-efficient-biological-treatment.pdf

www.grundfos.com, www.grundfos.com. [Online]
Available at: https://product-selection.grundfos.com/product-detail.product-detail.html?custid=GMA&productnumber=98787825
[Accessed 14 November 2019].